A study of the integration of semi-transparent photovoltaics with sunscreen structures in a major transportation infrastructure tunnel

David Yuan-Jae Sun

A Thesis in the Department of
Building, Civil and Environmental Engineering

Presented in the Partial Fulfillment of the Requirements
for the Degree of Master of Applied Science (Building Engineering) at
Concordia University
Montréal, Québec, Canada

August 14, 2019

CONCORDIA UNIVERSITY

CONCORDIA UNIVERSITY

School of Graduate Studies

This is to certify that the thesis prepared

By: David Sun

Entitled: A Study of the Integration of Semi-transparent Photovoltaics with Sunscreen Structures in a Major Transportation Infrastructure Tunnel

and submitted in partial fulfillment of the requirements for the degree of

Master of Applied Science (Building Engineering)

complies with the regulations of the University and meets the accepted standards with respect to originality and quality.

Signed by the final examining committee:

_____ Chair
Dr. L Wang

_____ Co-Supervisor
Dr. A. Athienitis

_____ Co-Supervisor
Dr. K. D'Avignon

_____ Examiner
Dr. L. A. C. Lopes External (to program)

_____ Examiner
Dr. U. Eicker

_____ Examiner
Dr. L. Wang

Approved by _____
Dr. F. Haghighat, GPD
Department of Building, Civil, and Environmental Engineering

_____
Dr. Amir. Asif, Dean
Gina Cody School of Engineering and Computer Science

Date _____

Abstract

A study of the integration of semi-transparent photovoltaics with sunscreen structures in a major transportation infrastructure tunnel

David Yuan-Jae Sun

This thesis presents a study of the energy consumption of a major underwater road tunnel in Québec and the possible integration of photovoltaics, as well as other energy efficiency measures. A novel application of semi-transparent photovoltaics (STPV) integrated with sunscreen structures (SS) installed at the portals of the tunnel is presented as a retrofit primarily for the tunnel lighting system, but with auxiliary benefits to other major systems and road safety conditions. A study on the operational power and energy use of the heating, lighting, and ventilation systems was performed to estimate the potential energy and monetary savings of this application.

Lighting subsystems account for up to 50% of the energy consumption of a typical tunnel. Day-time lighting levels account for over two-thirds of the total system lighting power; their periodic nature creates daily peaks in the tunnel's energy load profile.

The 1.3 km long Louis-Hippolyte-La Fontaine underwater road tunnel, located in Montréal, Québec is presented as a representative case study for cold climates. A model of the lighting system was developed using recorded data from a supervisory control and data acquisition

(SCADA) system and calibrated using metered data provided by the electric utility. This model was used to evaluate the energy and power demands of the lighting system, in comparison to estimates of other major systems that consume electricity in the tunnel.

Additionally, a daylighting model was created with the DIVA-for-Rhino daylighting plug-in for the Rhinoceros and Grasshopper software using detailed construction plans. This was used to evaluate the function of the semi-transparent photovoltaic sunscreen (STPV-SS) structure as a shading device to gradually reduce the contrast between the outdoor and indoor environments. Its primary goal is to reduce the lighting requirements necessary for the safe adaptation of the human visual system (HVS) of motorists entering the tunnel and reduce the black hole effect and glare from the sun during critical glare hours (CGH). Different STPV options with varying transparencies and visible light transmittances (VLT) were considered to determine the option most suitable for tunnels. Matrix-based STPVs achieve their degree of transparency by alternating between opaque PV material and transparent glass. Intrinsically STPVs are process-induced materials such as thin-film or organic PVs whose transparency is an innate characteristic. Energy saving and energy production potential from the STPV system is greatest with matrix-based STPV options, however, safety conditions suffer greatly from poor visibility, resulting from poor uniformity of the transmitted daylight. The most balanced option was low VLT intrinsically STPV technology, which resulted in better daylight uniformity, and lower artificial lighting demands. Low VLT intrinsically STPV options also have higher PV efficiencies than their high VLT counterparts. It also resulted in the highest reduction in equivalent veiling luminance (disability glare) for drivers during CGH. Reductions in lighting system requirements over the tunnel length, including the threshold, transition and interior lighting zones of the tunnel were considered. Results showed that the application of STPV-SS structures at entrances of the LHLF tunnel could reduce annual energy demands of the lighting system by between 10% to 18%, depending on the VLT of the structure.

Acknowledgements

I would like to thank my supervisors, Professor Andreas Athienitis and Professor Katherine D'Avignon for their unwavering support and the invaluable expertise they have provided throughout my Master's degree. I appreciate all the time you have invested in me and the opportunities that the two of you have encouraged and continue to encourage me to partake in; from applications for internships and scholarships, to participating in conferences and meetings, to working as a teaching assistant, I feel like I have experienced as much as a could as a Master student, thanks to you.

Thanks to all my colleagues and friends from CZEBS: Gilles Jean, thank you for your camaraderie during our work with the Ministry of Transport, which helped form the basis of my thesis work. Mostly though, I enjoyed your friendship and the advice you have given me these past two years. Dahai Qi, Jun Cheng, Maged Ibrahim, Katherine D'Avignon, for your work on the ventilation and heating estimates in this thesis. Costa Kapsis, for bringing me into the fold from your daylighting and illumination course so many semesters ago, and introducing me to the CZEBS lab and CanmetENERGIE (also thanks for the new apartment!). Charalampos Vallianos and Vasken Demarrdios, for being know-it-alls. You are always the first people I go to for help at the office. Olesia Kruglov, for your help with daylighting simulations and design aesthetics. Lynn Dee and Jiwu Rao, the office and labs would fall apart without the two of you. Thank you for always helping us with everything from

administrative tasks (that we as grad students are so horrible at) to setting up experiments and weather stations. All other members of the CZEBS solar lab for being a part of a supportive and fun work environment: Ali Saberi, Stratos Rounis, Bruno Marcotte, Zissis Innonadis, Remi Dumoulin, Navid Morovat, Camille John, Jennifer Date, Matheiu Pellesier, Sam Yip, and Matin Abtahi.

I would like to especially thank my Friends and Family who were supportive and encouraging of my decision to change careers and pursue graduate school: Mom and Dad, Wayne, Louis, Tracy, Phil, Hana. My friends Javed, Jason, David, Kim, Anthony, Li-Anne, Helena, Rose, Kate, and Saman. Graduate school is very stressful but being able to unwind with you all made it that much better.

Table of Contents

List of Figures

List of Tables

Nomenclature

Acronyms

ANSI/IES American Nation Standards Institute/Illuminating Engineering Society

BIPV Building integrated photovoltaics

CGH Critical glare hour

CIE International Commission on Lighting

CV(RMSD) Coefficient of variation of the root mean square difference

DOT Department of Transportation

GHG Green house gas

HVS Human visual system

LHLF Louis-Hippolyte-La Fontaine

MAD Mean absolute difference

MTQ Ministry of Transport of Québec

NMBE Normalised mean bias difference

PV Photovoltaics

RMSD Root mean square difference

SAM System advisor model

SS Sunscreen

SSD Safe stopping distance

STPV Semi-transparent photovoltaics

STPV-SS Semi-transparent photovoltaic sunscreen

Metrics

η	Luminous efficacy	lm/W
ϕ	Luminous flux	lm
E	Illuminance or luminous flux incident on a surface	lm/m^2
E_{min}	Minimum illuminance	lm/m^2
L_{seq}	Equivalent veiling luminance	cd/m^2
L_{th}	Threshold zone luminance	cd/m^2
L_{tr}	Transition zone luminance	cd/m^2
M	Luminous exitance	lm/m^2
N_{eff}	Effective PV efficiency	%
P_e	Estimated power output	kW
P_m	Measured power output	kW
R	Residuals	kW
U_o	Average illuminance	lm/m^2

U_o	Illuminance uniformity coefficient	n/a
VLT	Visible light transmittance	%
L	Luminance	cd/m^2

CHAPTER 1

Introduction

This first chapter explains the motivation behind this thesis, explains what the final objective is and presents a short outline of the next chapters.

1.1 Background

Tunnels are energy intensive infrastructure; studies of underground and underwater road tunnels around the world conducted by [1, 10] and in this study conducted by the Centre for Zero Energy Building Studies (CZEBS) indicate that their annual energy intensity can be as high as 1500 kWh/m. However, a preliminary study showed that the Louis-Hippolyte Lafontaine tunnel - the primary case study for this thesis - has an energy intensity exceeding 2500 kWh/m. Road tunnel systems have many of the same needs as buildings and consequently have similar service systems. These include major systems such as lighting, heating, and ventilation, as well as minor systems such as building services, communications and surveillance, UPS, pumping, and plug loads. Of these systems, the lighting systems usually contribute the most to annual energy consumption, with observed energy shares of up to 50% [1, 10, 11]. In tunnels, a significant portion of the lighting load comes from day-time

lighting requirements in the threshold and transition lighting zones. The intensity of the loads are correlated with the direct and indirect solar irradiance and are concurrent with the energy production of PV systems; this presents an opportunity to integrate semi-transparent photovoltaic (STPV) technology [12] with sunscreen structures (SS) [3,4], compounding their reductions to lighting system energy use [10, 13–19] with an integrated and cost-effective solution. The concepts of semi-transparent photovoltaic technologies and sunscreens will be elaborated on in Chapter 2.

1.2 Motivation

The motivation behind this thesis comes from the need to reduce the energy intensity of the underwater road tunnels. The major energy consuming systems of the Louis-Hippolyte-La Fontaine tunnel were identified and energy efficiency retrofits were explored for the tunnel's upcoming renovation which focused on achieving the following key objectives:

i) To analyse the current energy consumption and power demand profile of the tunnel and identify the most energy intensive systems

ii) Suggest retrofitting options for each of the major service systems that have a high potential for energy efficiency retrofitting

iii) Integrate local renewable energy generation

iv) Improve motorist safety during the winter by integrating an efficient road de-icing system

This thesis introduces the integration of semi-transparent photovoltaic (STPV) technology with sunscreen structures installed at the approaches of road tunnels as retrofitting option that integrates safety measures and energy savings for multiple systems. It proposes the novel application of a semi-transparent photovoltaic sunscreen (STPV-SS) presented in figure1.1. The structure introduces system-wide benefits throughout the tunnel including: improved visibility and driving conditions, reduced lighting system demands, reduced thermal

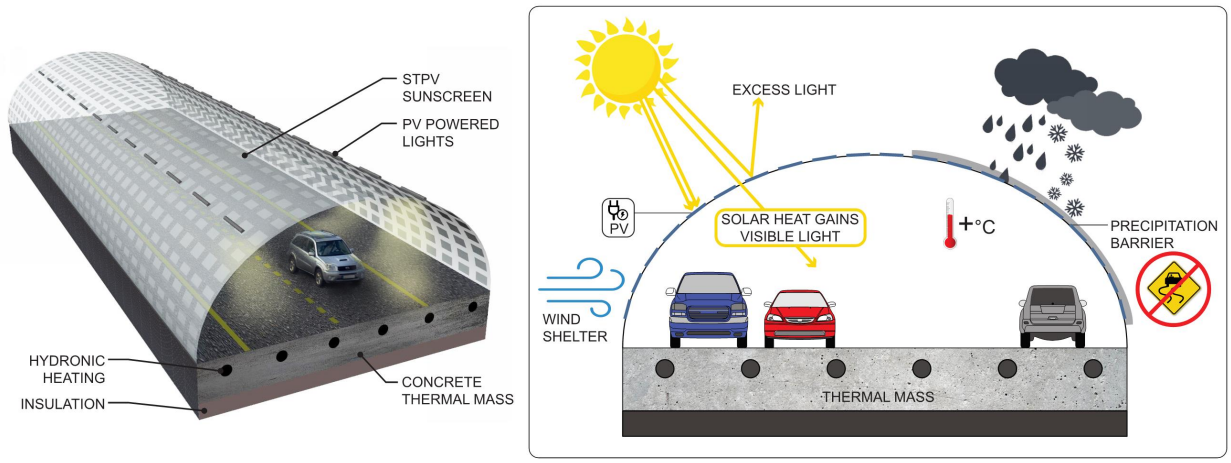

Figure 1.1: Schematic showing the integrative elements resulting from the application of semi-transparent photovoltaic (STPV) materials on tunnel sunscreen structures (SS).

demands for road de-icing systems, integrating renewable energy generation, and offsetting demand charges from local utilities.

The primary function of this type of structure (figure 1.1) is to recreate the threshold lighting zone of a tunnel. The threshold zone's function is to create a gradual transition - suitable for the adaptation of the human visual system - that reduces the sharp contrast in brightness between the exterior and interior environments. By replacing the intense lighting systems required in the threshold zone with transmitted sunlight, STPV-SS can significantly reduce the annual energy consumption of tunnel systems while also generating renewable electricity that can offset day-time lighting demands to the electric grid.

In parallel, the unique application of a partially enclosed STPV-SS can have auxiliary benefits to safety conditions and its related major service systems. Figure 1.1 illustrates many of the additional positive effects the structures can provide:

i) Solar heat gains to increase the temperature of the interior air and thermal mass of the tunnel leading to reduced radiative heat transfer coefficients for the thermal slab of the integrated de-icing system

ii) A wind shelter that reduces wind speeds at the approaches of tunnels [20], leading to reduced convective heat transfer between the thermal slab and cold air

iii) Shelter from precipitation, reducing thermal loads and improving road conditions for motorists

These effects are the subject of studies currently in progress. They provide benefits additional to the primary daylighting function of the STPV-SS but are not fully evaluated in this thesis.

1.3 Objectives

The overall objective of this study is to explore ways to integrate renewable energy, specifically solar photovoltaic technology into Québec infrastructure. Specifically, the objective of this thesis is to understand the inner working details of how tunnel systems operate and identifying potential systems that would benefit from the application of integrated photovoltaic systems. The following objectives are addressed in this work:

i) Analyzing the energy consumption and power demands of the major tunnel service systems

ii) Reducing the energy use of the lighting system

iii) Integrating localized renewable energy generation

iv) Improving the visual safety and performance of motorists as they approach the tunnel portal

1.4 Outline

The contents of this thesis can be summarized as follows:

Chapter 1 provides an introduction to the topic and insight to the motivation behind the work and sets the objectives.

Chapter 2 presents a literature review of tunnel service systems around the world, photovoltaic systems, and different daylighting simulation tools and metrics relevant to the thesis.

Chapter 3 presents the Louis-Hippolyte-La Fontaine Tunnel as a case study used in this work. The chapter gives an overview of the various electrical and mechanical systems of the tunnel, and their operation over a representative year. The annual energy use and energy share of each major system was estimated.

Chapter 4 analyzes the energy consumption and demand profile of the LHLF tunnel in detail. The discrepancy between estimated and measured energy use is investigated. The impact of each system on the local electric grid was examined and their financial cost was calculated. The chapter identifies one of the major systems of the tunnel suitable for energy retrofitting.

Chapter 5 presents semi-transparent photovoltaic sunscreen structures (STPV-SS) as a major net-energy saving retrofitting option for the Louis-Hipppolyte-La Fontaine. Different variations of the structure are explored and results are presented and discussed.

Chapter 6 concludes the work, mentioning some key aspects of the analysis performed in the thesis. It explains the limitations and sets objectives for future work.

CHAPTER 2

Literature Review

This chapter will give an overview of topics relevant to the research in this thesis. An overview of underground road tunnels will identify the minor and major power systems present in tunnels studied around the world; past and proven energy efficiency measures and retrofits will be identified for each major system. The next section will focus on the application of sunscreen structures in tunnels as a lighting system energy retrofit and visual safety improvement. An introduction of types of photovoltaic (PV) technologies, specifically semi-transparent photovoltaics (STPV) that can be integrated into a sunscreen structure (SS) will follow. Finally, different daylighting metrics and calculations and simulation tools that will be used to evaluate the performance of an STPV-SS structure will be introduced.

2.1 Tunnel Systems

Transport infrastructure such as tunnels have service systems that are more energetically complex than the typical road or bridge. In fact, the systems found in a tunnel are more similar to what is typically found in a building [2]. Their purpose is to carry out critical functions to ensure that the underground environment is safe and comfortable to drive in.

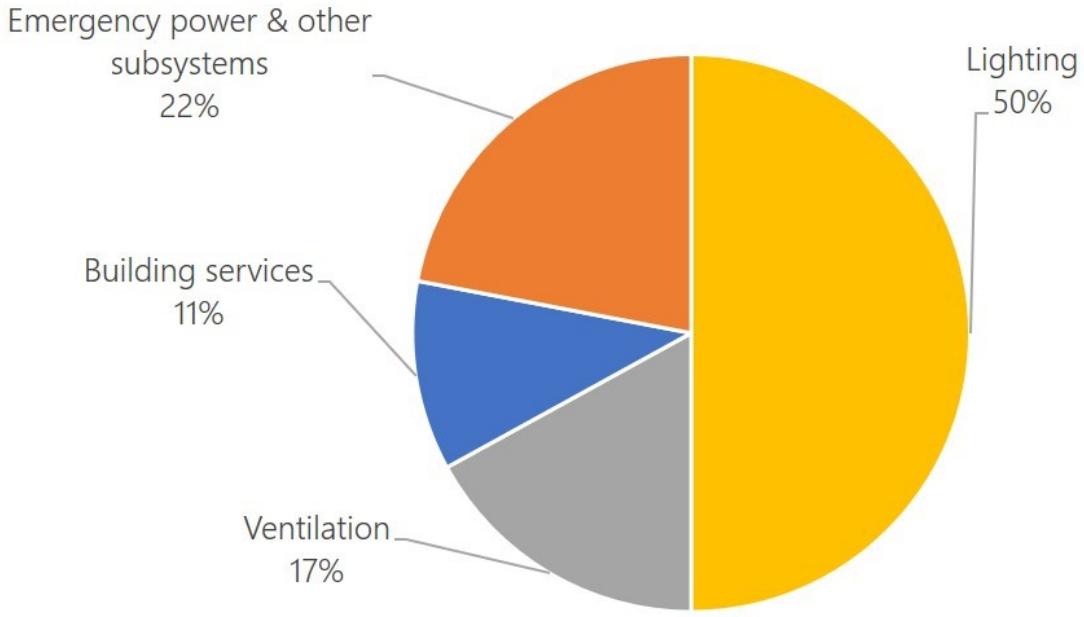

Figure 2.1: Energy share of major tunnel systems adapted from [1].

These services include heating to keep equipment within operating temperatures and prevent the formation of ice on the road, ventilation to exhaust airborne pollutants, and lighting to adequately illuminate the space. There are also many minor auxiliary building service systems that can also incur significant energy costs when their impact is aggregated (Figure 2.1).

2.1.1 Heating

Heating systems in tunnels can be responsible for annual peak loads and creating significant seasonal imbalances between peak loads that occur in the summer and winter; this can incur significant costs in the form of minimum demand charges from local utilities. They are a necessity in tunnels located in cold climates to prevent water from freezing in the drainage channels and piping networks used to supply water to fire protection cabinets and deluge systems. It is also necessary to heat equipment boxes located along the length of tunnels to keep monitoring equipment within operating temperatures in extreme cold conditions. Furthermore, the occupied spaces used by tunnel operators needs to be heated during the winter. The combination of these heating subsystems can account for a significant energy

share of the annual consumption in underground road tunnels.

There are many retrofitting options available for heating systems in tunnels that can help reduce their impact on annual energy consumption and monthly peak loads. These include:

- Insulating domestic water mains to reduce thermal loads
- Installing a dry pipe sprinkler system to reduce heating demands
- Supplying thermal energy using geothermal boreholes and heat pumps
- Supplying thermal energy using river-water source heat pumps

2.1.2 Ventilation

During normal operation, ventilation is used in tunnels to exhaust pollutants created by vehicles during normal operation and in the event of vehicular collisions in the tunnel. The pollutants that are monitored in tunnels and used to control the operation of fans are typically carbon monoxide and carbon dioxide. In the event of an emergency - such as a vehicular collision or fire - ventilation fans change functions to provide emergency fire attenuation by removing heat and smoke to assist emergency response teams and to replace unburned potentially explosive gasses with oxygen [21]. Ventilation is responsible for 17% of the annual energy consumption in tunnels [1]; however, when activated they are usually responsible for the occurrence of system-wide peak loads due to the relatively high nominal power required to adequately exhaust air both under normal and emergency operation conditions.

Large capacity axial ventilation fans are typically used in tunnels but there are two major types of ventilation systems that can provide better efficiency [1, 10]:

- Passive ventilation with vertical shafts
- Longitudinal ventilation jet fans

Additionally, the application of visibility and air quality-based controls for ventilation systems can reduce energy consumption in tunnels that operate their fans excessively due to lack of information.

2.1.3 Lighting

A recent survey conducted by the Realistic Energy Efficient Tunnel Solutions (REETS) project concluded that lighting accounts for over 50% of tunnel operational energy demands [1]. Additionally, a study of four tunnels in the Netherlands [11] affirms the estimate that lighting can be responsible for 50% of annual energy use. This identifies lighting as the highest potential system for energy savings. A study identified peak shaving as a method to reduce operational costs [22] while another suggested several electric storage systems that could smooth load behaviour in tunnel systems [11]. This is because the demands of tunnel lighting systems are much higher during the day than conventional road and building lighting systems because they are used to ensure the safe visual adapation of drivers as the transition from the bright exterior environment to the darker interior environment [2]. Drivers must be able to simultaneously visually adapt to the change in brightness while performing all the necessary tasks of driving. If there is no adaptation to the underground environment, the difference in contrast at the entrance of the tunnel will be so high that it will cause drivers to experience the black hole effect [3]: being unable to see past the tunnel portal because of this glare effect may cause drivers to panic and slow down, leading to increased traffic conditions, or increasing the chances of a vehicular collision. An example of this can be seen in Figure 2.2. Table 2.1 shows that depending on the environment surrounding the tunnel, the difference in luminance can vary greatly. This means that a tunnel's susceptibility to large contrasts in brightness is largely dependent on their unique environmental factors. Additionally, the combination of high vehicular speeds and high contrast in brightness may lead to visual impairment because of the inability of the motorist's HVS to adapt. This can cause visual impairment and lead to accidents in an enclosed area with many high speed objects. To reduce the contrast between the two environments, lighting intensity must be high at the extremities of tunnels. This is why tunnel lighting systems end up being the largest consumer of energy, annually [2].

The International Commission on Illumination's technical report "Guide for the Lighting of Road Tunnels and Underpasses" [3] and the American National Standards Institute's standard practice on tunnel lighting [4] are international standards that describe the best lighting practices for underground tunnels. They both divide tunnels into 5 different lighting

Table 2.1: Examples of typical veiling luminances at tunnel portals provided by [3].

Driving Direction	$\mathbf{L_{sky}}$ (kcd/m^2)	$\mathbf{L_{road}}$ (kcd/m^2)	$\mathbf{L_{environment}}$ **(kcd/m^2)**			
			Rocks	**Buildings**	**Snow**	**Meadow**
N	8	3	3	8	15(V) 15(H)	2
E-W	12	4	2	6	10(V) 15(H)	2
S	16	5	1	4	5(V) 15(H)	2

(V) Mountainous country with mainly steep surfaces facing motorists

(H) Flat, horizontal scene, country

NOTE: In the southern hemisphere, N and S should be interchanged

zones called the the access, threshold, transition, interior and exit zones (Figure 2.3). The required level of lighting in each zone is dependent on its preceding zone to maintain a consistent decrease in lighting requirements that is suitable for the adapatation of the human visual system (HVS). The luminance requirements in the threshold and transition zones are calculated using equations 2.1, 2.2, and 2.3. These zones reduce the contrast in brightness that is experienced by motorists by gradually reducing the intensity of lighting (see Figure 2.4). Their luminance requirements (L_{th} and L_{tr}) are a function of the equivalent veiling luminance (L_{seq}), which both standards [3, 4] state should be measured at the safe stopping distance (SSD) from the tunnel portal using a polar diagram superimposed over the view of a motorist (Figure 2.5). The SSD is the minimum distance that is required to detect obstructions in front of motorists and bring the vehicle to a halt. The speed limit is a major factor in determining the SSD. The interior lighting zone maintains the minimum luminance needed for motorists to navigate in underground tunnel environments. This minimum luminance is typially very small compared to the luminance in the threshold zone since motorists have theorectically adapted to the darker environment with the help of the transition lighting

zone [3, 4].

Table 2.1 shows reference data for typical luminances of different tunnel environments.

$$L_m = \frac{\tau_{ws} L_{atm} + L_{ws} + L_{seq}}{\tau_{ws} \tau_{atm}} \tag{2.1}$$

where:

L_m = Real measured luminance (cd/m^2)

L_{atm} = Luminance atmosphere (cd/m^2)

L_{ws} = Luminance of the windscreen (cd/m^2)

L_{seq} = Total equivalent veiling luminance (cd/m^2)

τ_{ws} = Transmission factor of a typical windscreen

τ_{atm} = Transmission factor of the atmosphere

$$L_{th} = \frac{L_m}{\frac{1}{C_m}\frac{\rho}{q_c \pi} - 1} \tag{2.2}$$

where:

L_{th} = Luminance required in the threshold zone of the tunnel (cd/m^2)

L_m = Real measured luminance

C_m = Minimum required perceived contrast

q_c = Contrast revealing coefficient

ρ = Reflection factor of the target object

$$L_{tr} = L_{th}^{(1.9+t)^{-1.4}} \tag{2.3}$$

where:

L_{tr} = Luminance required in the transition zone of the tunnel

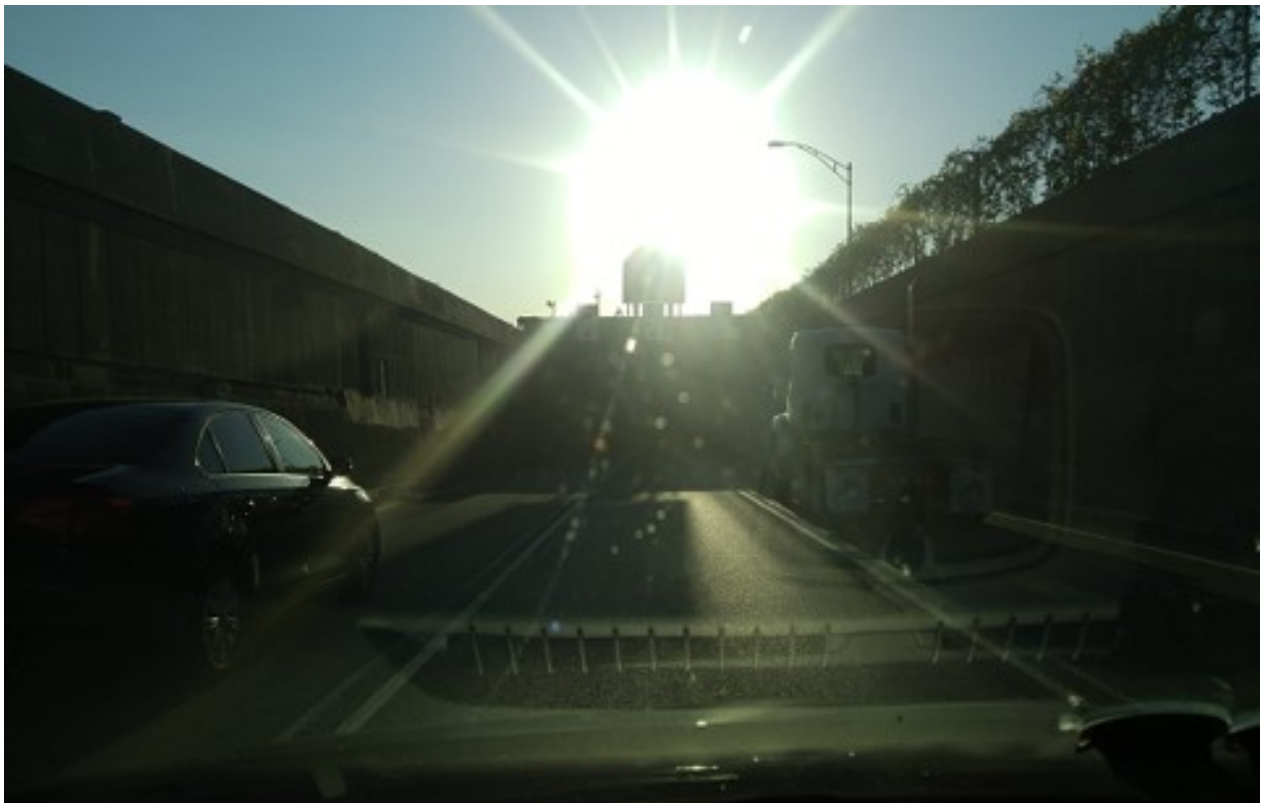

Figure 2.2: A photo taken by D. Sun at approximately the safe stopping distance from the tunnel portal at the Louis-Hippolyte-La Fontaine tunnel [2].

t = Time spent in the tunnel (s)

L_{ws} = Luminance from the windscreen

L_{seq} = Total equivalent veiling luminance

τ_{ws} = Transmission factor of the wind shield

τ_{atm} = Transmission factor of the atmosphere

There are many well-known retrofitting options for lighting systems in tunnels that can significantly reduce their impact on annual energy consumption and peak power demand [1, 10, 23]. These options include:

- Replacing less efficient luminaires with LED
- Using an active/adaptive lighting control system to reduce lighting when unnecessary

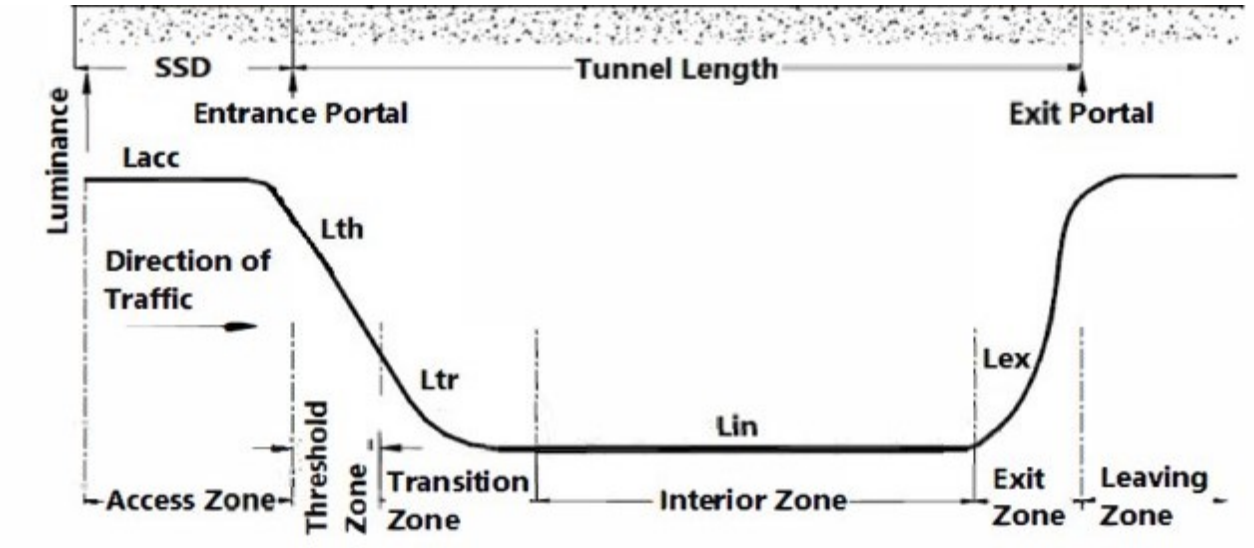

Figure 2.3: Typical longitudinal section of a tunnel, showing the different lighting zones that are active during the day. Figure adapted from [3].

- Using a dimmable lighting control system
- Installing sunscreen structures
- Replacing tunnel and road surface materials with more reflective materials
- Increasing the reflectance of the tunnel portal scene
- Using reflective daylight tubes

However, despite the availability of energy retrofitting options for tunnel lighting systems, current standards do not provide adequate guidance on these options [24]. As a result, lighting systems remain the largest consumers of energy in tunnels.

2.2 Sunscreen Structures

Sunscreen structures are installations at the approach of a tunnel used to reduce the contrast between the outdoor and inside brightness to facilitate the HVS's adaptation to a significantly darker environment. The transition from a dark to brighter environment is also considered with exit lighting zones and sunscreens installed immediately after the exits of

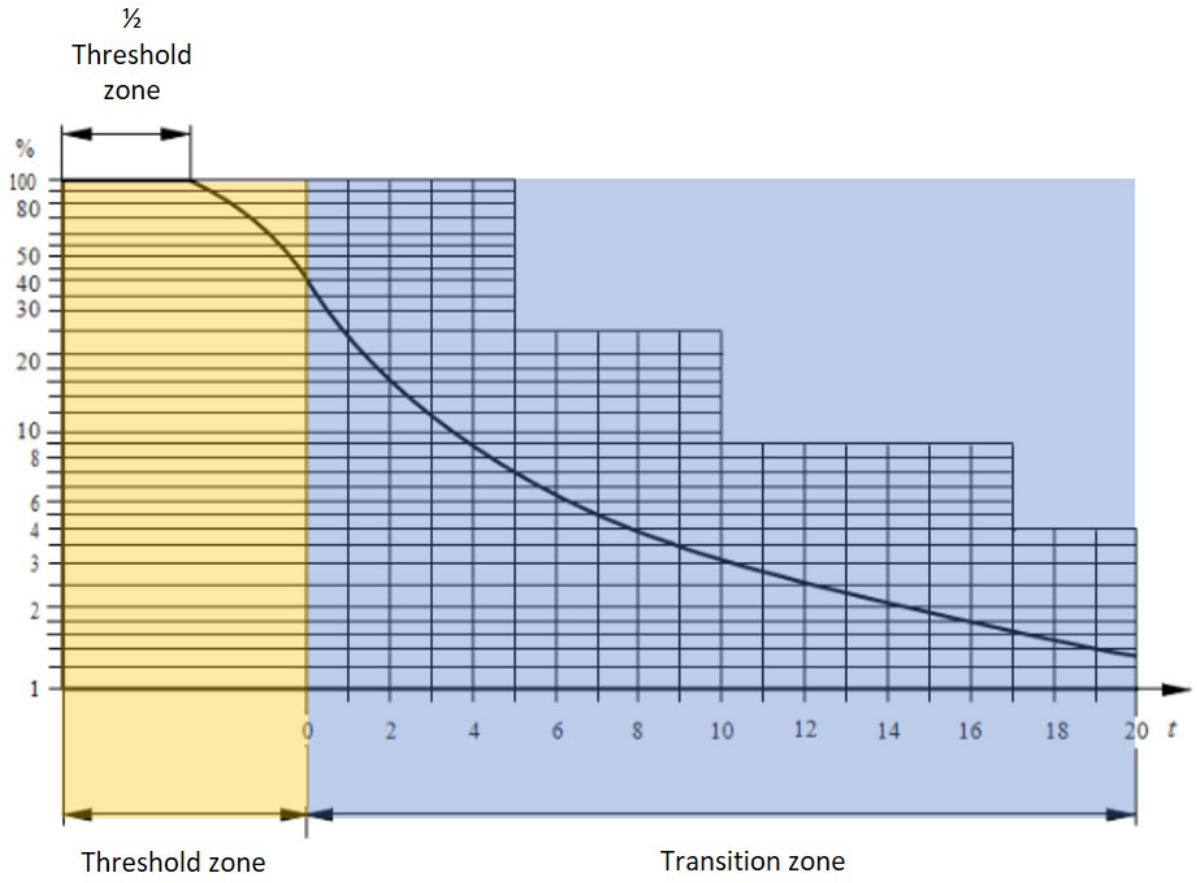

Figure 2.4: Luminance requirements in the threshold (yellow) and transition (blue) zones of underground road tunnels. Lighting requirements are reduced as a function of the amount of time motorists have spent in the tunnel. Figure adapted from [4]

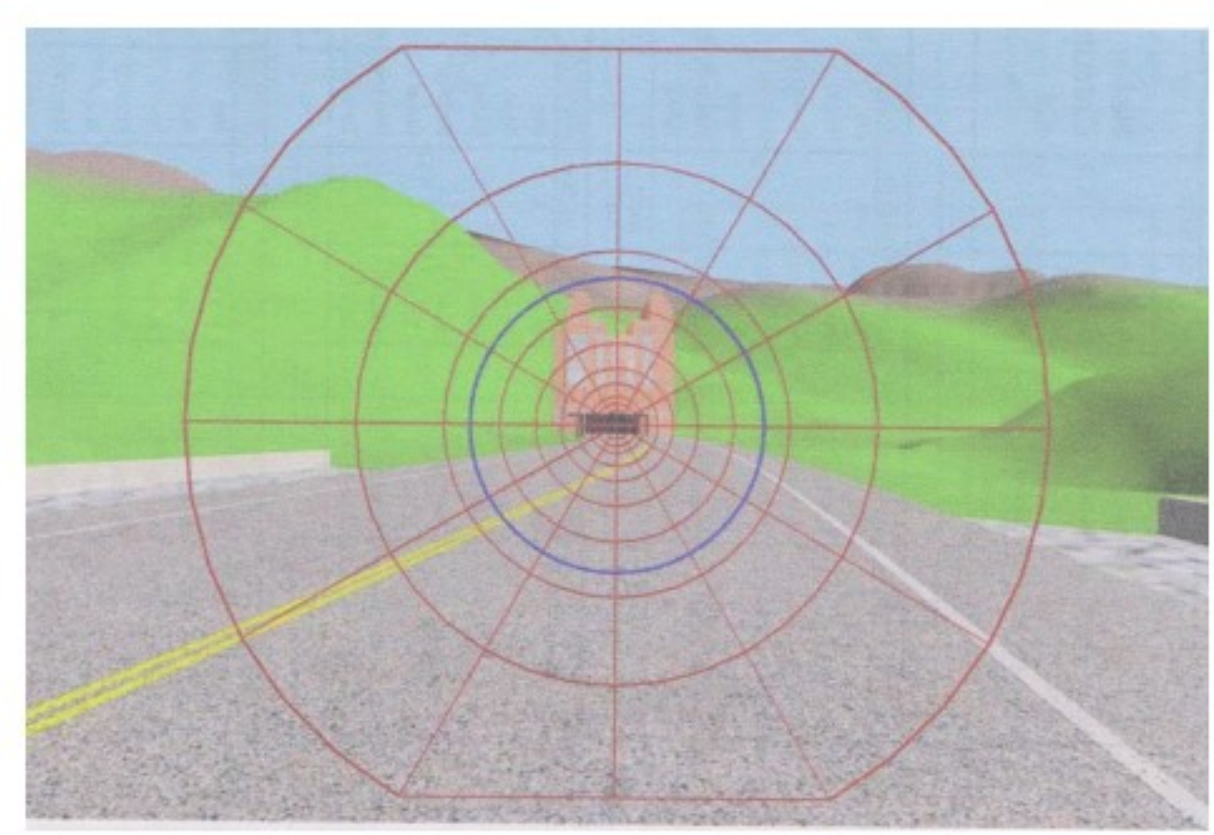

Figure 2.5: An image of the polar diagram used to evaluation of the equivalent veiling luminance as per the method suggested in [3]. Figure taken from [3].

tunnels [3, 4]. These structures can also reduce the energy consumption of lighting systems in tunnels [14–18] by using natural sunlight to reduce artificial lighting demands without additional intelligent control methods [13].

The use of sunscreens structures to reduce day-time lighting energy consumption is widespread around the world. An index called the Technological Readiness Level (TRL) is used to evaluate how close to widespread deployment a technology is in its development phase [25]. TRL is assessed using a 0 to 9 scale representing a range development phases from early stage conception to fully proven and commonly used. In their study to assess the potential of energy efficiency retrofitting measures for underground tunnels, [10] assigned sunscreen structures a TRL of 8, meaning that the technology is has been completed and qualified through tests and demonstrations.

Researchers have studied two methods of reducing energy consumption using sunscreen structures:

1) Displacement of the threshold zone outside the tunnel, allowing for natural sunlight to fulfil existing lighting requirements.

2) Reduction of lighting requirements through reducing the veiling glare experience by drivers approaching the tunnel. Additionally, this improves motorist safety and performance by reducing the black hole effect during CGH.

Displacement of the Threshold Zone

Sunscreen structures can effectively displace the threshold zone outside of the tunnel, allowing the transparency of the structure to provide enough natural daylight to adequately to replace artificial luminaires. When properly optimized, the structure can ensure that the luminance requirements of the threshold zone are met by transmitting natural sunlight [13–18]. When not enough daylight is transmitted through the structure, artificial lights can still be activated to increase illuminance on the road, however the duration at which they are active is greatly reduced. Since lighting loads can double during the day when the sun is shining, this can be an effective way of reducing energy use.

Reducing Lighting Requirements

Sunscreen structures provide shading from the sun, reducing the equivalent veiling luminance -amount of light reflected into eyes of drivers- as they approach the tunnel. This reduces the luminance requirements of the threshold and transition zones [13], [26], [19]. For tunnels oriented parallel to the East-West axis, the sunscreen can reduce the amount of sunlight that is directly in the line of sight of drivers during the early mornings and evenings.

Case Studies

The University of Granada has studied the use of pergola-like structures as sunscreens to save tunne energy. They have recognized the difficulty in acheiving adequate illuminance uniformity on the road with these types of structures [17]. To mitigate the negative effects of this method, they have tested the use of light diffusive materials in their pergolas sunscreens. Results showed that uniformity could be improved by using light diffusive materials as a transmission medium, but at the cost of significantly reducing the average illuminance on the road [18].

Another way to improve the homogeneity of light on the road surface is to use a semi-transparent tension structure made of polyester with PVC coating [15]. Results of this study showed that the sunscreen structure was able to achieve 76 to 100% energy savings in the threshold zone of the tunnel. When compared to the pergola-like sunscreen structures, the semi-transparent tension sunscreens resulted in better uniformity of light and greater energy savings [17].

The integration of semi-transparent photovoltaics as the light transmitting component of sunscreen structures is an application that has not been explored. Photovoltaic technology presents an opportunity to add energy production functionality to sunscreen structures that can reduce annual net-energy consumption and grid-power demand during the day. The next section will give an overview of different types of photovoltaics and semi-transparent photovoltaics that can provide different types of visible light transmission.

2.3 Photovoltaics

This section will give a brief overview of the context of photovoltaic solar energy in Canada and Québec and the different types of PV and STPV technologies available on the market that can potentially be integrated into sunscreen structures.

2.3.1 Context in Canada and Quebec

There has been an exponential decrease in average crystalline silicon PV technology price per watt between 1975 and 2013, resulting in an increase in global PV deployment. [27] shows that PV technology prices (relative to the value in 2015) have decreased from approximately 100 USD/W in 1975, to less than 1 USD/W in 2013. This decrease in module cost is attributed to variables such as efficiency and material costs that were stimulated by high-level mechanisms such as "research and development, learning-by-doing, and economies of scale" [27].

In Canada, the province of Quebec supplies nearly all of its energy needs through renewable sources, mainly hydroelectric power; however, Quebec still has an enormous and untapped energy potential: solar energy. In the Canadian Solar Industries Association's latest submission to the Commission sur les Enjeux Énergétiques du Québec, it is stated that solar energy can contribute to the reduction of greenhouse gas emissions and provide more economic development than any other form of energy source [28]. Solar energy is also expected to play a prominent role in the following provincial key policy objectives: "reduce greenhouse gas emissions, facilitate the electrification of transportation by contributing to energy surpluses, sustain regional development, foster development and innovation of renewable energies, and ensure the long-term security and diversity of Quebec's energy" [28].

Furthermore, in the 2015 annual report on PV technology status and prospects in Canada, published by CanmetENERGY [29], it is stated that the cost of solar energy is quickly dropping and is approaching grid parity in Quebec. Over a 10-year period (2004 – 2014), PV module prices have dropped drastically from 6.18 CAD/Watt to 0.85 CAD/Watt. As a result of this price drop, the industry has grown, creating 5400 new jobs in Canada from 2009 to 2014 . Despite the high potential in introducing solar energy to Québec, the province's

total installed grid-connected PV capacity in 2014 was only 0.401 MW out of Canada's total of 1843.08 MW. By the end of 2015, Canada's cumulative installed PV capacity grew to over 2500 MW, with the bulk of the increased installation occurring in Ontario [29].

2.3.2 Types of Photovoltaic Technologies

There are three main types of photovoltaic cells that are currently used to generate electricity. Crystalline Silicon based PV cells convert solar radiation into electricity using a planar crystalline lattice. These are the most common types of PV cells used in industry today, accounting for approximately 90% of modules sold. Crystalline Silicon based solar cells have an average efficiency[1] of 18.2% and are the most cost-effective option on the market [30].

Cadmium telluride (CdTe) and copper indium gallium diselenide (CIGS) are the two main types of thin-film PVs on the market. Of the two, CdTe is the second most used type of PV. They also have a lower material and manufacturing cost than crystalline silicon based PVs [12]. However, CdTe cells also have a significantly lower cell efficiency of 12.8% —incurring additional costs in materials, land, and labour required to achieve the same nominal power— making an installation of equivalent capacity more expensive using thin-film PVs than using their silicon based counterparts [30]. Advantages of CdTe thin film PVs are that they have a lower maximum power point efficiency temperature coefficient (making their power efficiency less sensitive to cell temperature) and they have higher power outputs under overcast conditions when compared to crystalline silicon cells [31]. One disadvantage is the toxicity of the elements used on thin film technologies (Cd, H2Se). This is not a problem during the operational lifespan of the module but rather at the end of its operational life when it needs to be handled and recycled.

Concentrated PV (CPV) use reflectors and/or lenses to concentrate solar radiation onto small but high efficiency multi-junction solar cells. They are one of the most efficient PV technologies (35-44%) since their PV cells become more efficient at energy conversion at higher irradiance levels [12]. However, CPV systems are limited in that they require a large, uninterrupted landmass to function and require expensive lenses and solar tracking systems

[1] Cell efficiency is defined as the ratio of energy output from the solar cell to the input energy from the sun.

since they only operate under direct solar radiation. CPV systems include complex mechanical and electrical subsystems which also need constant care, thus increasing maintenance costs when compared to typical stationary PV systems. That is why, "increased governmental support is required to build the manufacturing infrastructure required to scale CPV up to a cost-effective alternative to silicon solar cells" [30].

2.3.3 Semi-Transparent Photovoltaics

Photovoltaics are no longer uniquely installed in empty fields and on top of buildings but are being used to replace standard construction materials and elements. Such Building Integrated Photovoltaics (BIPV) have been used to replace roofs, walls, and windows. Semi-Transparent Photovoltaics (STPV) devices are a sub-category of BIPV devices that can replace building components that have light transmission (and shading) functions, such as overhangs and glazing units, to transmit sunlight for daylighting and electricity generation [32]. There is also on-going research that integrates heat collection functions into STPV glazing units using airflow as a coolant fluid [33], [34]. One crucial characteristic about integrating any type of material into sunscreen structures is its transmissivity – an optical property that represents the amount of visible light that passes through a type of material under standard conditions. Modern day STPV devices are categorized into 3 types based on how their transparency is achieved and the type of PV technology used [5], [35].

Matrix-Based Semi-Transparency

Matrix based semi-transparency (Figure 2.6) achieves the intended degree of transparency by alternating opaque crystalline-silicon PV cells with fully transparent gaps on a glazing unit, creating an opaque-transparent pattern [35]. These types of STPV devices are typically designed to resemble shading devices in windows such as fritted glass and shutter blinds.

Process-Induced Semi-Transparency

Process induced semi-transparency (Figure 2.6) applies the same principle as matrix-based semi-transparent PV devices, achieving its intended degree of transparency with a

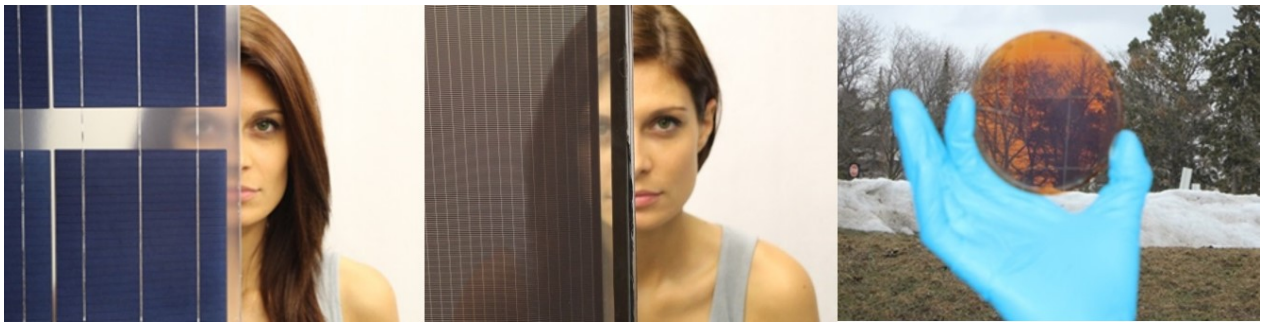

Figure 2.6: Summary of different types of STPV technologies. Left: Matrix-based semi-transparency, centre: Process-induced semi-transparency, right: Intrinsic semi-transparency. Taken with permission from [5]

sequence of opaque PVs and fully transparent spaces. The main difference is that the laser-etching technique can cut micro voids out of the PV material allowing for a finer degree of transparency that gives the illusion of the PV cells themselves being 'see-through' or 'tinted' rather than opaque. This technique has been applied to both crystalline-silicon and amorphous silicon PVs [5], [35].

Intrinsic Semi-Transparency

While Intrinsic semi-transparent PVs are still process induced, their transparency is an innate characteristic (Figure 2.6), rather than a physical modification of cells. They are thin-film, organic and perovskite PV technologies that are highly customizable in terms of transparency and shape [5], [35]. Some of the more recent PVs in this category allow for complete transparency and uniform transmission of sunlight, however, they are not as durable or efficient as silicon-based cells [36].

2.3.4 Applications of PV in transport

There is interest in developing decentralized renewable energy as means to supply electricity to remote areas. Decentralized production of energy, also known as distributed generation, serves the purpose of supplying electricity to load-centers in close proximity to the power station. This has the added benefit of reducing the cost of renewable energy generation by severing stations' reliance on energy infrastructure such as long-distance transmission

lines and by minimizing transmission and distribution losses. This also has the dual effect of reducing costs for conventional energy suppliers since demand in remote areas can be met by decentralized producers [37]. Highway and road infrastructure right of ways present an opportunity to use otherwise un-used land masses as means to produce decentralized energy using PV.

A recent study [38] conducted by Jochems at the Eindhoven University of Technology investigated whether PV farms could add value to road infrastructure in the Netherlands. The study focuses on several case studies for Photovoltaic Noise Barriers (PVNBs) that have been installed around the world, citing the multi-purpose use of land for noise control and energy production as one of the main advantages [38]. This is of particular interest to countries and organizations that want to take advantage of un-used right-of-ways along highways and intersections.

An example of this is shown in [38], which cites 3 case studies that examined losses incurred by soiling and particulate matter on PV systems integrated to road infrastructure. These 3 case studies reported losses between 4-8%, however, did not go into detail as to the exact reason why. This begs the question of whether conditions along a route with high traffic flows can impact the efficiency and durability of panels and if so, at what magnitude.

Oregon's Department of Transportation's (ODOT) proof of concept solar highway demonstration project is an example of successful implementation of PV technology along road infrastructure. The installation is a 104 kW grid-connected PV system that feeds the public utility grid during the day and draws electricity during the night to illuminate the adjacent highways. Oregon's DOT has planned an expansion project to double the demonstration project's PV capacity and install additional 1.75 MW and 3.0 MW roadside PV systems in the state. The ODOT has also published a Solar Highway annual report, authored by Good Company sustainability consultant, as a means to provide a process for other DOTs to follow when adopting PV projects in highway right-of-ways. [39].

Public-private partnerships with financial institutes are a way that departments of transportation (DOT) have begun utilizing empty right of ways to generate renewable energy [37]. These partnerships allow DOTs to benefit through by obtaining net metering and renewable energy credits without having to worry about building, operating, and maintaining the power

plants. It allows DOTs to achieve their intended goals of [37]:

1) Reducing greenhouse gas (GHG) emissions;

2) Creating savings by generating electricity at a lower rate than their utility;

3) Generating revenue using un-used state land;

4) Supporting a green and clean economy.

Two examples of department of transportations successfully applying these types of partnerships are the Massachusetts DOT (MassDOT) and Oregon DOT (ODOT) [37]:

MassDOT entered into an agreement to lease their property to a contractor who developed, built, operated and maintained the installed solar power plants. Under this contract, MassDOT agreed to purchase power directly from the developer at a favorable fixed rate for the duration of the lease [37]. This partnership allows all parties to benefit by allowing the developer to retain all incentives associated with generating renewable energy and gaining renewable energy credits, while MassDOT obtains all net metering credits. The state benefits financially by having zero upfront capital costs, utilizing federal tax incentives, obtaining favorable electricity rates, and adding revenue through their lease agreement.

ODOT entered into a similar agreement which directly involved the state's public utility company, Portland General Electric (PGE). PGE's role was to operate and maintain the solar power plant which was paid for and owned by the Bank of America. PGE benefits by feeding the energy produced to their grid to serve their customers, the state, and ODOT [37].

2.4 Daylighting

2.4.1 Lighting Metrics

There are six fundamental metrics used to measure and quantify light [40–42]: Luminous flux, ϕ (lm), is a measure of the amount of light that is emitted by a light source in all directions. It is typically used to indicate the brightness of a lamp in lumens. Luminous efficacy, η (lm/W), is a metric used to measure how well a light source converts power to lumens. Luminous exitance, M (lm/m^2), is the luminous flux that is transmitted through or

reflect off of a surface, per unit area. Illuminance, E (lm/m^2), is the amount of luminous flux incident on a surface, per unit area. The illuminance can come from many different sources, including surfaces that transmit and/or reflect luminous flux. Luminance, L ($lm/sr*m^2$), is the luminous intensity of light emitted from a source (per unit area of the source) at a particular direction per unit steradian. These six metrics describe all the fundamental interactions of light.

2.4.2 Glare

Glare is a general term that is used to describe visual impairment due to a large contrast in brightness but the term encompasses many different situations. There are two major types of glare:

i) Disability glare

Disability glare is measured using a metric called equivalent veiling luminance, L_{seq} (cd/m_2) and the terms are often used interchangeably. It is a representation of the amount of disruptive light that a person experiences from ocular light scatter or stray-light in their eyes and is a physiological response to a large amount of disruptive luminance which impairs the persons ability to see the contrast in brightness between an object of interest and the background scene [43–46]. This phenomena is mathematically defined as 2.4.

$$C = \frac{(L_b + L_o)}{(L_b + L_{seq})} \tag{2.4}$$

where:

C = Contrast factor

L_b = Luminance of the background scene (cd/m_2)

L_o = Luminance of the object of interest (cd/m_2)

L_{seq} = Equivalent veiling luminance (cd/m_2))

There are several computations for L_{seq} such as Holladay, Stiles/Crawford, Fry, Adrian, Hartman, Meskov, and Vos; these methods are slightly different but all follow the same format as equation 2.5 [41, 47–52].

$$L_{seq} = \frac{(kE_g)}{(\theta)} \tag{2.5}$$

where:

L_{seq} = Total equivalent veiling luminance (cd/m_2)

E_g = Illuminance at the observer produced by a glare source (lux)

θ = Angle of the glare source relative to the observer

k = Straylight parameter

While disability glare is a indicator for visual performance, it does not always indicate discomfort in an occupant.

ii) Discomfort glare

Discomfort glare or 'photo-aversion' describes a psychological response to a light source but doesn't necessarily affecting visual performance of the human visual system (HVS) [44]. The factors that typically effect discomfort glare metrics are the luminance, size, number, and position of glare sources, as well as the adaptation level of the observer. There exist many different models and scales to evaluate discomfort glare [53], however most have been developed using studies done in office buildings, where glare sources typically come from sunlight transmission through windows, artificial luminaires, and electronics [44]. Daylight glare probability is one of the most appropiate metrics for determining when an occupant will be uncomfortable [54]. However, discomfort glare and the indices developed to evaluate it do not apply to the glare experienced by drivers in this application because of the different tasks and level of concentration required when driving compared to working in an office environment. This is because there is a greater emphasis on the motorist's ability to detect moving objects as opposed to a building occupants comfort and productivity.

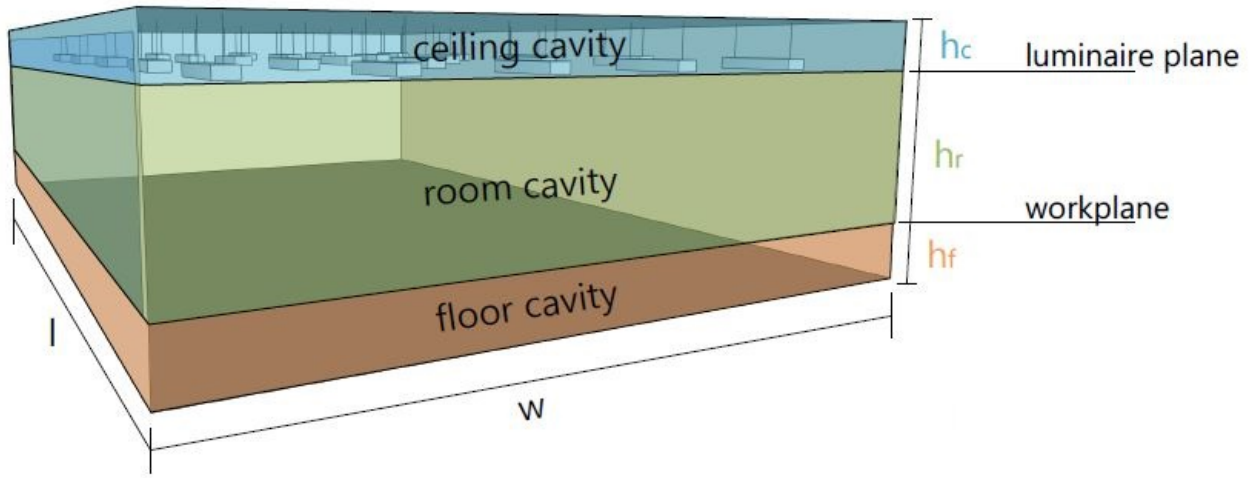

Figure 2.7: Illustration showing the three zones used in the zonal cavity method, taken from [6].

2.4.3 Radiosity method, zonal cavity method

The Radiosity method is a numerical model used to estimate the indirect lighting component reflected and incident on lambertian (diffuse or 'matte') surfaces in an enclosed room. This method assumes an infinite amount of diffuse reflections occuring from a primary source (ie the sun through a window) and secondary reflected source (reflection off a wall). A major limitation of the radiosity method is that direct specular reflections are not considered.

The zonal cavity method is a simplified concept based on the radiosity method used to calculate the light level in an enclosed room using inputs from light sources such as artificial luminaires and light transmission through windows. The method simplifies the geometry of the a room with many surfaces by subdividing them into three distinct surfaces (see Figure 2.7). These surfaces are the ceiling cavity, representing the space above the room's luminaires, the room cavity, representing the space below the luminaires and above the work-plane, and the floor cavity, representing the space below the work-plane. The zonal cavity method uses the same assumptions as the radiosity method and therefore suffers from the same inaccuracies.

2.4.4 Raytracing using Radiance

Radiance is a combination of tools that uses a combination of Monte-Carlo and deterministic ray-tracing to perform lighting calculations and simulate artificial lighting and daylighting levels. The daylighting engine is capable of estimating the direct, specular indirect, and diffuse indirect components of light incident on any surface [55].

Scene inputs are entered into Radiance using text descriptions of different object geometries, material properties, light sources, weather files, time, date, and location of the desired simulation. The scene inputs are received by a program called oconv which converts text based scene definitions into a binary model format called octree. This binary format is used to trace rays through the scene efficiently.

The outputs from the ray tracing lighting calculations include irradiance, spectral radiance, and glare indices which are displayed in the form of numerical data, data visualizations, and/or renderings [7, 55].

One of the primary advantages of Radiance over simplified lighting calculations is that complex geometries can be analyzed without having to be simplified to basic shapes and assumptions about material properties (lambertian surface assumptions). The Radiance lighting simulation engine is able to output three components of light (direct, specular indirect, and diffuse indirect). Whereas the radiosity method is limited to computing indirect component of light reflected from assumed lambertian surfaces in the scene. However, the limitation in directly using Radiance to study complex geometries is that scene inputs must be assigned using text. There are many tools such as DIVA that allow users to input CAD models of complex geometries directly into Radiance, making the tool much more accessible to building specialists.

Interfacing with Rhinoceros

The Radiance engine can be used as a standalone tool, and different geometries can by created using the text inputs described in [7]. However, it can also be interfaced with conceptual design environments of Rhinoceros [56] and Grasshopper [57] using an optimized plug-in called DIVA-for-Rhino [58]. This plug-in creates a user interface that allows for the complex geometries that can be created with Rhinoceros and Grasshopper to be used as

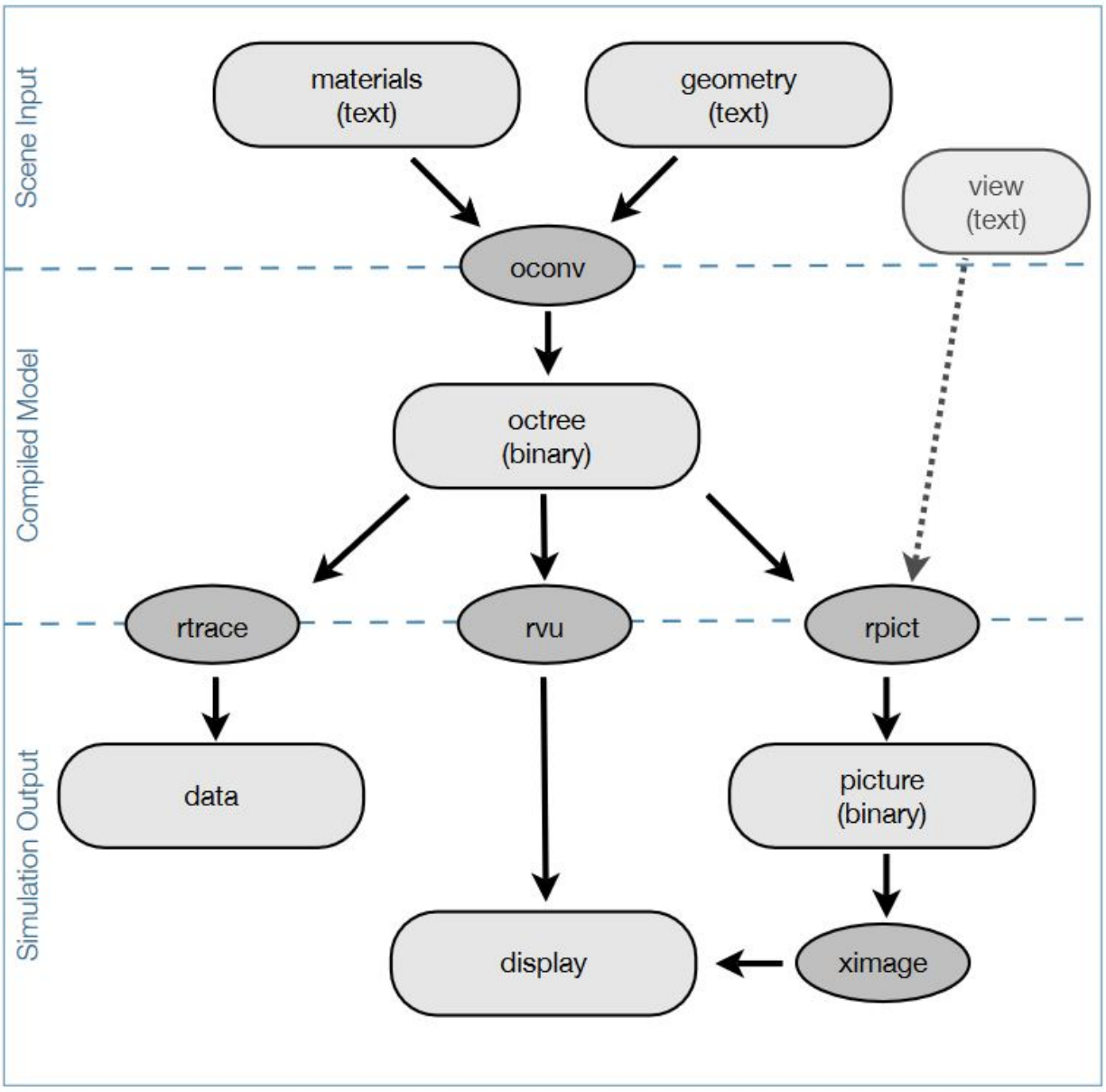

Figure 2.8: Radiance workflow [7]. rpict - program used to generate renderings from octree; rtrace - calculates radiance and irradiance; rvu - interactive rendering program; ximage - displays radiance format images

scene inputs in the Radiance workflow (Figure 2.8) to generate simulation outputs.

CHAPTER 3

The Louis-Hippolyte-La Fontaine Tunnel: A case study

This chapter introduces the Louis-Hippolyte-La Fontaine tunnel as a case study of an underwater road tunnel in a cold climate. Heating, lighting and ventilation systems are identified as the major tunnel systems contributing to energy use throughout the year. The annual power demand profile and energy consumption of these main systems were be estimated using numerical methods to determine the energy share of each system and compare them, when available, to literature. The energy share of heating systems for a tunnel in a cold climate (which is scarce in literature) will be presented.

3.1 Introduction/Purpose

The island of Montreal would be an isolated land mass without vital transportation infrastructure such as tunnels and bridges. This scant amount of connections are the only option for vehicles to pass to and from one of Canada's largest metropolitan cities, making them high-priority structures in the event of an emergency situation or natural disaster. The Louis-Hippolyte-La Fontaine Tunnel (see Figure 3.1), an 1.4km underwater road tunnel constructed in 1967, is one of these main traffic arteries that traverses the St Lawrence

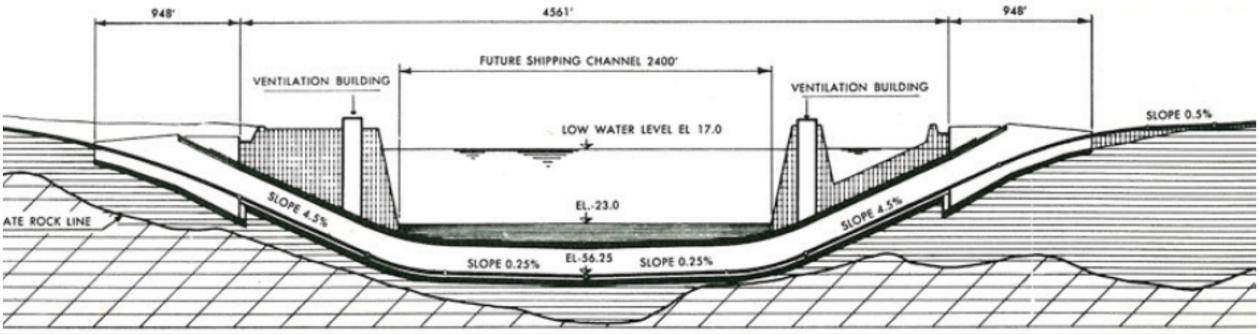

Figure 3.1: Longitudinal cut of the Louis-Hippolyte-La Fontaine tunnel [8].

River. With a dual circulation tube construction, with three traffic lanes in each direction, the tunnel has an annual average daily traffic (AADT) flow of 120,000 vehicles travelling at a speed limit of 70km/h, providing safe passage for approximately 4.4 million vehicles annually. The tunnel uses two ventilation tower buildings to house 16 powerful extraction and supply ventilation fans. The towers are multi-level service buildings used by the tunnel operators and to house necessary monitoring and emergency equipment such as generators and a UPS [8].

The climate in Montréal is classified as humid continental or hemiboreal (köppen climate classification Dfb). The city is subject to diverse weather conditions; average temperatures can drop to as low as -9.8°C in the Winter and as high as 21.1°C in the Summer. Climatic data from over the past 25 years show that the geographic area receives an average of 1048mm of precipitation annually [59]. This implies that drainage, heating, and cooling are important components of building systems in the area.

The Louis-Hippolyte-La Fontaine tunnel has the task of creating an underground environment that is safe and comfortable for drivers under any condition. It is equipped with systems to carry out operational and emergency situation functions such as ventilating out polluted air, illuminating the road, providing fire protection services, drainage, and heating. For tunnels to reliably provide services for such a massive amount of vehicles per day, their system energy use is substantial. A survey was sent to underground tunnel operators globally to gain information on the annual energy consumption of their tunnel. Figure 3.2

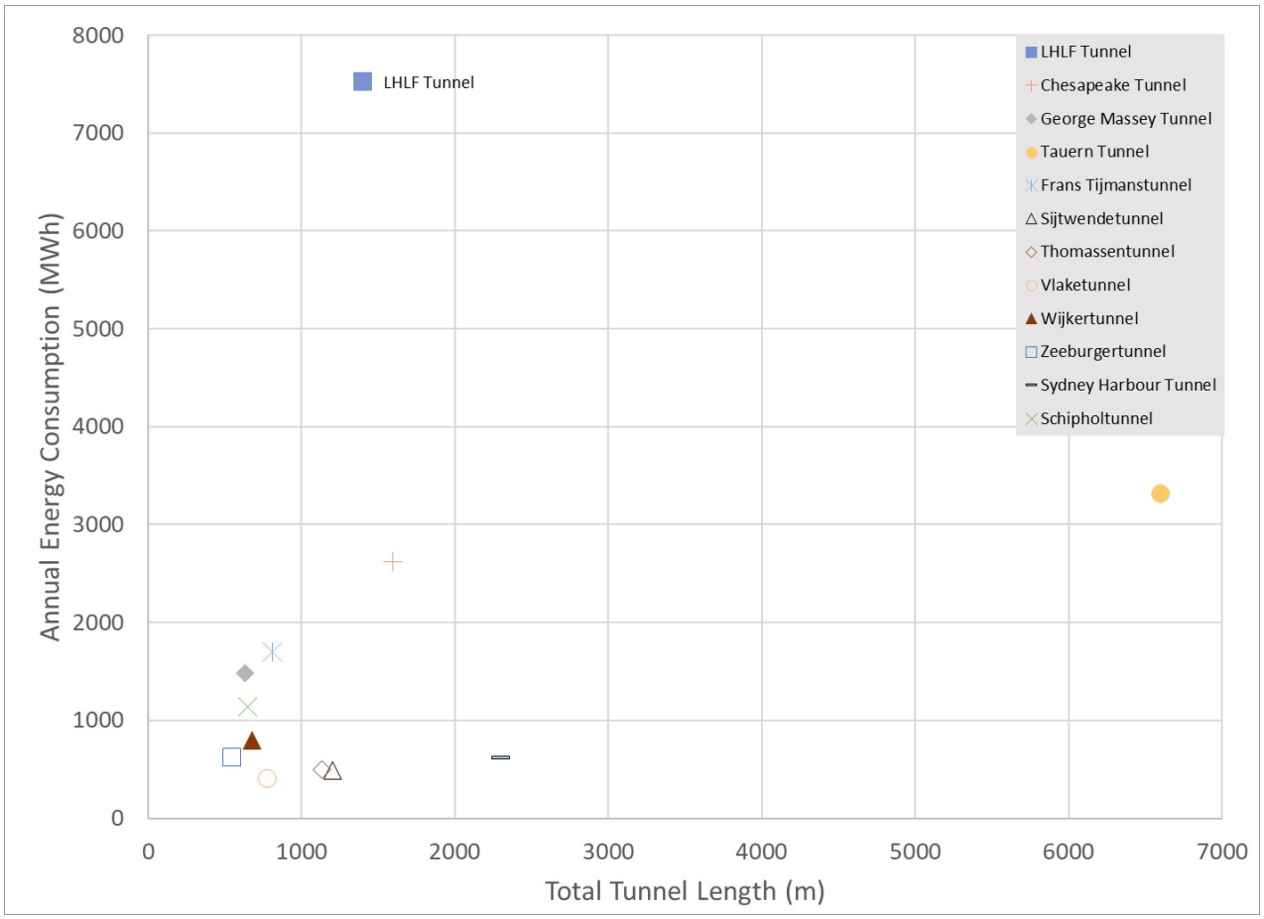

Figure 3.2: Survey results showing the energy consumption and effective tunnel length of underground road tunnels around the world.

shows that the average annual energy consumption of the LHLF tunnel over the past five years (2011-2016) is abnormally high when compared to reference tunnels that were surveyed around the world. Its energy intensity (MWh/m) makes the LHLF tunnel an outlier in this small sample.

Furthermore, the LHLF tunnel is equipped with four diesel generators, enabling it to maintain operation in case of grid power outages. An example of when such a back up system can be useful was during the 1998 North American ice storm, the underwater tunnel was an important transportation artery, connecting Montréal to the south shore, that remained functional.

This chapter will provide a breakdown of the LHLF tunnel total energy use profile to the subsystem level to better understand the energy use of the main subsystems of the LHLF

tunnel, specifically the lighting system. This information will be used to provide counsel on what energy efficiency provisions are most suitable for future renovations.

The energy use of the tunnel system components will be broken down into its three major subsystems according to literature: heating, ventilation and lighting. Two years worth of historical data collected from a centralized supervisory control and data acquisition (SCADA) system and technical drawings and specifications will be used to model the components of each subsystem. The share of each subsystems energy use will then be compared to literature and the model results will be compared to observed consumption using recorded metering data from Hydro-Québec[1].

3.2 Description of Tunnel Service Systems

Road tunnels have many of the same operational systems as buildings such as ventilation, heating, lighting, and various building services. Tunnel system energy use is on a similar scale in terms of operational consumption: between 2011 and 2016, the LHLF tunnel had a mean annual energy intensity of 244kWh/m^2. This is comparable to the average energy intensity of commercial and institutional buildings in Canada, which is 1.14GJ/m^2 (316.7kWh/m^2) [61].

In the context of tunnels around the world, the LHLF tunnel had a mean linear energy intensity of 2710kWh/m, whereas information from tunnel operators participating in a survey revealed the mean energy intensity of underwater immersed tunnels to be 1001 kWh/m, annually [4]. From the tunnels surveyed by the research team, only four out of eleven tunnels had an energy intensity greater than 1000 kWh/m and none exceeded 2000 kWh/m.

Similar to buildings, road infrastructure energy retrofits such as the LHLF tunnel would benefit from a better understanding and predictability of their system loads. This section will describe the three subsystems that are most likely responsible responsible for majority of tunnel annual energy consumption: heating, ventilation, and lighting.

[1]Hydro-Québec is the public utility that manages the generation, transmission, and distribution of electricity for the Province of Québec [60]

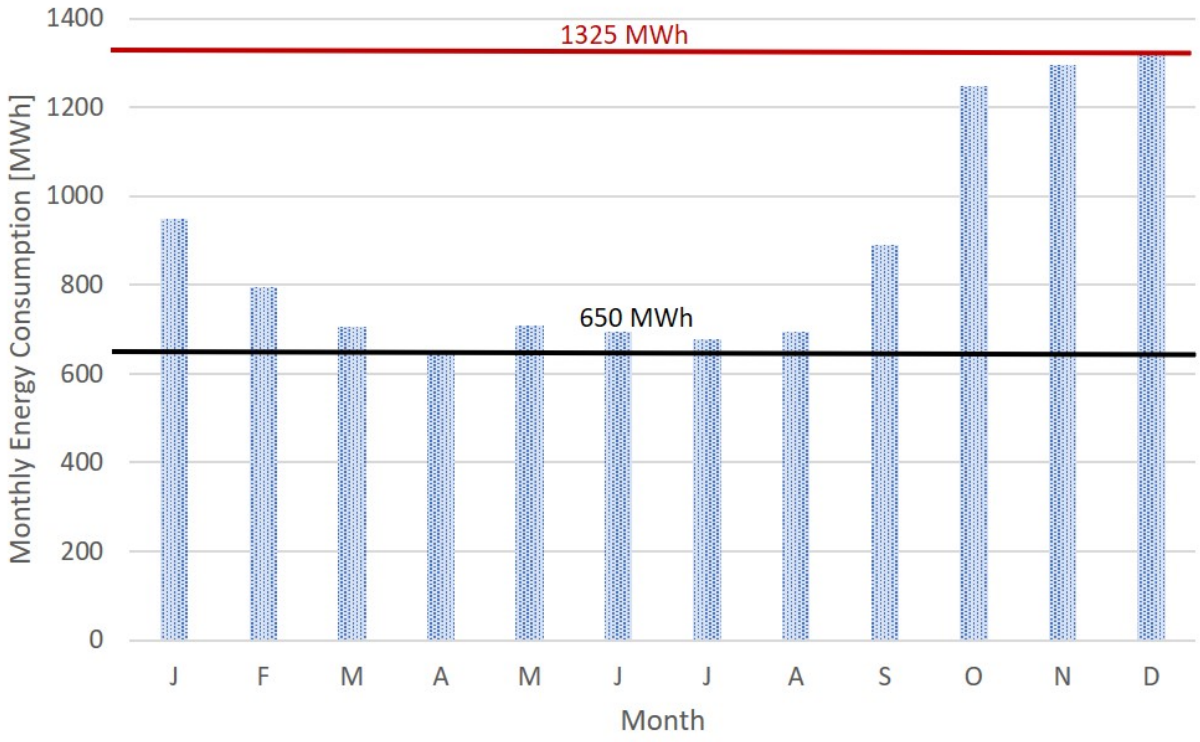

Figure 3.3: Monthly energy consumption over 2015-2016

3.2.1 Heating

One of the main systems responsible for the tunnel consuming significantly more energy than expected is heating. Normally, heating is not relevant due to the location and climate of most of the tunnels studied in [4] and Concordia's survey of international tunnels. However, during the cold Montréal winter, monthly energy consumption in the tunnel almost doubles when compared to the summer (Figure 3.3). This suggests that significant temperature dependent heating loads exist in the LHLF tunnel.

The heating system of the LHLF tunnel consists of resistive heating elements that are used to prevent water from freezing in its drainage and piping systems, to melt ice and snow, and to warm occupied spaces during the winter. The following list is a summary of the heating elements in the LHLF tunnel that were analyzed:

i) 48 fire protection cabinets located in the tunnel circulation tubes

ii) 4 fire protection cabinets located in the ventilation towers

iii) 88 drainage sumps, each equipped with 350W heating elements to prevent ice formation

iv) Heat traced piping throughout the length of the tunnel, including domestic water mains, fire protection supply mains, and supply pipes to fire protection cabinets,

v) Heated drainage channels and drainage trenches to prevent ice from forming and causing blockages

vi) De-icing systems in the entryways to the garages of the ventilation towers to melt ice and snow

vii) Space heating elements in occupied spaces inside the ventilation towers and pumping stations.

These heating elements can be broken down into eight subsystems, summarized in Table 3.1. The total capacities of these heating subsystems were estimated by reading their listed specifications in the operator's manual [8]. On site verification of a few elements that were accessible were done during site visits.

Table 3.1: Heating element specifications

Heating Subsystem	**Element**	**Specified Capacity (kW)**
Fire Protection System	Fire cabinet heating	30
	Supply main heat tracing	144
	Piping heat tracing	14.4
Domestic Water	Supply main heat tracing	252
Drainage	Drainage trench heat tracing	138
	Drainage channel heat tracing	200
Deicing	Garage entrance pavement heating	69.6
Occupied Spaces	-	160.5
	Total:	**1008.5**

3.2.2 Ventilation

The ventilation system of the tunnel consists of 8 supply fans totaling a capacity of 1006kW, and 8 extraction fans totaling a capacity of 896kW; detailed specifications are summarized in Table 3.2. The two ventilation towers on the North and South side of the tunnel that each house 4 supply and 4 extraction fans (Figure 3.1). Their purpose is to ventilate the tunnel space of harmful concentrations of pollutants such a CO_2. The control system for the fans use CO_2 set points to activate and deactivate the fans, however, on-site measurements have demonstrated a large discrepancy between measured concentrations of pollutants and the activation of the fans. The CO_2 sensors need to be re-calibrated in order for fan controls to operate properly. Consequently, the supply and exhaust fans are operated manually at the discretion of the tunnel operators and it is not clear what signals the need for ventilation in the traffic tubes. However, tunnel operators claim that the ventilation system is only operated in the summer. During warmer seasons, the ventilation system must operate to exhaust pollutants from the tunnel. However, during the cooler seasons, a piston effect caused by a combination of traffic flow and the buoyancy of air in cold temperatures is enough to naturally ventilate the tunnel.

Table 3.2: Ventilation fan specifications

Fan Description	**Number of Fans**	**Estimated Capacity (kW)**	**Total (kW)**
Supply Fan Type 1	5	149	745
Supply Fan Type 2	1	74.6	74.6
Supply Fan Type 3	2	93.2	186.4
Exhaust Fan	8	112	896
		Total:	**1902**

3.2.3 Lighting

The tunnel's lighting system is equipped with a combination of over 3000 high pressure sodium (HPS) luminaires of varying nominal powers between 100W to 400W. These lumi-

naires are split into different lighting stages that are activated when needed. Over the course of a year, this system accounts for approximately 50 percent of the tunnel's energy consumption and, at its maximum power, is responsible for 40 percent of the peak power demand in the winter. Approximately a third of the lighting system is active 24 hours a day, while the remainder is only activated during day-time hours, when outdoor conditions are bright. The cyclic nature of this 400kW day-time lighting load creates daily peaks in the load profile of the tunnel, highlighting the importance of understanding the lighting system of the tunnel in the context of this thesis. This following section will summarize how the lighting load profile was estimated.

The tunnel under study uses a lighting control system that evaluates outdoor brightness using measurements of luminous flux incident on a horizontal surface. Depending on how bright these measurements indicate it is outside, day-time lighting subsystems are turned on or off. However, this is not fully representative of what drivers experience when they approach dark tunnel environments and therefore, the lighting control system is limited. A better representation of what motorists experience (glare, black hole effect) can be given by evaluating luminance sources from their point of view [3].

3.3 Modeling Systems

The only point of measurement available for the electricity consumption of the LHLF tunnel is the Hydro-Québec meter located immediately outside of the tunnel (Figure 3.4). Therefore, only the cumulative power output of the all tunnel electrical systems was measured. This can only provide information on the instantaneous load of the entire system. To understand the contribution of each subsystem on the entire system load, it is necessary to model their power and energy individually. This section will go into detail about how each of the three major subsystems were mathematically modeled using a combination of recorded control signals, and electrical measurements.

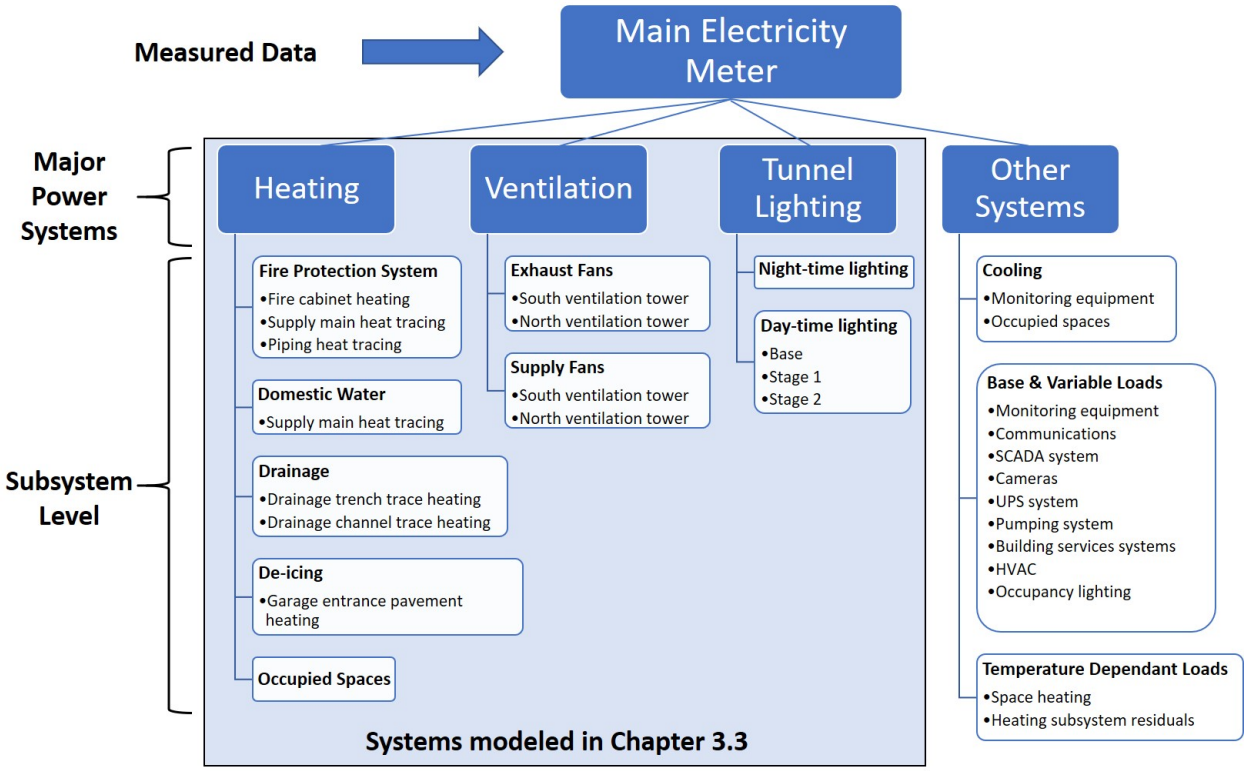

Figure 3.4: Location of energy measurements taken and provided by the local utility.

3.3.1 Modeling of Lighting Systems

The Louis-Hippolyte-La Fontaine tunnel has a reactive lighting control system that uses measurements of outdoor illuminance on the horizontal plane to determine when day-time lighting stages should be activated. A model of the lighting system, based on historical records and activation thresholds of each lighting stage, was created to simulate lighting loads and energy consumption.

Estimating the load profile of the tunnel's lighting system was a two-step task. The first step was determining each HPS luminaire's nominal power (including its accompanied ballast) and their designated lighting stage using the tunnel operator manual [8] and the most recent lighting renovation construction plans. A summary of this information is provided in Table 3.3. This information was used to determine what the total increase in power would be after activating a lighting stage. The increase in lighting power [W] use upon activation of a lighting stage was calculated using equation 3.1.

$$P_i = (n_{100W} P_{100W})_i + (n_{150W} P_{150W})_i + (n_{250W} P_{250W})_i + (n_{400W} P_{400W})_i \tag{3.1}$$

Where

P_{100W} is the rated power of one 100W HPS light and its ballast

n_{100W} is the number of 100W HPS lights

P_i is the power of each lighting stage

i denotes the name of each stage (night, day, stage 1, stage 2, and stage 3)

The next step was to determine what triggers the activation of each lighting stage. This information was provided in the tunnel operator manual [8]. The lighting intensity of each tunnel approach is controlled based on outdoor illuminance conditions. Two Class 2 ambient light photo-diode sensors[2] installed at the entrances of each tunnel tube are used to measure the luminous flux incident on the horizontal plane. As it becomes brighter outside, more

[2]The sensor has a measurement range of 0 to 10,000fc with a ± 1% accuracy in standard operating conditions.

lighting is required inside the tunnel to reduce the extreme contrast between the outdoors and underground environment. This in turn reduces the impact that the black hole effect has on motorists as they transition between environments. The control system increases lighting intensity as a step function, activating additional stages of lighting at different activation thresholds. The activation thresholds of each lighting stage and the associated increase in power use are described in Table 3.4. The illuminance readings for every 15-minute interval were recorded in the tunnel's SCADA system and used to determine the load profile of the lighting system for the year 2015-2016.

The base lighting load and increases in power linked to the activation thresholds for the Day, Stage 1, and Stage 2 lighting stages are shown in Table 3.4.

Table 3.3: Lighting fixtures assigned to each lighting stage in the Eastbound and Westbound circulation tubes.

Type of Lamp	**Lamp Power** [W]	**Ballast Power** [W]	**Total Power** [W]	**Number of Lamps**				
				Night	Day	S1	S2	S3
Eastbound Tube	100	30	130	339	175	40	0	0
	150	35	185	380	165	34	0	0
	250	39	289	32	16	44	35	0
	400	65	465	32	30	90	132	0
Westbound Tube	100	30	130	357	177	40	0	0
	150	35	185	373	169	38	0	0
	250	39	289	30	10	42	14	0
	400	65	465	30	30	90	122	0

3.3.2 Heating

The heating system was modeled using the installed capacity of each heating element (see Table 3.1) and the control signals recorded by the SCADA system. The data acquisition system indicates either the activation signal and/or the 15 minute-average current, or voltage

Table 3.4: Lighting Stages and Activation Thresholds.

Lighting Stage (i)	**Activation Threshold** [lux]	**Lighting Power** [kW]
Night	Always On	276
Day	1200	143
Stage 1	6000	133
Stage 2	15000	139
	Total:	**691**

of each heating subsystem, allowing us to calculate the demand charge of each time-step using equations 3.2 or 3.3.

$$DemandCharge_i = S_i C \tag{3.2}$$

Where:
S_i is the analog signal indicating if a heating element is on or off; 0 = off, 1 = on, and
C is the capacity of the heating element in kilowatts.

$$DemandCharge_i = \left\{ \left(\frac{1}{\sqrt{3}} V_{AB} I_A \right) + \left(\frac{1}{\sqrt{3}} V_{BC} I_B) \right) + \left(\frac{1}{\sqrt{3}} V_{CA} I_C) \right) \right\}_i \tag{3.3}$$

Where:
V_{AB} is the voltage between phase A and B in volts, and
I_A is the Phase A current (I) in amps.

The following assumptions were made:

1 All heating elements in the fire protection cabinets are 750W in magnitude. This value was determined by inspection of a sample fire protection cabinet. The assumption is

that all fire protection cabinets in the circulation tubes are identical and thus require the same capacity of heating.

2 The magnitude of each of the electrical heat tracing of the 4-inch supply pipes is 600W. This value was determined by inspection of one of the heat traced 4-inch supply pipes. The assumption is that the same capacity of heating is used for all similar supply pipes in the tunnel.

3 The magnitude of the heating elements used to maintain operating temperature inside housing for electronic equipment in the tunnel is negligible. While these heating elements exist in order to keep equipment within operating temperatures, they were not available for inspection. However, it was assumed that their magnitude was negligible due to the low operating temperatures of the equipment and the insulation of the housing for the equipment.

3.3.3 Ventilation

The ventilation system, consists of 8 supply fans and 8 evacuation fans (see Table 3.2). Similarly, the demand charge of each fan was determined using 15-minute averages of the speed and current of each fan, recorded by the SCADA system using equation 3.4 for fans controlled by a variable frequency drive (VFD).

$$DemandCharge_i = (1.732 I_2 U_1 \frac{N_2}{N_r})_i PF \tag{3.4}$$

Where

U is the rated voltage (V) of the fan

N_2 is the measured motor speed (m/s) of the fan

N_r is the rated motor speed (m/s) of the fan

The following assumptions were made:

1 The measurements of current recorded by the SCADA system were taken as the input of the motors. An assumption was made that the current supplied is equal to the current transmitted to the fan.

2 Power Factor is constant at 0.8 for all fans which is typical for induction motors in this size range. This simplification is false, the variable speed fans used in the LHLF tunnel have a variable power factor that is dependent on fan speed. At low fan speeds, the fans should operate at low power factors and at high fan speeds, power factor should increase. This can potentially lead to extreme differences in measured power demand.

3 Fan speed and voltage are linearly proportional (Equation 3.5).

$$\frac{U_2}{U_r} = \frac{N_2}{N_r} \tag{3.5}$$

Where:

N_r is rated motor speed (m/s) of the fan

U_r is the rated voltage (V) of the fan

N_2 is the measured motor speed (m/s) of the fan

U_2 is the calculated voltage (V) of the fan at N_2

3.4 Results

3.4.1 Subsystem Energy Share

Using the models described in the preceding sections, the energy consumption of each of the primary systems - heating, ventilation and lighting - was determined. Figure 3.5 shows the monthly energy consumption of the LHLF tunnel throughout 2015 and Table 3.5 summarizes the energy share of each system and compares it to literature [1].

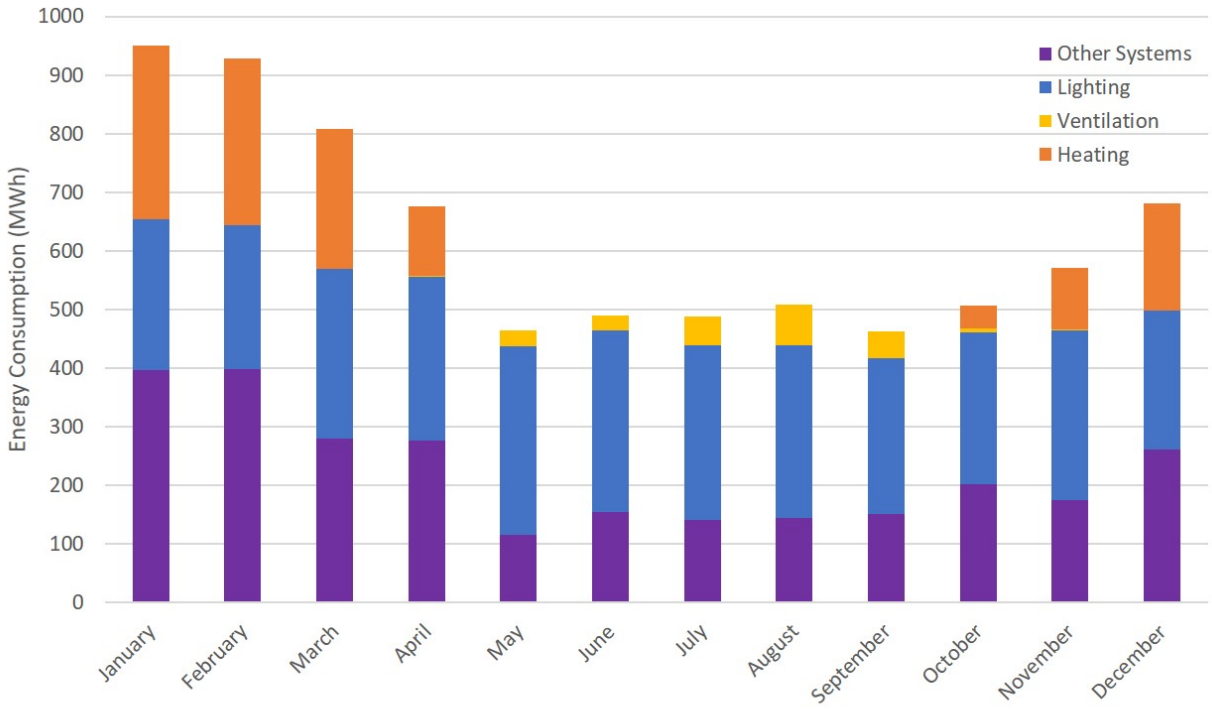

Figure 3.5: Monthly energy consumption breakdown of major systems over 2015-2016

The residual energy consumption between the summation of the three primary systems and the measured total energy consumption from HQ is significant. This is because it is not a complete model and only considers the three primary systems of interest. This difference will be referred to as the 'other' system loads and represents all other tunnel and building systems not considered in the model and modeling errors. While the other systems have a significant energy share of 36%, it is consistent with literature [10] which states that building services, emergency power, and other subsystems can be responsible for 33% of tunnel energy use. The energy share of the lighting system is consistent with literature which states that it has accounted for up to 50% of the annual consumption [10, 11]. Whether the estimate for heating energy consumption is reasonable is uncertain due to the lack of a reference tunnel with measured heating loads. Energy consumed due to ventilation appears to be low. Reference energy consumption is 17% whereas the estimate for the LHLF tunnel is only 2.9%. A decrease in energy share was expected due to the presence of a large heating system, but ventilation did not decrease proportionately with the lighting and 'other systems'.

Table 3.5: Annual energy use in 2015-2016 by subsystem

Subsystem Name	**Annual Energy Use** (MWh)	**Energy Share** (%)	**Reference Energy Share** (%)
Heating System	1270	16.9	n/a
Ventilation System	224	2.9	17
Lighting System	3306	43.9	50
Other systems	2740	36.4	33
HQ meter (Total):	**7530**	-	-

3.4.2 Error

ASHRAE Guideline 14 recommends using the following metrics (equations 3.6, 3.7, 3.8, and 3.9) to evaluate the uncertainty of a whole building model approach [62]. Since the model being evaluated for the LHLF tunnel only consists of systems that should theoretically only account for approximately 70% of the energy consumption of the tunnel, the equations represent the *difference* between measured and estimated values instead of error.

Root mean square difference (RMSD)

$$RMSD = \sqrt{\frac{\Sigma(y_i - \hat{y}_i)^2}{(n)}} \tag{3.6}$$

Coefficient of variation of the root mean square Difference (CV(RMSD))

$$CV(RMSD) = 100 \left[\frac{RMSE}{\bar{y}} \right] \tag{3.7}$$

Mean Absolute Difference (MAD)

$$MAD = \left[\frac{\hat{\Sigma}(|y_i - \hat{y}_i|)}{n} \right] \tag{3.8}$$

Normalized Mean Bias Difference (NMBD)

$$NMBD = 100 \left[\frac{\hat{\Sigma}(|y_i - \hat{y}_i|)}{n\bar{y}} \right] \tag{3.9}$$

Where:

n is the number of data points,

y_i = observed/measured value,

$\hat{y}_i$ = model estimated value of y, and,

$\bar{y}_i$ = arithmetic mean of the sample of n observations.

The difference between modeled results and HQ total measurements are high due to an incomplete model that only considers the three major power systems (heating, ventilation, and lighting) according to literature. Table 3.6 shows that the root mean square difference (RMSD) is higher than the mean absolute difference (MAD) of the 15-minute, hourly, and monthly estimated consumption. Since an incomplete model is being evaluated and RMSD is more sensitive to large variations between measured and estimated consumption, MAD is a better metric to evaluate the results. As expected, the MAD of the estimated consumption is very high and does not conform to the recommended minimum error of ASHRAE Guideline 14 [62].

The next chapter will discuss possible reasons for the discrepancy due to limitations in the numerical models by analytically inspecting the load profile of each system. Possible sources for the large discrepancy of loads will be investigated through an analysis of data's correlation with outdoor weather conditions and identification of existing, but un-modeled subsystems that can be potentially responsible.

Table 3.6

Metric	Interval		
	15-Minute	**Hourly**	**Monthly**
RMSE	89.0 kWh	354 kWh	300 MWh
CV(RMSE)	41.4 %	41.2 %	47.8 %
MAE	80.4 kWh	321 kWh	297 MWh
NMBE	37.4 %	37.4 %	47.4%

CHAPTER 4

Energy Analysis of Tunnel Systems

4.1 Introduction/Purpose

The previous chapter showed that the data recorded by the SCADA system approximates that 64% of the annual energy consumption of the LHLF tunnel is caused by the heating, lighting and ventilation systems. This is consistent with what reference studies have indicated [10]. However, 36% of the tunnel energy use is still unaccounted for and the estimates for average energy use over 15-minute intervals have a mean absolute discrepancy of 80.4 kWh using the data from the main electricity meter. The goal of this chapter is to discuss the results of the current tunnel model by analysing the 15-minute load profiles of the heating, ventilation, and lighting systems with the purpose of identifying sources of error. The residuals of the data set will be analysed by examining their relationship to weather conditions to hypothesize their source. Residuals are the difference between the power demand measured at the main electricity meter and the estimated power demand of the heating, ventilation, and tunnel lighting systems. Figure 4.1 shows how the residuals are calculated, what factors contribute to their magnitude, and what the sources of each parameter are.

A discussion about the analysis done on the improved results will follow. The energy

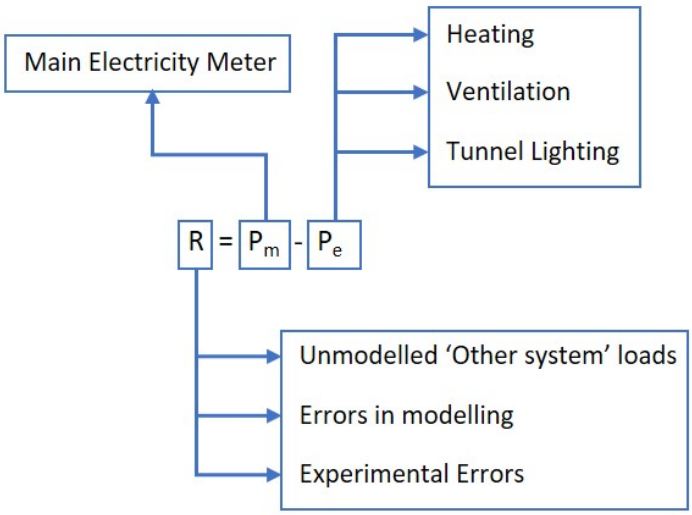

Figure 4.1: Equation used to calculated the residuals: R is the residuals, P_m is the measured power demand, and P_e is the estimated power demand.

consumption and financial cost from each subsystem (heating, ventilation, and lighting) will be analyzed individually to better understand the needs of the tunnel. Additionally, the impact that the tunnel has on the local electrical grid will be evaluated by looking at which systems are responsible for large seasonal variations and spikes in instantaneous power. This information will be used to determine the financial potential of applying different energy efficiency retrofits and to give insight on the priorities that the tunnel should have in a potential renovation project focused on reducing overall consumption.

4.2 Anomalies in Load Profile

Chapter 3.0 resolved that the models used to estimate the demand profile of the major service systems were able to represent a significant portion of the measured power usage of the LHLF tunnel. Figures 4.2 and 4.3 show the load profiles of the modeled systems superimposed on the measured HQ load profile over a five day period in the summer and winter respectively; they show how well the profiles of the heating, ventilation, and lighting systems represent the actual measured load of the entire tunnel. Figure 4.2 clearly shows that increases in instantaneous power are in alignment with the activation of day-time lighting and ventilation systems. Similarly in the winter, figure 4.3 shows that day-time lighting accurately represents increases in day-time peak loads in the measured profile; the measured profile is also in synchronization with the modeled load profile for the combined heating subsystems. However, there still exists a major difference between the total measured power and the power estimated by the combined models, which exists because the model was not meant to estimate all of the tunnel systems. While the three major systems that were modeled represent roughly 70% of the tunnels energy usage, they does not represent the complete picture.

This section will attempt to explain and reduce the difference between the total measured power demands of the LHLF tunnel and estimated power demand of the combined heating, ventilation, and lighting models. The results obtained from the models of these major systems will be analyzed individually to characterize sources of error in the model.

Three main types of errors related to the heating, ventilation, and lighting subsystems

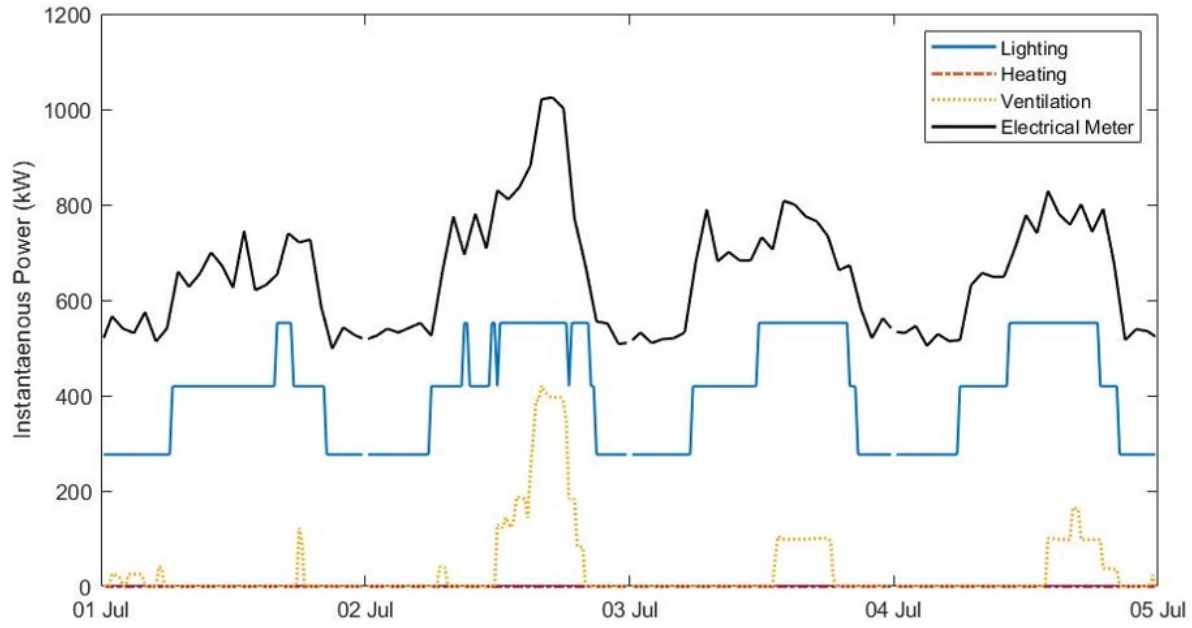

Figure 4.2: Estimated power demand of the lighting (blue) and ventilation (yellow) systems during the summer compared with the measurements taken at the main electrical meter (black).

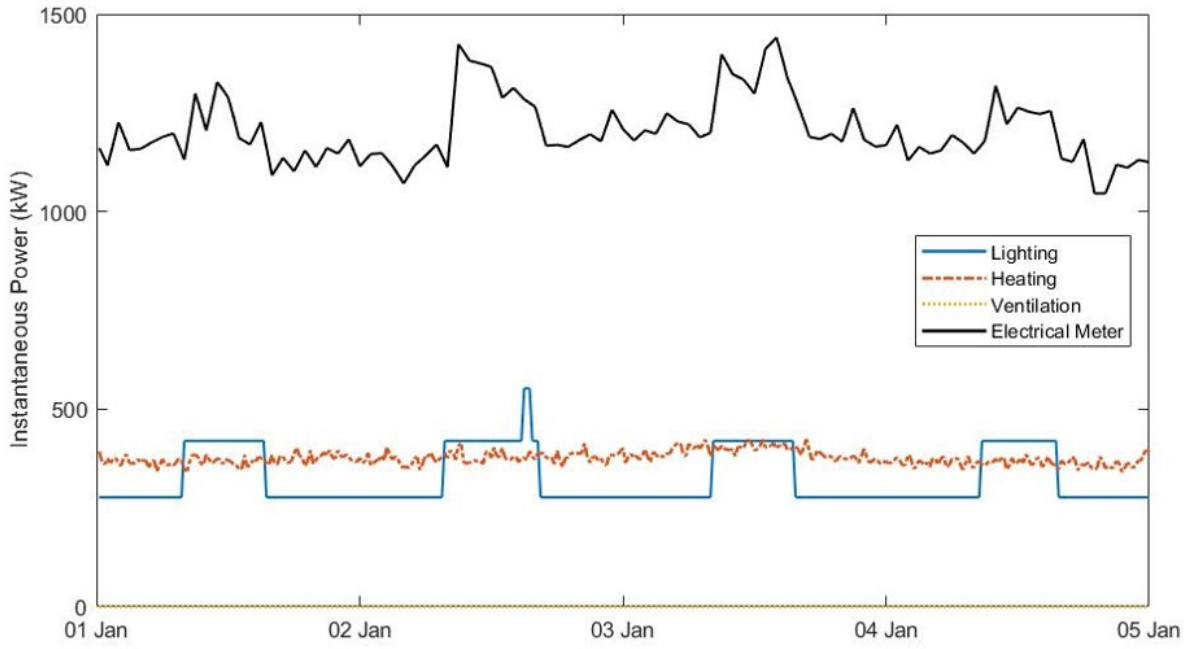

Figure 4.3: Estimated power demand of the lighting (blue) and heating (orange) systems during the winter compared with the measurements taken at the main electrical meter (black).

were analyzed. Significant spikes or drops in the demand profile of the residuals that correspond with an opposing spike or drop in one of the heating, lighting, and/or ventilation load profiles is an indicator that there is an anomaly in one or more of the models due to an over or under estimation. Figure 4.4 gives an example of the different types of anomalies that were analyzed by showing a time period when all types of anomalies were present.

Type A anomalies in the load profile are spikes that occur in the residuals profile that are not accompanied by an opposing drop in the heating, lighting, or ventilation load profiles. A drop is expected because the modeled loads should be inversely proportional to the residuals unless there is a modeling or measurement error. This can be due to an additional major system that was not considered in the model - such as the pumping system. An example of this can be seen in figure 4.4, encircled in red and labeled as Type A. Note that the spike in residual system power is also accompanied by a similar spike in the total load measured by Hydro-Québec, indicating that the spike represents a real load. Type A anomalies usually occur on consecutive nights between 10PM and 4AM. An explanation for this is night-time maintenance operations that were not considered in the lighting model; the sensor used in the lighting model determined the automated activation of the lighting stages, however they can also be manually activated by the tunnel operators in scenarios such as a scheduled maintenance service. There were 22 observed occurrences of Type A anomalies between 2015 and 2016 which corresponded with scheduled maintenance and renovations from the operator logbook.

Type B anomalies are due to an overestimation in the loads caused by heating elements in the tunnel. These are characterized by sudden reactions in the residuals; sudden large spikes in heating power, accompanied by an identical drop in residuals. The example in figure 4.4 shows that the residuals create a load profile that is symmetrical to the combined heating loads. The change in loads of both profiles are similar in magnitude and duration. In some cases, the residuals drop below zero due to such a large overestimation of heating; these errors are mainly restricted to the cold winter season. There were 28 observed occurrences of Type B errors between 2015 and 2016. These errors may be explained by the assumptions made in Chapter 3.3.2 and signal errors. Additionally, the errors can be explained by how the heating elements were grouped in the heating model, since some heating elements were

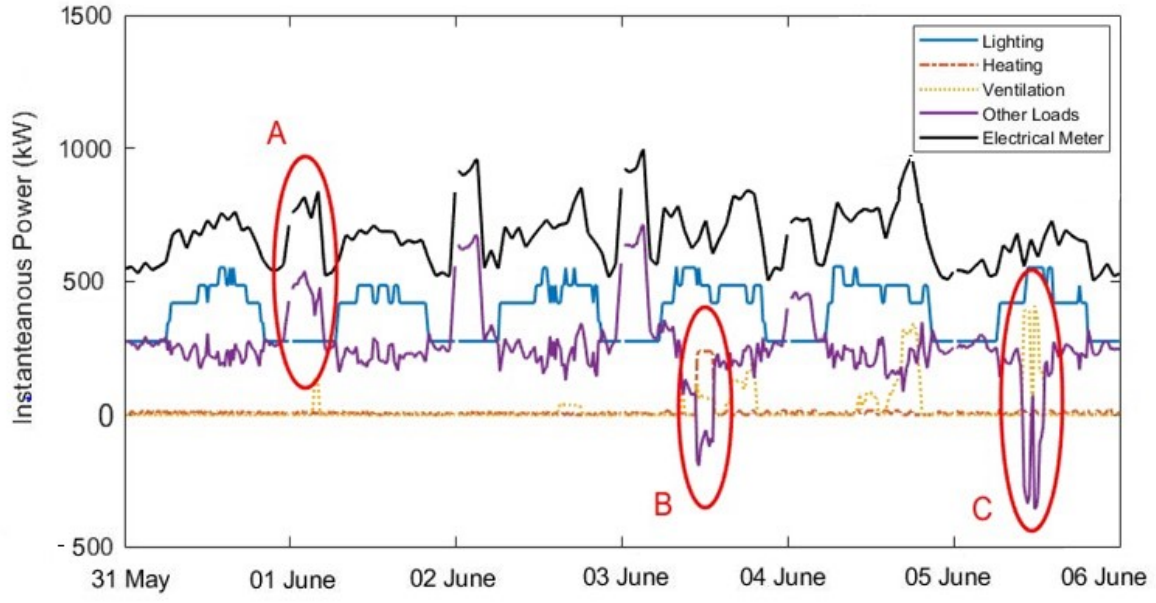

Figure 4.4: Examples of anomalies detected in the detailed analysis of the modeled tunnel profile occuring between May 31st and June 6th of the year 2015. Type A: Spike in power caused by unidentified source(s). Type B: Over-estimation of heating load(s). Type C: Over-estimation of ventilation load(s).

assumed to have the same activation signal. If these elements were improperly assigned, they could result in the significant differences observed in type B anomalies.

Type C errors are due to an overestimation in the ventilation system loads. Similar to Type B errors, they are characterized by reactions in the residuals (figure 4.4). These errors occur mainly during the summer. There were 21 observed instances of Type C errors between 2015 and 2016. These errors are assumed to be caused by the assumptions made about fan power factor in chapter 3.3.3.

4.2.1 Recommendations

Ventilation

According to the tunnel operator manual, the ventilation fans should be automatically controlled by CO_2 and CO sensors throughout the length of the tunnel, with the option

of being manually overrun by the tunnel operators. However, the recorded control signals for the ventilation fans showed that their operation did not correspond with the air quality criteria outlined in the tunnel operator manual [8]. Further investigation revealed that the ventilation fans were primarily manually operated based on qualitative information -such as odour- instead of automatically controlled using the measurements from the air quality sensors.

Additionally, at 9:00AM on August 20th, an RV transporting propane caught fire inside the LHLF tunnel and caused a major emergency closure and evacuation of the tunnel. However, the recorded voltage and current sent to the fans did not indicate that the ventilation fans were turned on. The lack of a spike in the data measured at the main electricity meter further supports the hypothesis that the fans were never turned on and therefore do not respond appropriately to fires.

In conclusion, the operation of the ventilation fans are considered to be unpredictable and cannot be modeled using any measured parameter. To accurately model and predict the operation of the ventilation fans in the future, the air quality sensors should be properly calibrated and the original control strategy should be implemented.

Correction to lighting

The preliminary model estimates that in 2015, lighting was responsible for approximately 43.9% of the annual energy consumption; this is consistent enough with what reference projects have shown [10, 11]. However, a closer look at the load profile shows that there a potential discrepancy between the modeled lighting load and the actual load. Residuals are made up errors from modeling and estimating the major systems (heating, lighting, and ventilation systems) and loads from all minor systems and subsystems that were not included in these major systems (see Figure 3.4). The residuals were calculated by taking the difference between the total measured instantaneous power and the cumulative estimated loads of the 3 modeled systems. They can be used as an indicator for abnormal behaviour in the modeled results. Figure 4.5 shows the load profile of the lighting system and the residuals. There is a inverse relationship between the residuals and lighting loads; when the day-time lights are supposed to turn off, there is an instant reactionary spike in the residuals. Due to the

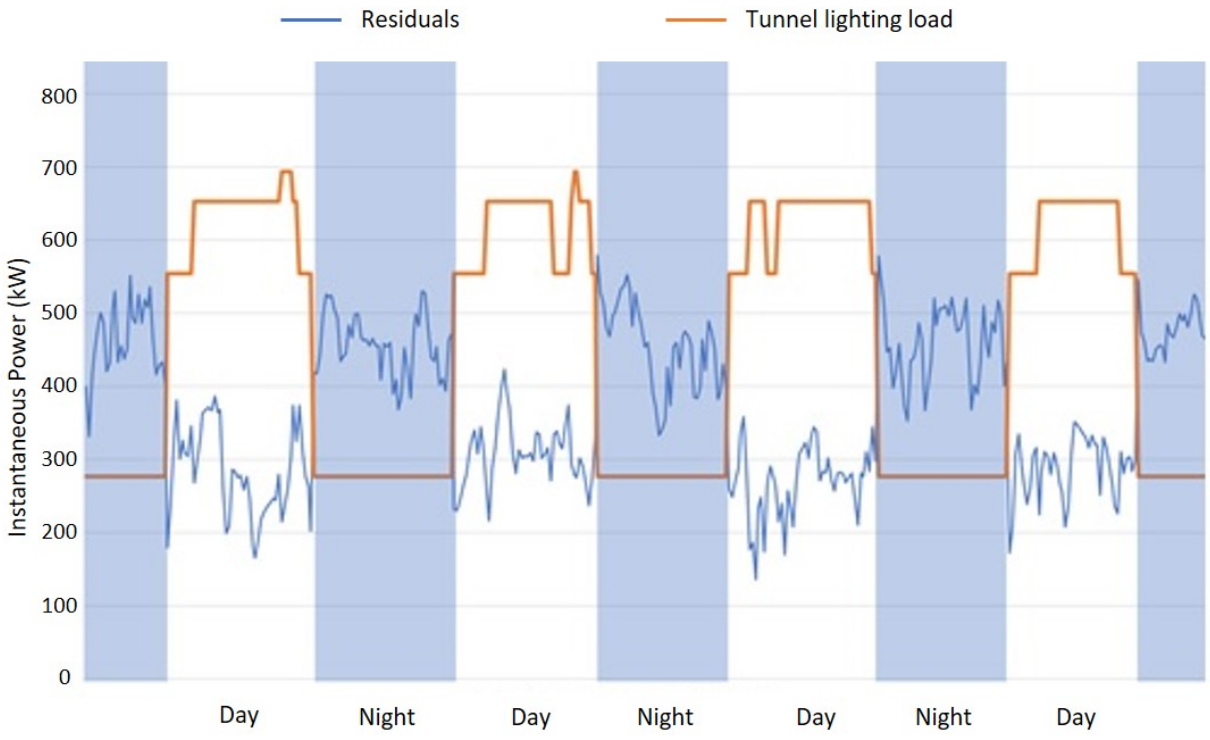

Figure 4.5: Discrepancy between day-time and night-time lighting loads.

apparent dependency of the residuals on lighting loads and the fact that there are no other system loads that use the same illuminance readings as an activation signal, this sudden variation in residuals suggests that there is an overestimation in the day-time lighting load or an underestimation in the base night-time lighting load.

This discrepancy between the lighting loads can be the result of inconsistent information between what is communicated in the lighting plans and what is actually present in the tunnel. Two adjustments were made to the lighting model to account for this difference:

i) A correction of the day-time lighting system capacity was made using on-site electrical measurements.

ii) The night-time maintenance schedule was applied to the load profile to account for the abnormal activation of the lighting system.

The voltage and current of each of the day-time lighting stages (Day, Stage 1, and Stage 2) was measured. All day-time lighting stages were turned on by the tunnel operator and measurements of each circuit were taken using a multimeter. These measurements revealed that the modeled lighting capacity was overestimated by 34 kW. Since this small adjustment does not account for the large spike in residuals, the only possible explanation is that there is a underestimation of the night-time lighting load. Unfortunately, the circuit for the base night-time lighting system was inaccessible and it was not possible to validate its capacity. The validated lighting system capacities which were used to in new calibrated model are summarized in Table 4.1.

Table 4.1: Comparison between the lighting system capacities shown in technical drawings vs corrected capacities measured on site.

Lighting Stage (i)	**Activation Threshold** [lux]	**Lighting Power** [kW]	**Corrected Lighting Power** [kW]
Night	Always On	276	n/a
Day	1200	143	141
Stage 1	6000	133	117
Stage 2	15000	139	123
	Total:	**691**	**657**

4.3 Residual Systems

According to the estimates of the heating, lighting and ventilation systems produced at the end of chapter 3, a significant share 36.4% of the annual energy consumption of the tunnel is unaccounted for and categorized as residuals. The residuals can be largely attributed to loads from the other systems described in figure 3.4; while this energy share falls within the expected range (according to studies of other under-water tunnel systems [10]), modeling and experimental errors can make the energy share of the other systems seem larger than

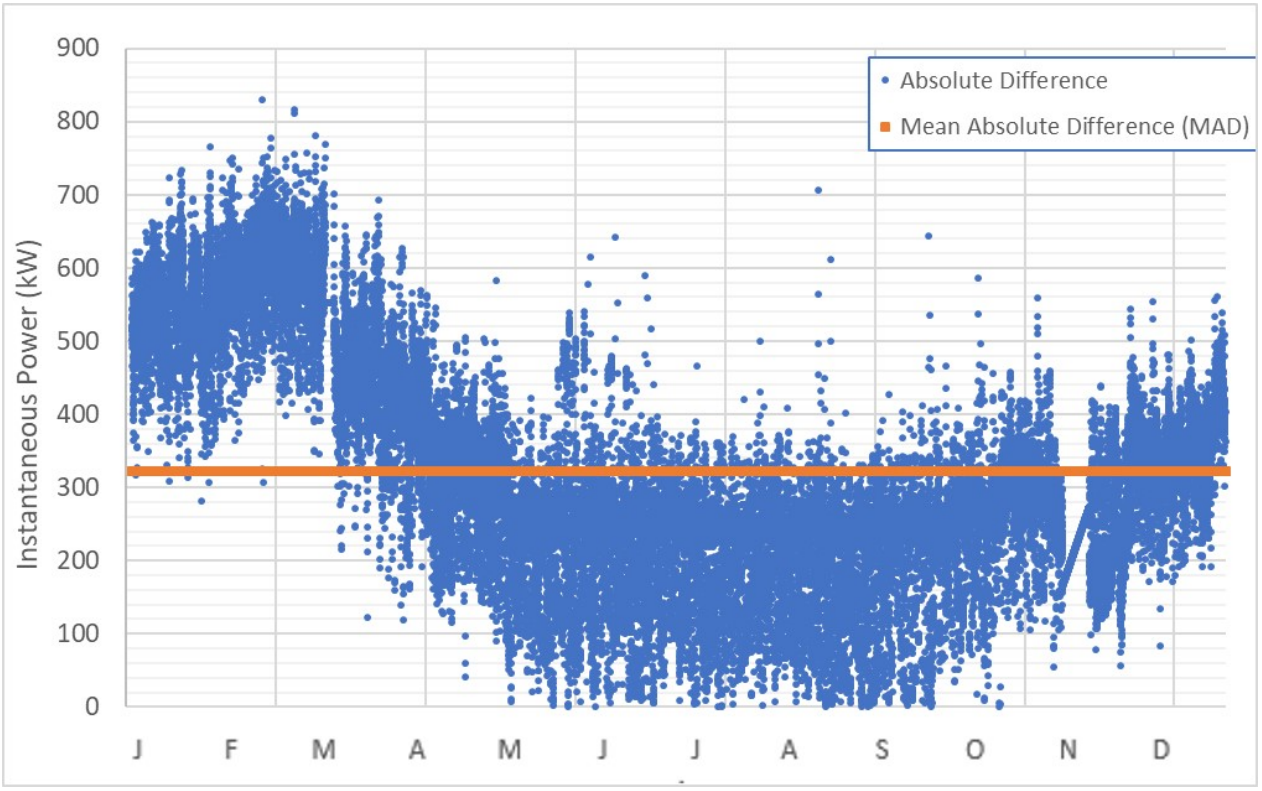

Figure 4.6: Absolute error of the combined heating, ventilation, and lighting model throughout the 2015-2016 year.

it actually is. The prominent increase in power demand during the winter months in figure 4.6 illustrates that the residuals have a large seasonal variation that is likely temperature-related. This suggests that modeling errors have lead to the exclusion of significant heating subsystem loads. Further investigation into the data will be done to characterize the residuals and identify a minimum annual base-load and if possible, temperature-related loads. This will give insight into what subsystems could be responsible for each type of load as opposed to referring to such a large group of subsystems as a singular component.

The other system loads can be divided into two groups:

i) Continuous minimum base load

Based on information from literature [11] and technical manuals [8], the base loads of the LHLF tunnel likely consists of minor systems that are constant throughout the entire year. These systems include space lighting (underground spaces with no daylight), 24hr surveillance and operational equipment, monitoring and data acquisition

equipment, SCADA system, air ventilation for occupied spaces, minor appliances, and a UPS system.

ii) Variable loads

The variable loads that have not been modeled in detail, consist of components that are constantly changing in magnitude. These systems with variable loads can be **daily** and change throughout a 24 hour cycle; or they can be **seasonal** and change throughout the year.

Instantaneously variable loads include systems that have sharp dips in their demand profile over a short period of time. In the context of this case study, variation of their loads can be clearly observed over a 24 hour cycle. This can include a range of systems such as the tunnel lighting systems which cycle on and off every day, or an elevator or automated garage door that is activated on demand.

Seasonally variable loads can include heating subsystems that were not considered in the initial numerical model due to modeling errors, air conditioning (cooling) systems, and errors in the ventilation fan model. The residual heating and cooling systems are temperature dependent and only operate during their respective seasons (winter and summer, respectively). The ventilation fans are frequently operated during the summer when buoyancy has less of an impact on air pollution inside the tunnel tubes. This fits with what is observed in figure 4.6, which shows that there is a large seasonal variation in the residuals of the tunnel.

Determining the base load

To determine the minimum base load of the tunnel system, we need to isolate it from the variable loads that exist in the system. Based on the work done in Chapter 3, it is known that heating, ventilation and the day-time lighting systems are the major variable loads in the system. A closer look at figure 4.6 shows that there are likely temperature-related loads in the residuals that were not accounted for in the heating system model. Therefore, to identify the base-load of the tunnel using a statistical approach, the data set must use a period when temperature-related loads are not present. The only period of time when

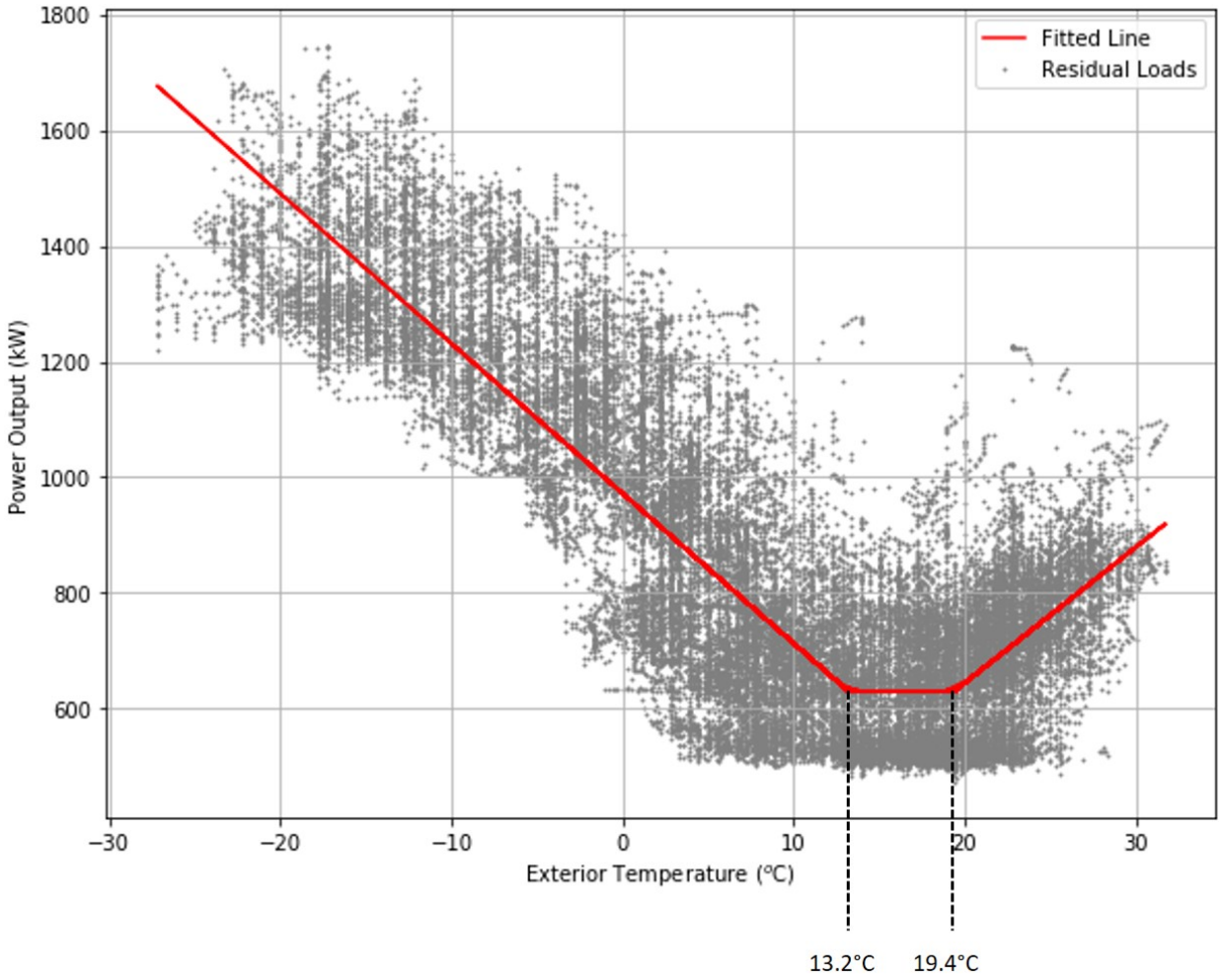

Figure 4.7: Scatter plot showing the relationship between the instantaneous power measured at the main electricity meter and exterior temperature. $r^2 = 0.77$

these heating loads are not present is during the summer. However, another component that has been overlooked is the cooling of occupied spaces and equipment. This must also be considered for when determining a base load for the tunnel since cooling will not be present during the winter. Since it has been established that the variable heating, ventilation, and cooling loads are temperature-related, a correlation with exterior temperature can be used to separate them from the base loads.

A correlation between the measured instantaneous power of the system (dependant variable) and exterior temperature (independent temperature) was made using 15-minute recorded data from a local weather monitoring station and the main electricity meter. Figure 4.7 shows

that system power demand increased as temperature decreased when temperatures were below 13.2°C (± 0.0931°C); there is an equilibrium band where temperature no longer affects system power demand between 13.2°C (± 0.0931°C) and 19.4°C (± 0.141°C); finally, when temperatures rise above 19.4°C (± 0.141°C), system power demand increases linearly with temperature. This suggests that the major systems with seasonal variation are related to temperature and are likely components of heating and cooling systems. Furthermore, the equilibrium band (see figure 4.7) indicates that these same systems have a minimal impact on total system power demand during days with moderate temperatures, when heating and cooling demands are lowest or non-existent. This supports the hypothesis that the seasonally variable loads are components of heating and cooling systems. A linear regression for the cooling related loads was made to estimate their capacity and loads throughout the year.

The LHLF tunnel has a series of minor systems that form a continuous base load throughout the year that is independent from exterior temperature conditions. These systems fall into the category of residuals that were not numerically modeled. Figure 4.7 shows that there is a high density of data points that cluster between a 500 to 600 kW power output. The data in the cluster occur in the equilibrium band, when loads are mostly temperature-independent and have minimal impact on the total power output of the tunnel. This allows us to identify the 500 kW threshold as the base load of the tunnel. Of the 500 kW baseload, the only modeled system that is known to be activated continuously throughout the year is the night-time lighting system (276 kW). This leaves a 224 kW difference which makes up the base load of the minor systems.

Estimating the temperature-related residuals

A significant portion of temperature-related residuals that are active during the winter can be observed in figure 4.6. These points likely originate from inaccuracies in the heating model or other systems related to heating in the winter. By determining the magnitude of these loads, the difference between real and modeled data can be better explained. To determine the magnitude of the temperature-related residuals, the residuals in figure 4.6 were plotted as a function of temperature to create a correlation (see figure 4.8). Using the fitted line in figure 4.8, the peak of the residual temperature-related loads during the cold

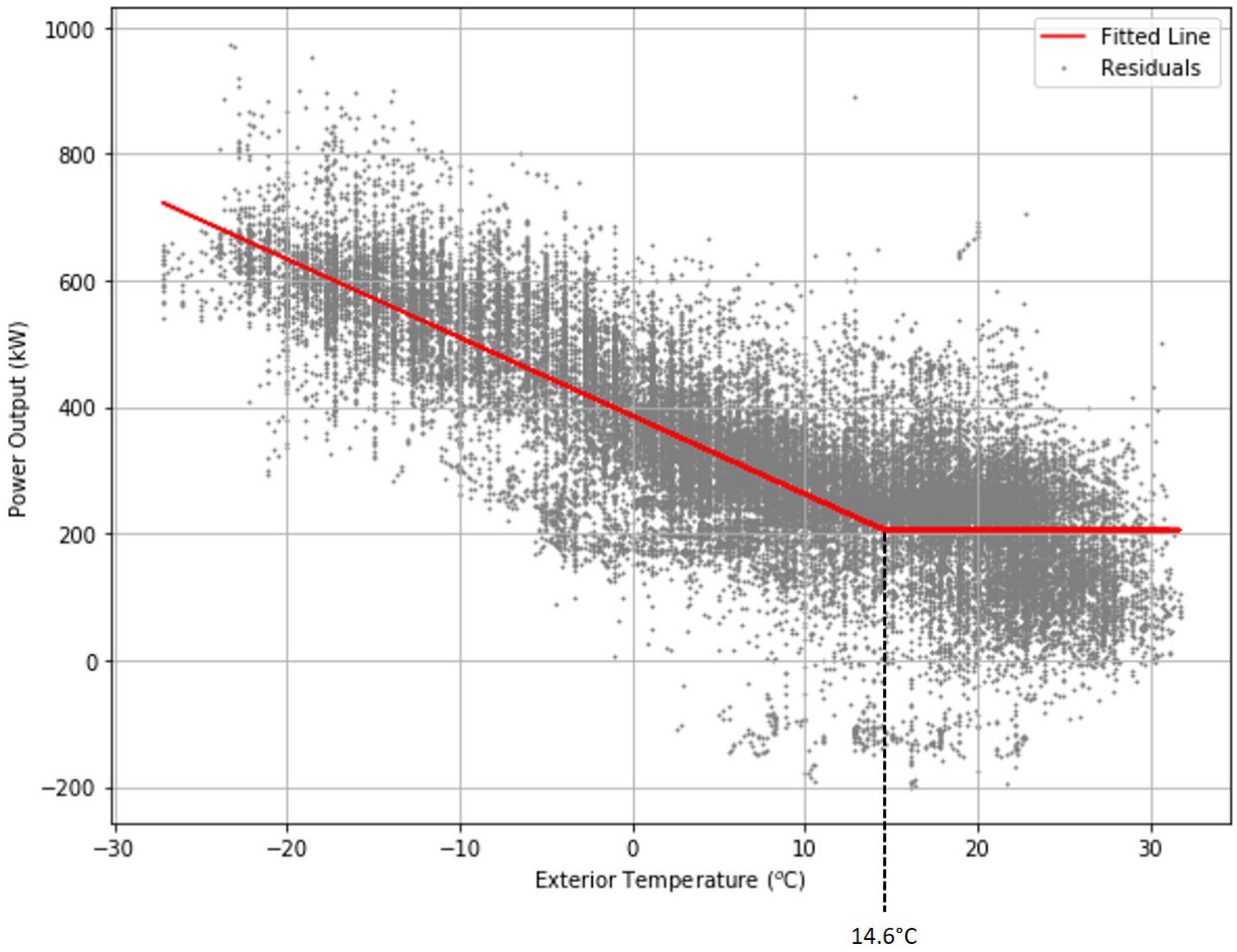

Figure 4.8: Scatter plot showing the relationship between the residuals and exterior temperature. $r^2 = 0.65$

season was determined to be 510.612 kW. It is important to note that while it is likely that these temperature-related loads are part of the heating system, it is not a claim that can be made with absolute certainty; this analysis simply shows that there is a correlation between these loads and the exterior temperature. Figure 4.8 also shows that there are no significant temperature-related residuals that occur during the summer when temperatures are high.

Variation in data

Furthermore, there is a large variation between the data predicted by the fitted line and real data plotted on figure 4.7 and 4.8. This can be explained by several phenomena. Primarily, temperature readings inside the tunnel were taken during the winter and summer

months using a mobile weather station retrofitted onto a vehicle. The data showed that there is a temperature gradient along the length of the tunnel, with temperatures increasing closer to the center of the underwater structure. This can be explained by heat exchange between the interior air of the tunnel and its warmer surroundings consisting of concrete, soil, and river water. The constant flow of vehicles through the tunnel also transmits thermal energy to the interior of the tunnel from combustion. This temperature gradation can lead to significant differences in interior and exterior temperatures, explaining the variance of the temperature-related loads. Secondarily, the different types of controls used for the different heating subsystems can also be a source of variance; three heating subsystems are controlled using specific temperature set-points that activate different capacities of heating instead of increasing linearly with temperature. Finally, the variation can also be explained by temperature independent loads that exist in the tunnel but cannot be correlated with the exterior temperature of the tunnel.

In summary, this analysis shows that the continuous base-loads and temperature-related winter loads that are present in the residuals contribute significantly to the difference between modeled and measured data. Table 4.2 shows the magnitude of these two types of loads and the estimated energy consumption that they are responsible for throughout the year. The base loads are responsible for 68% of the difference between modeled and measured power. Results show that regression of the temperature related loads is susceptible to systemic errors and can lead to over-estimations of residual energy consumption. This can be explained by the variation and uncertainty related to the fitted correlation with temperature. The important conclusion is that temperature-related loads are present and significant in this model and that an improved heating model can reduce the difference between modeled and measured power and energy consumption.

Table 4.2: Breakdown of the residual loads

Type of Load	**Capacity (kW)**	**Annual Consumption (MWh)**
Base	213.0	1865.9
Temperature-related (winter)	510.6	1349.9

4.4 Economics

This section will look at the resulting financial cost of the LHLF tunnel energy consumption between 2011-2015, with a focus on 2015-2016 for a detailed system breakdown. Using this data, the financial potential of each subsystem retrofitting will be calculated using Hydro-Québec's rate M structure.

4.4.1 Hydro Quebec Rate M

The Louis-Hippolyte-La Fontaine tunnel qualifies as a Rate M client of Hydro-Québec. This rate is intended for medium-power customers; to qualify, consumers maximum power demand must be at least 50 kilowatts (kW) over the last 12 monthly billing cycles and must not exceed a power demand of 5000 kW [9]. This structure includes a power demand charge (cost per kilowatt) to ensure that Hydro-Québec is adequately compensated for the equipment used to respond to a consumer's constantly varying loads. The demand charge is set to the maximum power demand - regardless of its frequency - of their facilities over the past month. Energy (kWh) is billed at a general rate per unit consumed. The rate M structure has two tiers of prices based on the customers consumption. The first 210,000 kWh consumed is charged at a standard rate and a discount is applied to the remaining consumption (see Table 4.3). The rate structure also has a conditional minimum demand charge which stipulates that the customer must pay a minimum of 65% of their maximum power demand from the last 12 monthly billing cycles [9]. This condition exists to penalize customers for having large seasonal imbalances in their power demand, particularly during the winter.

Table 4.3: Hydro-Québec's Rate M Structure as per [9].

Type of Fee	**Description**
Demand Charge	$14.46 per kilowatt of billing demand
Energy Consumption	¢4.99 per kilowatt-hour for the first 210,000 kilowatt-hours ¢3.70 per kilowatt-hour after the initial 210,000 kilowatt-hours

Minimum Demand Charge

Hydro-Québec has an interest in being able to reliably predict the magnitude of peak demand from their numerous and varied customers. This is so that they can provide and maintain the appropriate infrastructure required to service their electric grid during moments of peak demand. Hydro-Québec includes a minimum demand charge in their rate structure to incentivize their medium-sized customers to maintain a balanced demand profile over the last 12 months. The structure penalizes consumers that increase their demand significantly throughout the year by charging a minimum demand charge equal to 65% of their 12-month peak. Any monthly peak that falls below the 65% threshold will be charged for their minimum demand, regardless of their actual demand [9].

4.5 Subsystem Energy Consumption

The share of each annual energy consumption of the major systems (heating, ventilation, lighting, and residual systems) is summarized in Table 3.5 in chapter 3. Figure 4.9 illustrates the daily energy consumption of the tunnel broken down by the major systems and shows that consumption doubles during the winter due to the activation of the heating system.

Lighting is the biggest consumer of electricity, responsible for 43.9 % annually. This is because the system has a base load of 276 kW, combined with daily peaks that last the duration of daylight hours ranging from 417 to 657 kW depending on the outdoor brightness. An energy share of 43.9% is reasonable considering the critical function that lighting has during the day for underground tunnels. Furthermore, literature indicates that this energy share is typical for the underground tunnels in their study [10, 11].

Aside from the combined consumption of the residual systems, heating is the second largest consumer of electricity, despite being a seasonal winter load. The combined heating systems are responsible for 17% of the total system energy share. This is likely to be an underestimate considering that a large portion of the residual system loads are temperature-related. If temperature-related residual loads are grouped together with the heating system, their combined energy share could increase from 17% up to 34%.

The peak power of the tunnel is an important metric that can incur significant financial

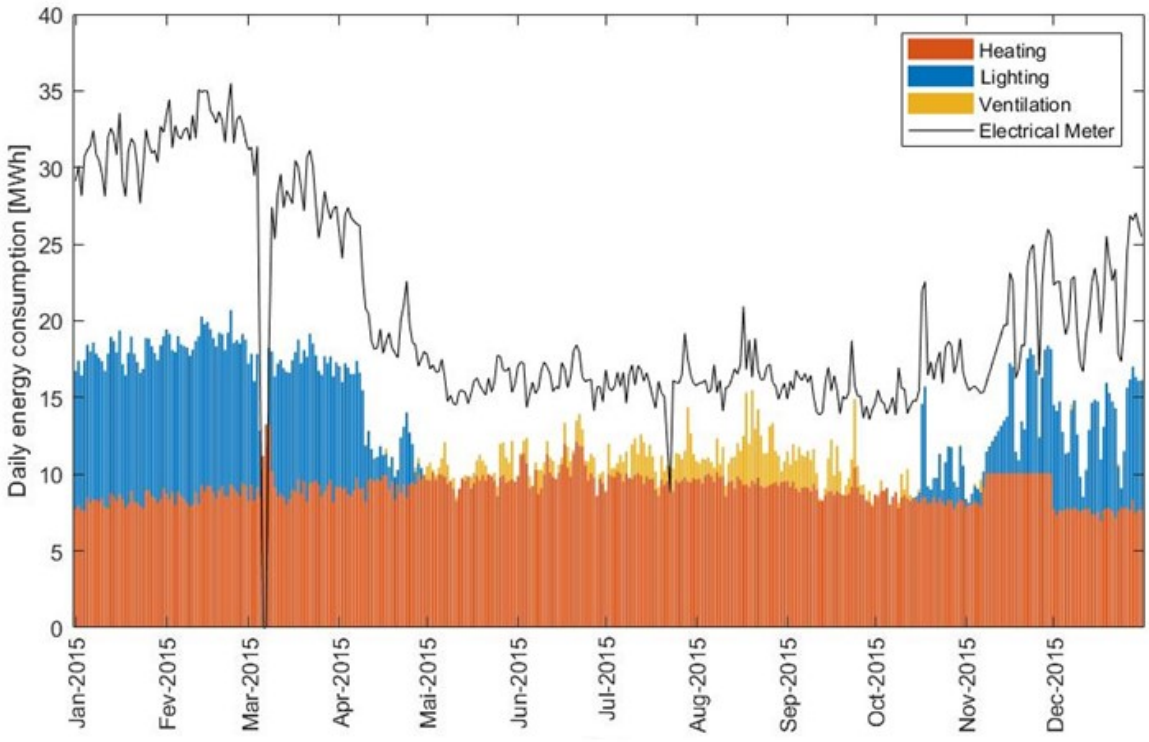

Figure 4.9: Estimated daily energy consumption of each subsystem for the 2015-2016 year.

costs. Table 4.4 shows the contribution of each major system on the monthly peak power demand of the tunnel. Since the LHLF tunnel is charged a demand charge and minimum demand charge, it is clear lighting is the single most demanding system in the tunnel.

4.6 Cost Analysis

This section will apply Hydro-Québec's rate M structure the LHLF tunnel systems. Using the calibrated model of the tunnel demand and energy consumption, a breakdown of the utility bill will attribute the operational financial cost to each of the major tunnel systems. This information will be used to determine the financial potential of renovating each system and ultimately decide on a system to evaluate.

Table 4.4: Estimated monthly peak power loads of the LHLF tunnel showing the contribution of each of the major service systems.

Month	Heating (kW)	Ventilation (kW)	Lighting (kW)	Residuals (kW)	Peak (MW)
January	511.2	0	552.5	744.0	1.651
February	535.6	0	691.5	817.0	1.746
March	468.2	82.9	691.5	768.8	1.595
April	388.6	246.7	691.5	627.3	1.396
May	0	577.3	552.5	575.3	1.080
June	0	474.1	691.5	641.8	1.131
July	0	531.9	552.5	499.7	1.099
August	0	861.0	552.5	706.6	1.226
September	0	782.2	691.5	536.2	1.277
October	363.0	533.3	691.5	585.8	1.177
November	399.4	143.1	552.5	537.1	1.326
December	421.0	202.6	552.5	561.5	1.398
Annual	535.6	0	691.5	817.0	1.746
Max	535.6	861.0	691.5	817.0	1.746

4.6.1 Consumption & Demand Charges

The cost of electricity was calculated using the estimated energy consumption and load profile of the heating, lighting, and ventilation systems (figure 4.10). A weighted average for each system was used to account for the tiered cost structure of HQ's Rate M. The monthly demand charge of each system was calculated using the resulting loads of each system that occurred during the entire system peak load.

The system responsible for the highest financial cost from January 1st, 2015 to December 31st, 2015 is the lighting system, followed by the combined residual systems, the heating system and then the ventilation system. The lighting system is the largest contributor to

the annual peak load and also consumes the most energy. This is because the system has a significant base lighting load of 276 kW, which can more than double everyday for the duration of all daylight hours (approximately 4020 hours per year). Figure 4.10 shows that improvements to the lighting system will yield the highest financial gain

4.6.2 Minimum Demand Charges

The minimum demand charge was determined by first determining the peak load of the 12 months between 2015 and 2016. During this period, the annual peak demand was 1745kW which occurred on February 24th between 8:45 and 9:00 AM during the winter. This peak load was driven equally by the lighting and heating systems of the tunnel. Due to the seasonal nature of the heating system, these high magnitude peaks only occur during the winter season. The minimum demand according to Hydro-Québec's guidelines, is 1135 kW; this minimum demand was surpassed for the majority of the year except for the summer months of May, June, and July. Although the minimum demand was not exceeded during these moments, the difference with actual peak demand was very close and the incurred penalties were minimal. This shows that the LHLF tunnel system has an acceptable seasonal balance between winter and summer demand but is on the cusp of being subjected to penalties if winter demand increases. Additionally, any renovations that exclusively improve summer seasonal demand might by offset by this demand charge if winter demands remain static.

The minimum demand charge between January 1st and December 31st, 2015 totaled less than 0.2% of the annual energy cost of the tunnel. Furthermore, between 2011 and 2016, monthly peak power demand was less than the minimum demand only 13 times; costing the Ministry of Transport less than 20,000$ over the five year period. While this amount is not significant compared to the total operational costs of the tunnel, it once again demonstrates the combined system's sensitivity to change.

Table 4.4 shows that the heating system is responsible for seasonal imbalance in the LHLF tunnel since it is only active during the winter. This means that improvements to the heating system is the most impactful way to prevent future penalties in the form of minimum demand charges. Additionally, Table 4.4 also shows that there is no clear relationship between the magnitude of monthly lighting power demand and the time of year. Therefore, any

improvements to the lighting system will also help avoid minimum demand charges. This is pertinent information for designers hoping to renovate the tunnel system with significant changes to its operational power demand.

Table 4.5: Summary of the financial cost of operating each tunnel system according to Hydro-Québec's Rate M structure.

System	Energy Cost ($)	Demand Charge ($)	Penalty ($)	Total Cost ($)
Heating	54,418	40,948	0	95,366
Lighting	153,318	80,281	604	234,203
Ventilation	11,192	39,884	638	51,714
Others	129,573	70,586	130	200,289
Total	350,503	231,699	1,372	583,574

4.7 Conclusion

This chapter helped resolve the source of the residual loads analytically by identifying tunnel systems that were not modeled and observing the behaviour of the residual loads based on parameters such as temperature and season. A group of systems that created a continuous base load was identified in figure 4.6, and the magnitude of temperature related loads was estimated for the warm and cold seasons. This helped establish confidence in the estimates made in chapter 3 on the energy consumption of the heating, lighting, and ventilation systems, despite the large difference between total measured data and estimated data.

Additionally, the following conclusions were reached by applying the Rate-M structure to the demand profile and of the heating, lighting, and ventilation systems:

- Lighting has the highest financial potential in terms of an energy retrofit.
- Lighting and heating loads during the winter should be reduced to ensure proper seasonal balance according to HQ guidelines.

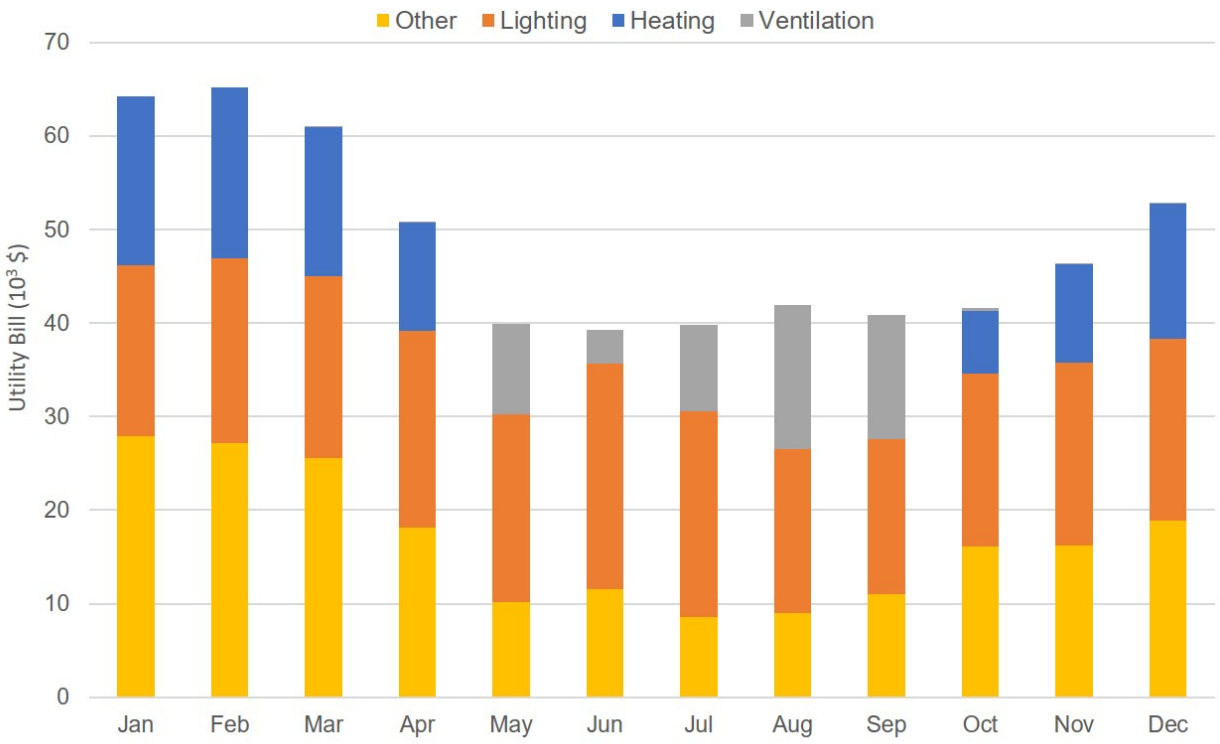

Figure 4.10: Utility costs broken down by different systems.

- Seasonal demand balance is very sensitive and any increase to the heating system of the tunnel will result in significant minimum demand charges.
- Improvements in lighting system efficiency and reduction of lighting loads will be the most beneficial retrofit.
- Self-production and storage of electricity during the winter could help offset minimum demand charges in a new tunnel renovation that increases winter-time consumption and loads.

The next chapter will explore a novel application of semi-transparent photovoltaics to tunnel sunscreen structures as an energy retrofit option that will primarily impact lighting energy use and power demand.

CHAPTER 5

Application of Semi-Transparent Photovoltaics in Transportation Infrastructure for Energy Savings and Solar Electricity Production: Towards Novel Net-Zero Energy Tunnel Design[1]

5.1 Introduction

Chapter 4 established that the lighting system of the LHLF tunnel has the highest financial potential for an energy efficiency retrofit. Reductions to the energy consumption and peak power demand of the lighting system will directly contribute to a reduction in the utility bill of the tunnel. This chapter will explore how the application of a novel semi-transparent photovoltaic sunscreen structure (STPV-SS) can provide benefits to the LHFL tunnel.

A STPV-SS is an adaptation of a sunscreen structure which is installed at the entrances and exits of underground road tunnels to reduce lighting system requirements and improve motorist visual performance (Figure 5.1). Using semi-transparent photovoltaic (STPV) ma-

[1]This is a continuation of the work presented in a journal paper (with the same title) that is in its final reviewing stage, to be published in Progress in Photovoltaics.

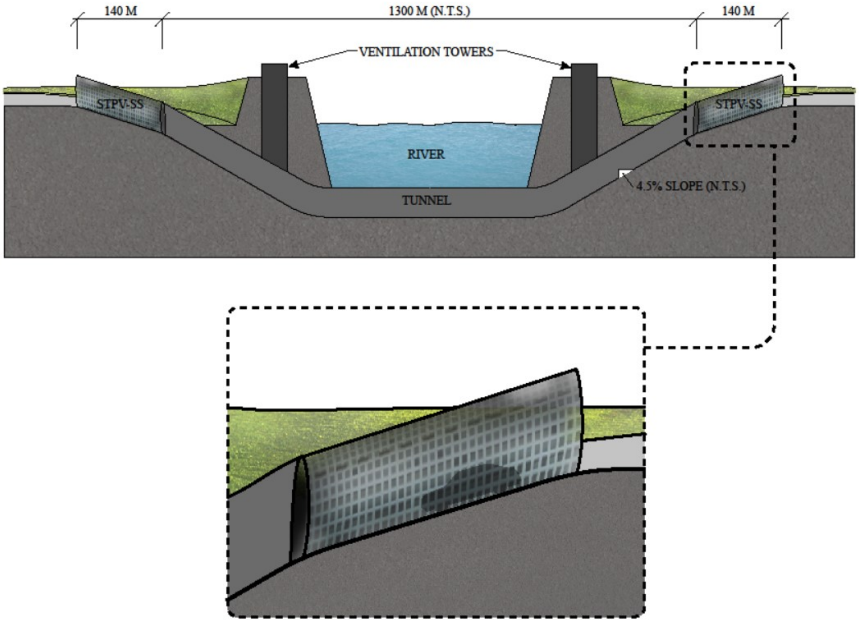

Figure 5.1: Longitudinal view of the LHLF tunnel with semi-transparent photovoltaic sunscreens (STPV/SS). Rendering by O. Kruglov.

terials to build a sunscreen structure introduces the benefits of producing solar electricity locally and transmitting visible light to supplement the tunnel lighting system [2]. Solar photovoltaics that are semi-transparent naturally fit with sunscreen structures and tunnel lighting systems because of two reasons:

1) The transparency and/or translucency of the STPV materials allows for the uniform transmission of daylight through the sunscreen structure, improving the uniformity of light on the road [2]. This addresses one of the primary problems with pergola sunscreen structures [17, 18].

2) Solar energy production profiles of properly oriented PV cells are concurrent with tunnel lighting system demands [2]. This increases the likelihood that the solar energy produced by the structure is used immediately and does not need to be stored or exported to the electric grid.

Additionally, STPV-SS structures act as partial covers and extensions to tunnels. Preliminary studies have shown that in the case of the LHLF tunnel, adding a partial shelter that sheds precipitation away will reduce demands for snow-ploughs and de-icing salts on the tunnel approaches. These two mechanisms of snow removal and de-icing greatly reduce the durability of reinforced concrete; avoiding them can reduce maintenance costs and increase the life-cycle of the tunnel. The transparency of the structure allows it to function similar to a greenhouse (see Figure 5.2), increasing the temperature inside through solar heat gains from the sun. Furthermore, a wind tunnel study showed that the convective heat transfer coefficient between the concrete road slab and air would be significantly reduced. Figure 5.3 shows that temperatures steadily decrease towards the center of the LHLF tunnel from the Westbound and Eastbound directions. The interior of the tunnel has an average surface temperature that is 2 to 3 °C warmer than exterior temperatures. Hypothetically, the STPV-SS extensions to the tunnel can further increase surface temperatures on the approaches, and deeper inside the tunnel.

The application of a STPV-SS (see Figure 5.2) that is fully integrated with the lighting, heating/de-icing, and ventilation systems of a tunnel is a financially intensive endeavour. There must be significant functional and financial incentives associated with this type of application for it to be considered in a new tunnel construction or renovation project. The innovative use of STPVs in this application stems from their dual purposes. The opaque photovoltaic cells and/or transparent photovoltaic materials act as daylighting shading devices, utilizing daylight transmission to reduce energy use, while simultaneously generating renewable energy. Both aspects play a fundamental role in designing net zero energy systems [31], including tunnels [11,63]. The energy analysis shows that current lighting design is responsible for daily peak loads. Since the tunnel lighting loads and PV generation are both concurrent with daylight hours, STPV sunscreen structures would naturally contribute to balancing the tunnel load profile [2]. Additionally, a sunscreen structure would add another functional incentive for its application by improving safety conditions for motorists.

This chapter will use the LHLF tunnel as a case study to quantitatively evaluate the following anticipated benefits associated with the application of STPV-SS structures:

i) **Reduce net-energy use of the LHLF tunnel through local PV system pro-**

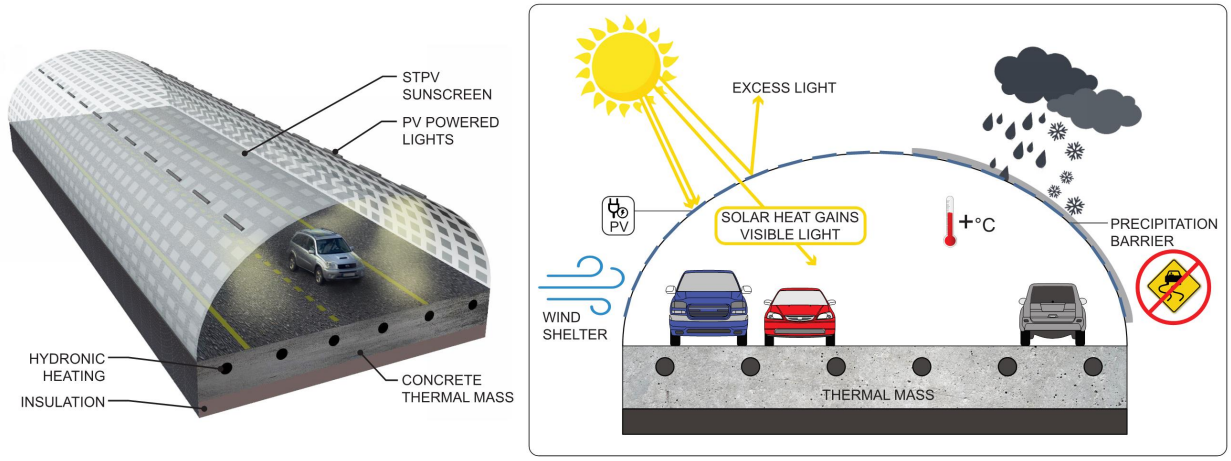

Figure 5.2: Conceptual overview of the functions of a STPV/SS. Rendering by O. Kruglov.

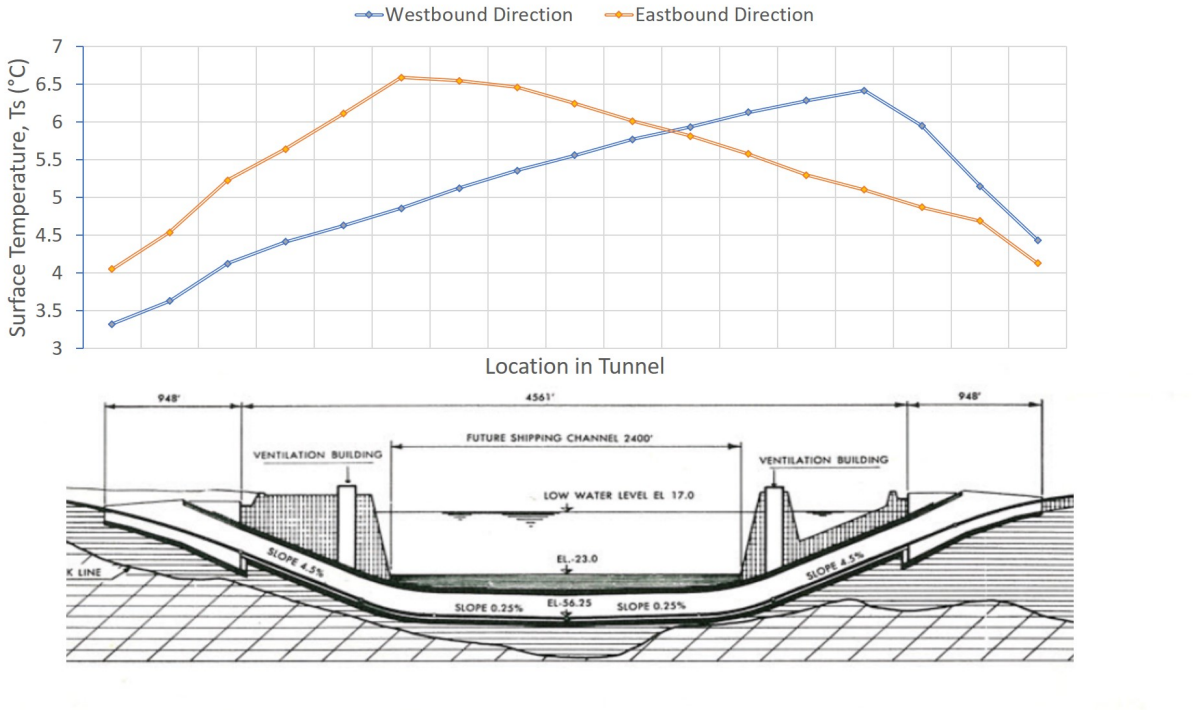

Figure 5.3: Visualization of the average road surface temperature during October and November of 2017. This data was obtained with daily measurements using mobile weather stations.

duction:

A PV model in System Advisor Model (SAM) will be used to simulate the annual and hourly energy production of the integrated STPV system component of the sunscreen structures.

ii) **Reduced net-energy use and power demand from the lighting system**:
Annual daylighting simulations will be used to generate illuminance conditions under different STPV structures. These conditions will be used as an input to the tunnel lighting model to evaluate energy savings.

iii) **Reduced annual utility bills**:
The energy savings from items i) and ii) will be applied to the tariff structure of the local utility to evaluate the potential savings on the tunnel's annual energy bill.

iv) **Improved visual performance by reducing the disability glare experienced by motorists**:
A 3D Rhinoceros model integrated with the Radiance engine will be used to simulate the uniformity of the luminous flux incident on the road surface due to daylight and the effects of disability glare on motorists from their perspective.

The next sections will go into detail about the development of the models of the LHLF tunnel and STPV-SS structures that were used to simulate and evaluate the application of STPV-SS structures.

5.2 3D Model Description

A 3D model of the east-bound and west-bound approaches and their proposed STPV sunscreens (Figure 5.4) was created using a computer-aided design software called Rhinoceros [21]. This Rhinoceros model was used in conjunction with the Radiance daylighting engine, using a graphical algorithm editor called Grasshopper, to perform the necessary simulations and evaluations.

5.2.1 Tunnel Approaches

The tunnel approaches were modeled using details from construction and renovation plans from the LHLF case study. The surrounding area which consists of flat grasslands at a slight inclination outwards were included to account for reflected light. There are also retaining walls that end flush with the surrounding grassland. These structures partially shade the surface of the road, creating an uneven distribution of light on the road.

The LHLF tunnel length is 1.3km long, however only the portions of interest were modeled because running simulations for the entire length would be computationally exhausting. It is also unnecessary since most of the structure is underground. To reduce simulation time, each of the tunnel approaches were modeled, simulated, and analyzed separately. Limitations were also applied to the physical boundaries of the model so that it would start at the safe stopping distance (SSD), 140m from the tunnel portal, and end at an appropriate distance into the tunnel where the road was no longer exposed to the sunlight. These models were used in the next section to determine the height and shape of the STPV-SS structures so that they would reduce the amount of direct sunlight exposure that drivers receive.

5.2.2 STPV-SS Structure

The STPV-SS structures were also modeled using Rhinoceros. The tunnel approaches were used as a base model where the STPV-SS models could be developed. A rendering of the proposed STPV-SS is shown in Figure 5.4. The original approach can be seen on the left; on the right, the STPV-SS sits on the edges of the retaining walls and extends 140 meters from the tunnel portal, creating a partially enclosed space. A simple half cylindrical geometry was used as a base structure for simulations and analysis so that running the Radiance daylighting engine would not be too computationally demanding. The radius of the base structure was selected based on the physical restrictions of the LHLF case study; the minimum clearance for vehicles to travel through the tunnel needed to be respected in the design and the width of the structure needed to span the distance between the surrounding retaining walls. A radius of 5m was chosen to satisfy the width and height requirements at a distance of 140m from the tunnel portal. Only the south-facing sides of the STPV SS

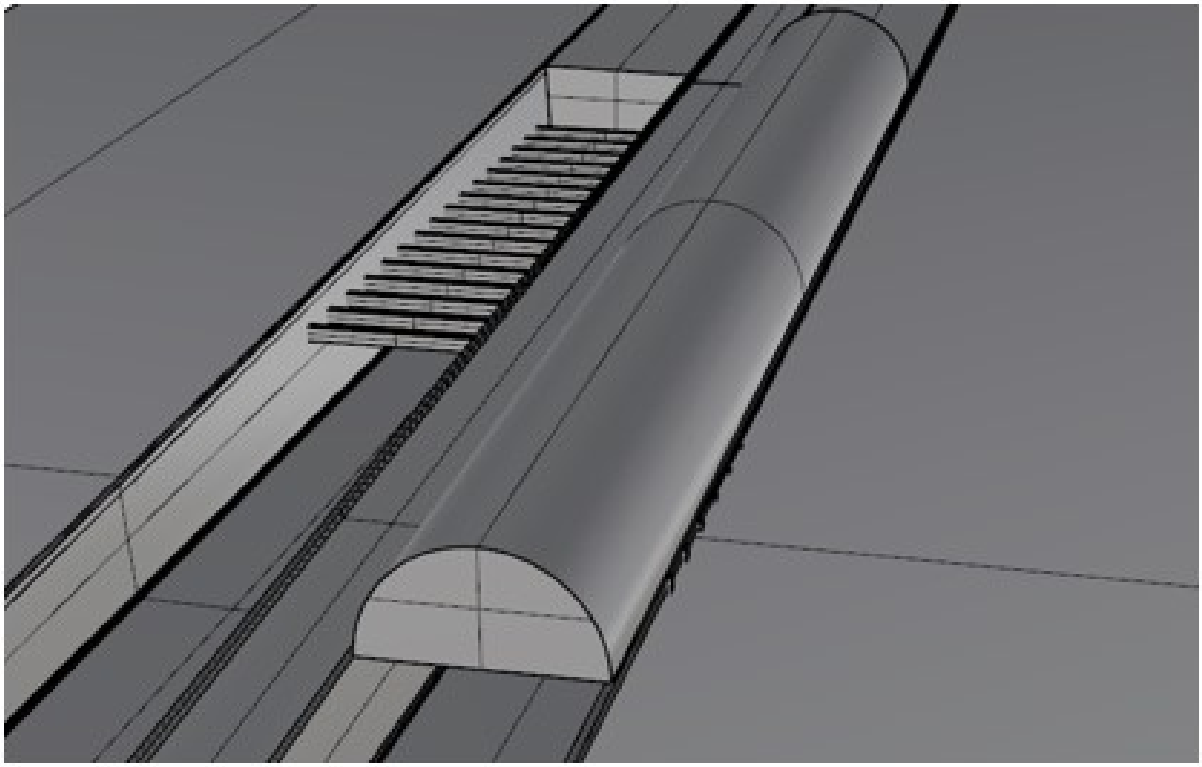

Figure 5.4: 3D Rhinoceros model of the tunnel approach with a curved surface representation of the STPV cover.

structures were integrated with photovoltaic material since the north-facing surface would not receive direct solar irradiation.

In addition to the simplified base structure, an interdisciplinary team of architects and engineers explored creative geometries for the STPV-SS structure that would fulfil the functions of a sunscreen but also have an aesthetic design that fits with the landmark area.

Models identical to the example of an STPV-SS shown in Figure 5.4 were created for each exit and entrance of the tunnel using the CAD software, Rhinoceros. Using DIVA to interface the geometry with the Radiance daylighting engine, annual simulations and visualizations were generated to evaluate lighting and glare conditions under the structure.

Scenarios

Intrinsic and matrix-based STPV technologies were considered for integration with sunscreen structures. An intrinsically transparent structure would distribute sunlight onto the

road surface more evenly and lead to better safety conditions for motorists. A structure whose transparency is matrix-based would create patterns of shadows on the road, leading to poor uniformity and increase the risk of motorists experiencing the flickering effect. However as a technology, matrix-based STPVs have much higher PV efficiencies and would be more effective at reducing net-energy use. The visible light transmittance (VLT) is another important factor that will be evaluated. The VLT of the STPV-SS is anticipated to have impacts on PV efficiency, lighting system demands, and disability glare conditions. Additionally, an intrinsically translucent STPV will be studied to determine if the transmission of diffuse light under the structure can improve uniformity conditions, as stated in [18]. Table 5.1 shows all the different scenarios that will be considered so that the anticipated benefits of a STPV-SS can be adequately evaluated:

Table 5.1: A summary of the different scenarios of STPVs that will be evaluated in this chapter.

Name of Scenario	Description of Scenario
Base	Base case scenario without any STPV-SS
I20	Intrinsically transparent STPV-SS with VLT of 20%
I30	Intrinsically transparent STPV-SS with VLT of 30%
I40	Intrinsically transparent STPV-SS with VLT of 40%
I50	Intrinsically transparent STPV-SS with VLT of 50%
IT20	Intrinsically **translucent** STPV-SS with VLT of 20%
M20	Matrix-based transparent STPV-SS with VLT of 20%
M30	Matrix-based transparent STPV-SS with VLT of 30%
M40	Matrix-based transparent STPV-SS with VLT of 40%

Simulations

The following list shows all the different simulations and models that will be used to properly evaluate the STPV-SS:

1) Annual Illuminance simulations using DIVA4Rhino to interface the Rhinoceros model

with scene inputs for the Radiance daylighting engine. The illuminance uniformity under the length of the STPV sunscreen was calculated for every hour of the year using the simulation results.

2) Visualizations using DIVA4Rhino for the same reasons as 1). Visualizations were created to show the perspective of drivers and used to analyze glare conditions by calculating the veiling luminance [3].

3) The numerical lighting model from chapter 3 (equation 3.1) and annual illuminance simulation results were used to calculate what the lighting demand would be with the addition of a STPV-SS. New lighting control activation signals were determined using simulated illuminance data as the input instead of recorded measurement data.

4) Annual energy production profiles of the STPV sunscreen system were simulated using System Advisor Model (SAM).

Radiance parameters for simulations

The radiance parameters used in all daylighting simulations were selected using the radiance primer document [7]. This document gives an overview of all the simulation parameters and provides recommended settings catered for different purposes. Preliminary simulation were done using minimum settings (see table A.1 in Appendix A) to greatly reduce simulation time. The simulations used for the analysis of the STPV-SS in this thesis were done using the 'accurate' settings from table A.1 to ensure that light reflected off of multiple surfaces are included in the results. 'Maximum' settings were not used because of the minimal improvements to the accuracy of the simulation results were outweighed by the significantly greater rendering and simulation times. Table A.2 in Appendix A gives a short overview of the impact of each parameter on simulation and rendering time.

5.3 Net-Energy Use

This section uses the case study of the LHLF tunnel to evaluate the net-energy reduction that STPV-SS structure can provide. Any improvements made to the net-energy use of the

tunnel will directly reduce the monthly and annual energy bills of the tunnel.

5.3.1 Methodology

The integration of STPVs with sunscreen structures is expected to reduce the annual energy consumption and day-time power demand of the tunnel lighting system in two ways:

i) Solar energy production that is concurrent with day-time lighting demands can be used instantly, potentially offsetting daily peaks induced by the intense lighting system and reducing net-energy use.

ii) The transparent nature of the STPVs can help avoid the activation of high intensity lighting stages by allowing motorists to naturally adapt to darker lighting conditions while under the sunscreen structure.

The energy savings from i) and ii) combine to create financial savings on annual energy bills.

Solar Energy Generation

The solar energy generation of the matrix-based and intrinsic STPV-SS structures of varying visible light transmittances (VLT) will be simulated using a software called System Advisor Model (SAM). Only the south facing sides of the susncreens should have photovoltaic material since the solar exposure of a north facing PV system will be very low. The location was set for the city of Montréal and a local weather file from Environment Canada [59] was modified so that it could be used as a model input for SAM. The total surface area available for coverage with photovoltaic material is 2420m^2 for all structures. Since the software is unable to simulate production on a curved surface, the portion of the STPV-SS covered in PV material was discretized into equivalent flat surfaces using a straight-line approximation (Figure 5.5). These surfaces were used to estimate the PV generation of the curved STPV sunscreen structures. The cumulative chordal distance of the straight line approximation had a percent difference of just 2.2% when compared to the actual curved length of the structure's real arc. This difference was considered when inputting the surface area available for PV material in the SAM model.

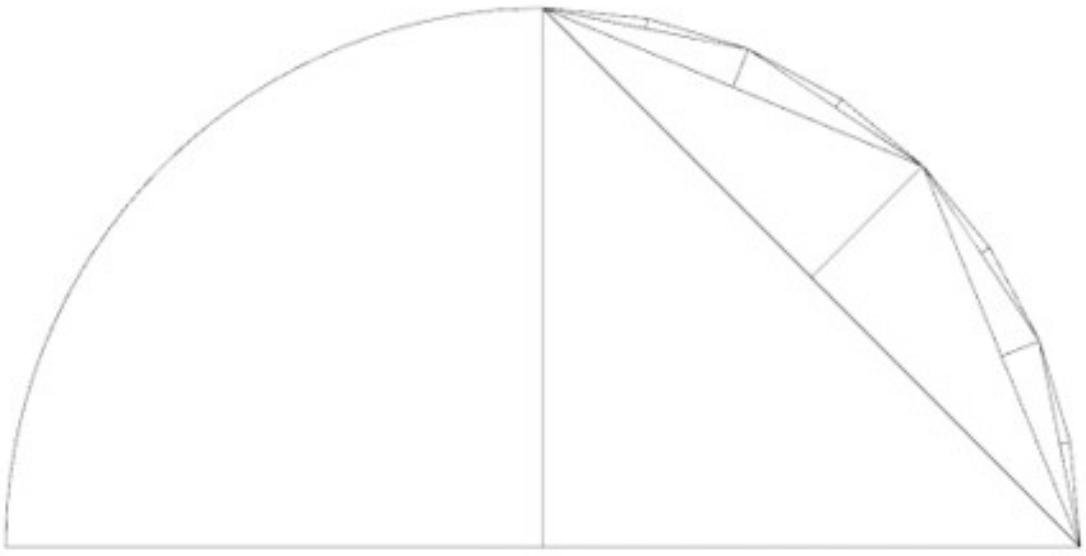

Figure 5.5: Cross-sectional view of the straight-line approximation method used to create the equivalent flat surfaces. These surfaces were used to estimate the PV generation of the STPV sunscreen structures.

Lighting System Demand

The lighting system of the tunnel was modeled in Chapter 3 using equation 3.1. The model used measurements of the luminous flux incident at the entrance of the tunnel as a control input for the level of lighting intensity required in the threshold and transition zones of the tunnel. In this chapter, it will be used to determine the reduction in lighting requirements when an STPV-SS structure is used to reduce the amount of luminous flux that is transmitted to the road. A reduction in lighting requirements would lead to a direct decrease in power demand and annual energy savings for the tunnel.

To determine the new illuminance conditions at the tunnel portals, hourly illuminance conditions were simulated using Radiance and used as the control input for the lighting model. Due to the shading from the semi-transparent sunscreens, the lighting conditions upon entering the tunnel should be more suitable for the adaptation of the human visual system, thus less intense lighting would be required. It is anticipated that this will result in significantly reduced frequency of activation of the day-time, S1 and S2 lighting stages

throughout the year while maintaining the existing standard for road illuminance in the threshold and transition zones of the tunnel.

5.3.2 Evaluation

Solar Energy Generation

The reduction in net-energy use of the STPV-SS scenarios were evaluated under the assumption that any excess power production would be exported to local utilities in exchange for energy credits. Results from the SAM simulations showed that semi-transparent photovoltaics can have significant impacts on the net-energy use of the LHFL tunnel: Table 5.2 shows that depending on the transparency and type of STPV that is used, net energy use can be reduced by 1.3% to 7.2%, annually. A trend can be observed in the effective transmittance of the structures; the structures with higher VLT have lower PV efficiencies and lower annual energy yields. Additionally, the nature of transparency of the sunscreen has an important impact; the PV efficiency of the sunscreens that used intrinsically transparent PV technologies were approximately 25% lower than structures whose transparency were matrix-based [2].

Table 5.2: PV production of each STPV SS type and transparency [2].

Scenario	$\mathbf{A_{pv}}$ (m^2)	$\mathbf{P_{max}}$ (kW)	$\mathbf{N_e}$ (%)	**Energy Generation** (MWh)	**Net Energy Reduction** (%)
I50	2420	38.72	1.6	58.5	0.9
I40		53.2	2.2	80.5	1.3
I30		67.8	2.8	102.6	1.7
I20		82.3	3.4	124.6	2.1
M40	1452	217	9.0	331.1	5.3
M30	1694	254.1	10.5	387.5	6.3
M20	1936	290.4	12	442.4	7.2

Lighting System Demand

The new lighting control activation signals resulted in a significant reduction in use of the high intensity lighting stages. Figure 5.6 shows that sunscreens with lower VLTs saw an increase in Night and Day-time lighting stages, but a significantly reduced amount of hours with the more power intensive S1 and S2 lighting stages. The reduced frequency of day-time lighting activations lead to a reduction in lighting system energy use between 9.5 and 18% (table 5.3). Once again, structures that had higher VLTs resulted in the least amount of energy savings.

Table 5.3: A summary of the energy savings resulting from reduced lighting stage activation according to radiance simulations.

Scenario	Energy Consumption (MWh)	Energy Savings (%)
Base	3475	-
I20	2850	18
I30	2927	16
I40	3037	13
I50	3147	9.5

Annual Energy Bill

The new annual energy bill for the year 2015 was calculated by subtracting the energy saved by generating solar energy and reducing day-time lighting use from the estimate made in Chapter 4, Table 4.5, and applying it to the cost of energy for Rate M consumers described in Chapter 4.6. Table 5.4 shows that STPV-SS structures with lower effective transmittances are optimal for reducing energy bills. The total savings are presented as a range since the Rate M structure has a 2-tier cost of energy that is dependant on the monthly consumption of the client and it is not possible to determine which tier the savings contribute to.

Additionally, the integration of an energy storage system for peak load shaving with the STPV-SS structure introduces the potential for even more annual savings. By strategically

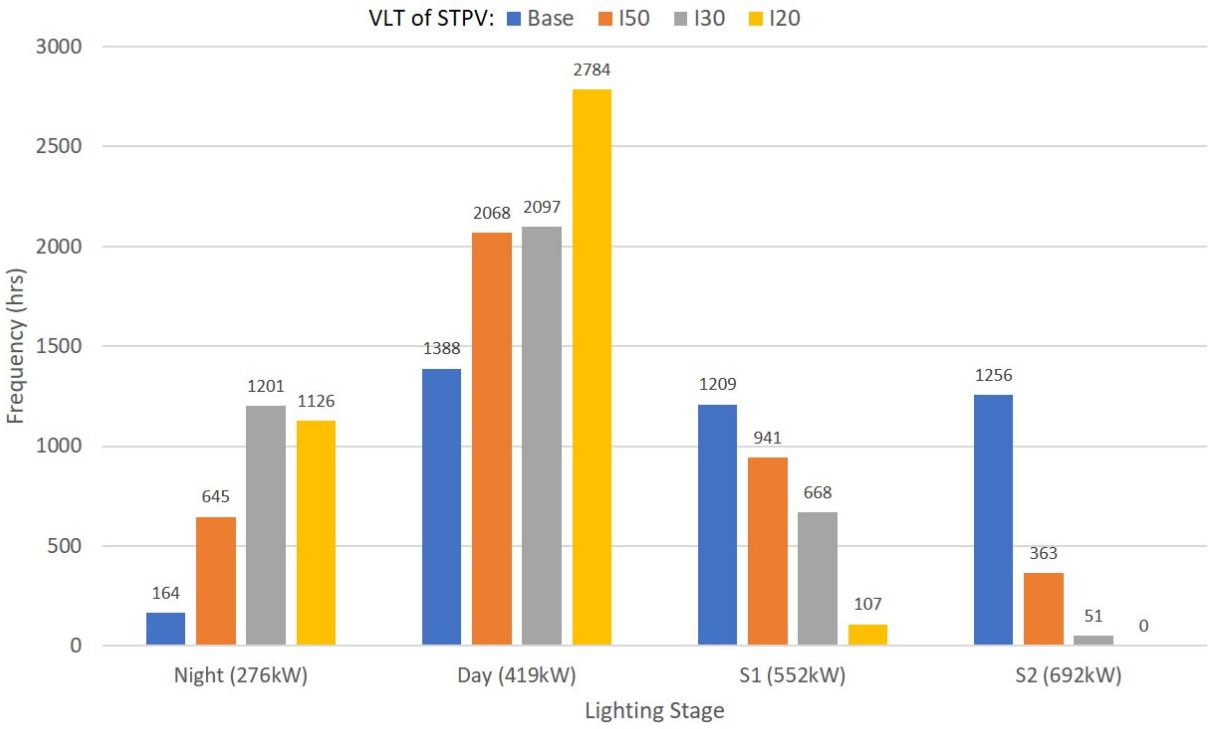

Figure 5.6: The frequency at which each lighting stage is active during the 4018 daylight hours under the application of different STPV-SS.

Table 5.4: A summary of the potential net energy and financial savings that different transparencies of STPV-SS can provide.

Scenario	**Energy Generated from PV** (MWh)	**Reduced Lighting Energy Use** (MWh)	**Total Savings** ($)
I20	124.6	625	27,735 to 37,405
I30	102.6	548	24,072 to 32,464
I40	80.5	438	19,184 to 25,872
I50	58.5	328	14,300 to 19,285

storing and using the energy produced by a photovoltaic system, monthly and annual peak loads can be reduced, leading to lower monthly demand charges [64].

5.4 Visual Safety of Drivers

A fundamental requirement in designing safe transportation infrastructure is ensuring that drivers can detect the presence and movement of objects and vehicles on the road [3, 4]. The design of tunnel lighting systems differ from conventional practices used to illuminate buildings and streets. In addition to adequately illuminating an underground space, tunnel lighting systems are also used to reduce the contrast between the outdoor and indoor environment during the day. By decreasing the contrast between the bright outdoors and dark underground, visual impairment from glare, and sudden changes in traffic conditions can be reduced. If not addressed adequately, these factors can all contribute to increased potential for accidents for motorists as they enter tunnels [2].

5.4.1 Methodology

To evaluate how well the proposed semi-transparent photovoltaic sunscreen improves motorist safety, the following will be studied:

i) The illuminance uniformity on the road surface. The luminous flux incident on the road (illuminance) throughout a typical year will be simulated using the Radiance daylighting engine. The uniformity of the illuminance will be evaluated using a metric recommended by the CIE [3].

ii) Equivalent veiling luminance (disability glare). Visualizations of all daylight hours in a year will be simulated using the Radiance daylighting engine. These will determine the amount of veiling luminance that motorists are exposed to while approaching the tunnel entrance.

New simulated conditions are expected to improve or maintain the same level of uniformity and drastically reduce the intensity and occurrence of disability glare during CGH.

Illuminance uniformity

A major principle in designing transportation lighting systems is to ensure that the contrast of brightness is adequately uniform (using 5.1) along the entire road. A phenomenon that drivers experience due to poor road illuminance uniformity is known as the flickering effect which can cause visual impairment, and in extremely rare cases, seizures. Additionally, transitioning between sections of road with high contrast can hinder the human visual system's ability to adapt and cause visual impairment [3, 4]

The CIE measures the distribution of illuminance from light sources on the road to evaluate how uniformly lit roads are and as in indicator for visual impairments such as the flickering effect. Guidelines stipulate that the uniformity coefficient, U_o of the luminous flux incident on the road surface should be greater than 0.4. U_o is defined as the ratio of the minimum measured illuminance, E_{min}, over the average measured illuminance, E_{avg}, for a given moment in time (Equation 5.1).

$$U_o = \frac{E_{min}}{E_{avg}} \tag{5.1}$$

To evaluate U_o, annual daylight simulations were used to determine the illuminance conditions on the road located before the tunnel entrances. The area defined for analysis is shown in Figure 5.7; the surface is slightly inclined at a slope of 4.5% and is 11.1m wide and

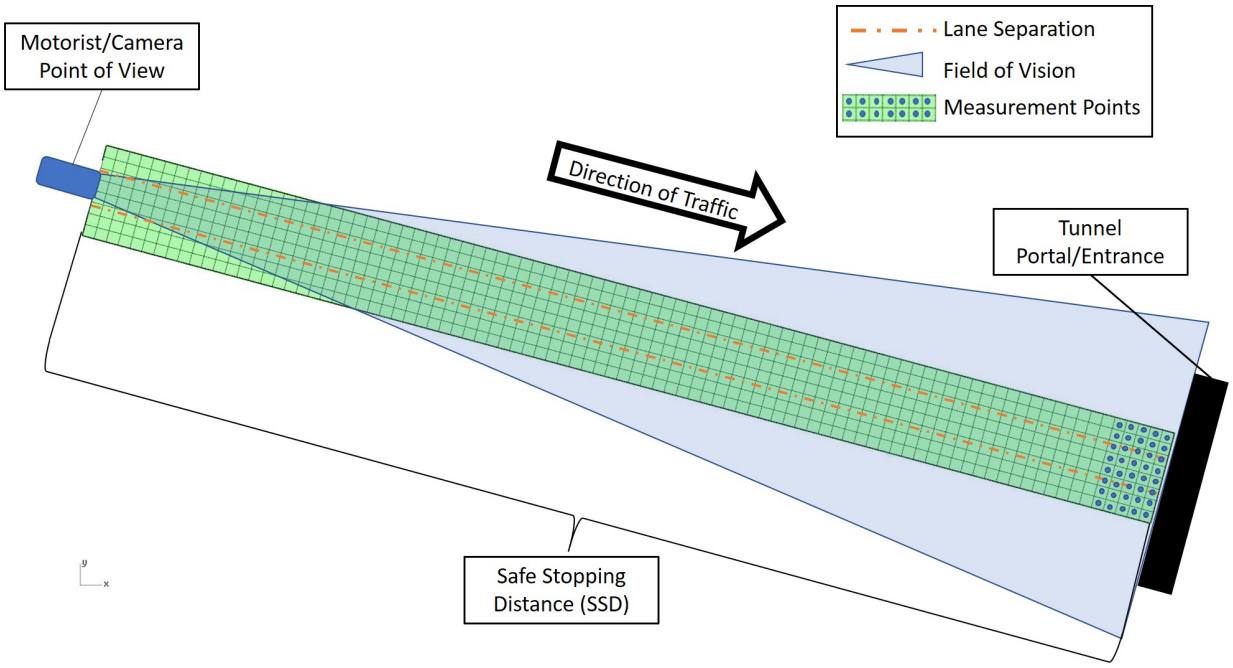

Figure 5.7: Layout of the analysis grid used for annual illuminance simulations

140m long. This area was divided into a total of 90 rows and 6 columns creating a total of 540 analysis surfaces; the average illuminance of each surface was computed using the Radiance daylighting engine. Using this information and equation 5.1, the average illuminance of each row was used to compute E_{min} and E_{avg} to observe how the luminous flux changes with progression into towards the tunnel portal. Next the uniformity coefficient was calculated for every day-light hour of the year to evaluate the performance of each STPV scenario for all possible positions of the sun.

Veiling Luminance (Disability Glare)

To get a visual idea of what drivers experience during CGH, Figure 5.8 shows visualizations generated using daylighting simulations. These figures illustrate the contrast in luminance between a glare source and its background, from the perspective of a driver at the SSD with and without a sunscreen structure shading part of the sun.

While these visualizations are enough to anecdotally understand the impact that sunscreens can have on the glare experienced by drivers, it is not enough to make any concrete conclusions. It is important to communicate to designers what this means in terms of lighting

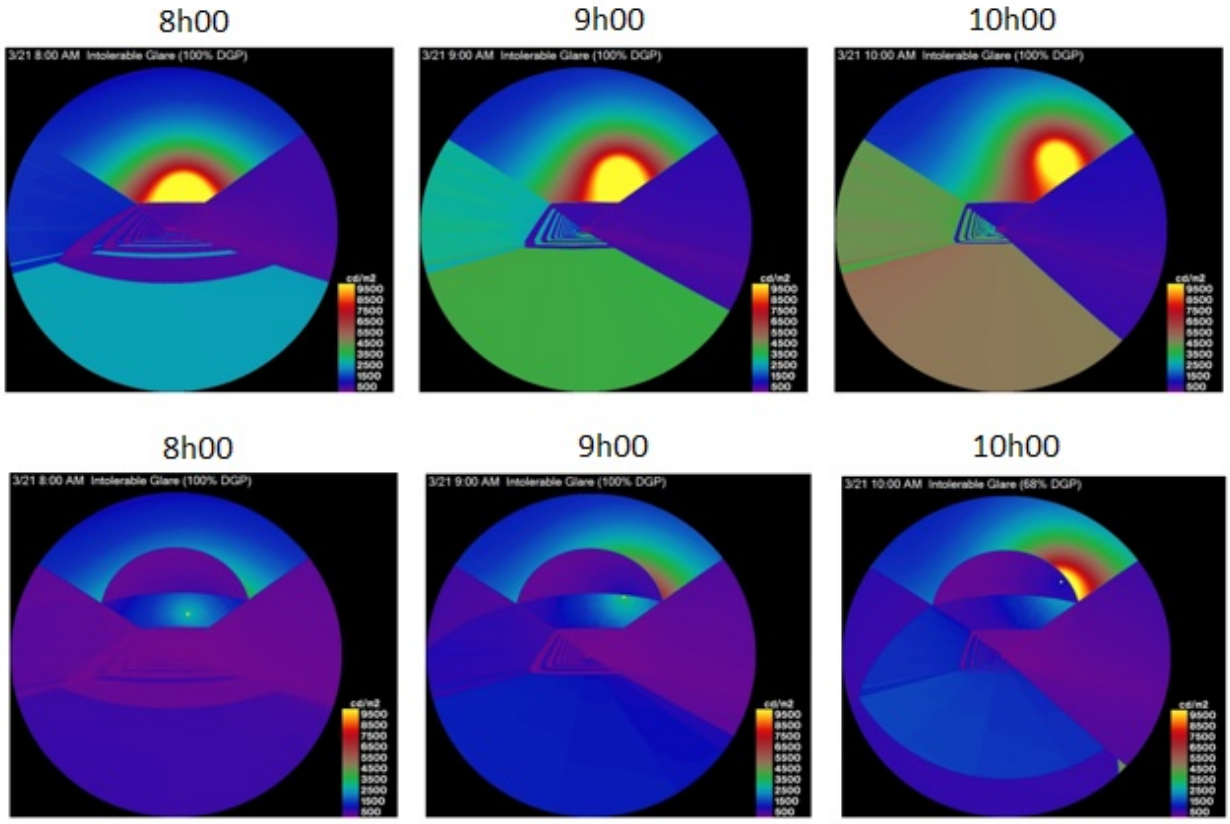

Figure 5.8: False-colour images generated using DIVA and Rhinoceros. Top: illustrates what drivers experience during CGH of the day when the sun is directly in their line of sight. Bottom: illustrates the impact that adding an intrinsically STPV-SS would have on driver experience during CGH [2].

requirements for tunnels. Tunnel lighting designers use a metric called the equivalent veiling luminance (L_{seq}) to calculate the lighting requirements inside the threshold and transition zones of the tunnel. This metric is used to quantify the loss of retinal image contrast of the human visual system (HVS) due to extreme contrast in straylight [44, 45]. It is a measure of the amount of light that is required to change contrast thresholds by the same amount as the glare source. This offsets the impact that the glare source has on the HVS.

Perspective of motorists

Point-in-time glare simulations will be used to generate the visualizations necessary to determine the equivalent veiling luminance. The Illuminating Engineering Society [4] and International Commission on Illumination [3] use similar viewpoints of tunnels to determine the luminance requirements inside the threshold zone. However, since the metric is relative to the persons' point of view, the visualizations must be generated from the perspective of motorists. This was done by placing a camera view in the virtual Rhinoceros model, at the safe stopping distance (SSD) from the South and North entrances of the tunnel (Figure 5.9). These camera views - placed at approximately the height of a seated driver - were used to simulate visualizations of motorists' perspectives (Figure 5.10) and evaluate the glare conditions for different sunscreen models. The geometry of the vehicle (window, window frame, hood, and steering wheel) was not considered since every vehicle type will have different characteristics and these details would have minimal impact on the final result. Furthermore, any additional shading caused by vehicle's geometry would reduce glare effects; therefore by ignoring vehicle geometry, the results used for analysis would be more conservative.

Critrical glare hours

In addition to the perspective of the motorist, the position of the sun is a major parameter that determines whether there will be significant disability glare. Critical glare hours (CGH) are moments when the sun is directly in the line of sight of motorists [2]. Figure 5.11 shows an example of disability glare conditions during a CGH and illustrates why they are considered a critical conditions for tunnel approaches. Through a still image, it is difficult to perceive the distance between the two neighbouring vehicles, and close to impossible to tell if there is

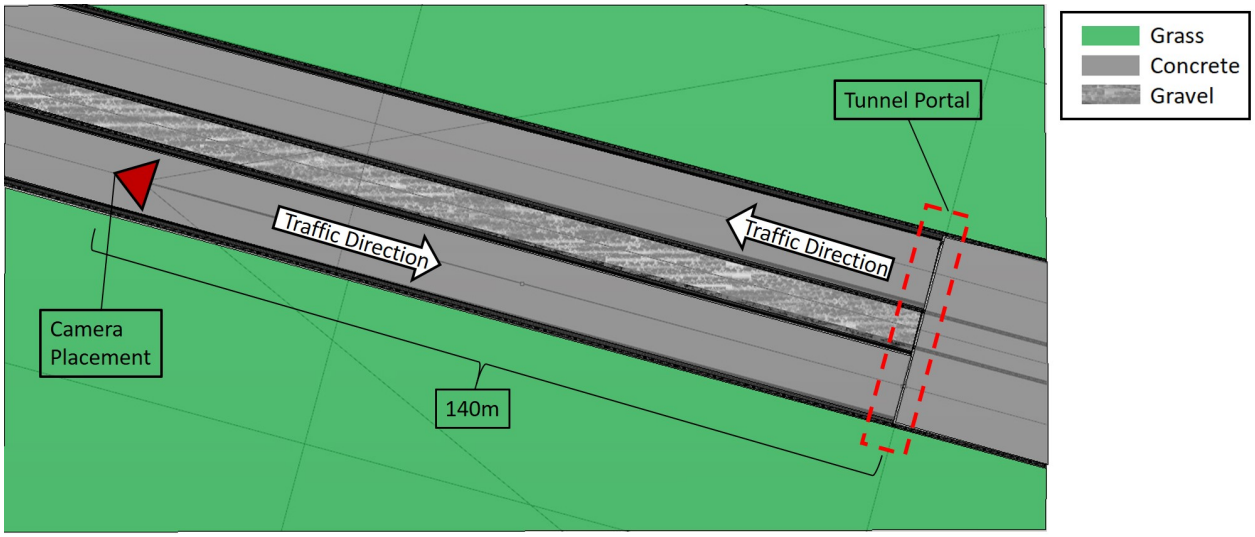

Figure 5.9: Topview of 3D rhinoceros model interfaced with DIVA - shows the placement of the camera representing motorist perspective.

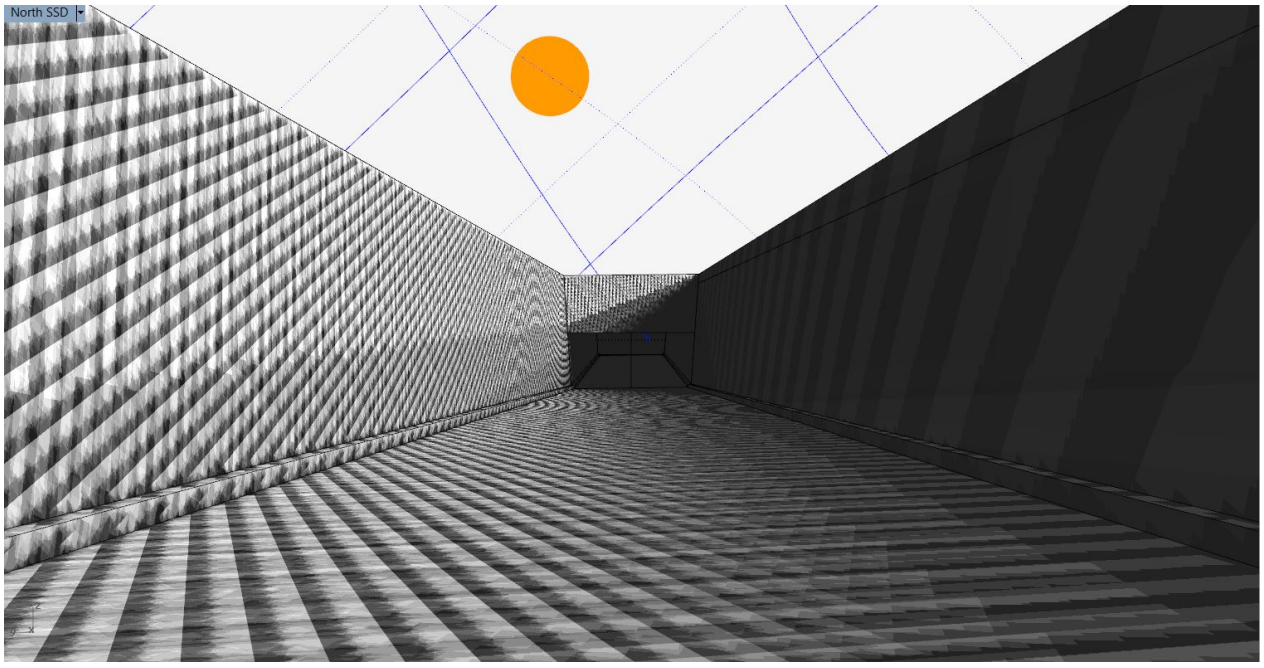

Figure 5.10: A perspective view taken from the Rhinoceros interface; this image represents the view from the camera placed at the SSD from the tunnel portal.

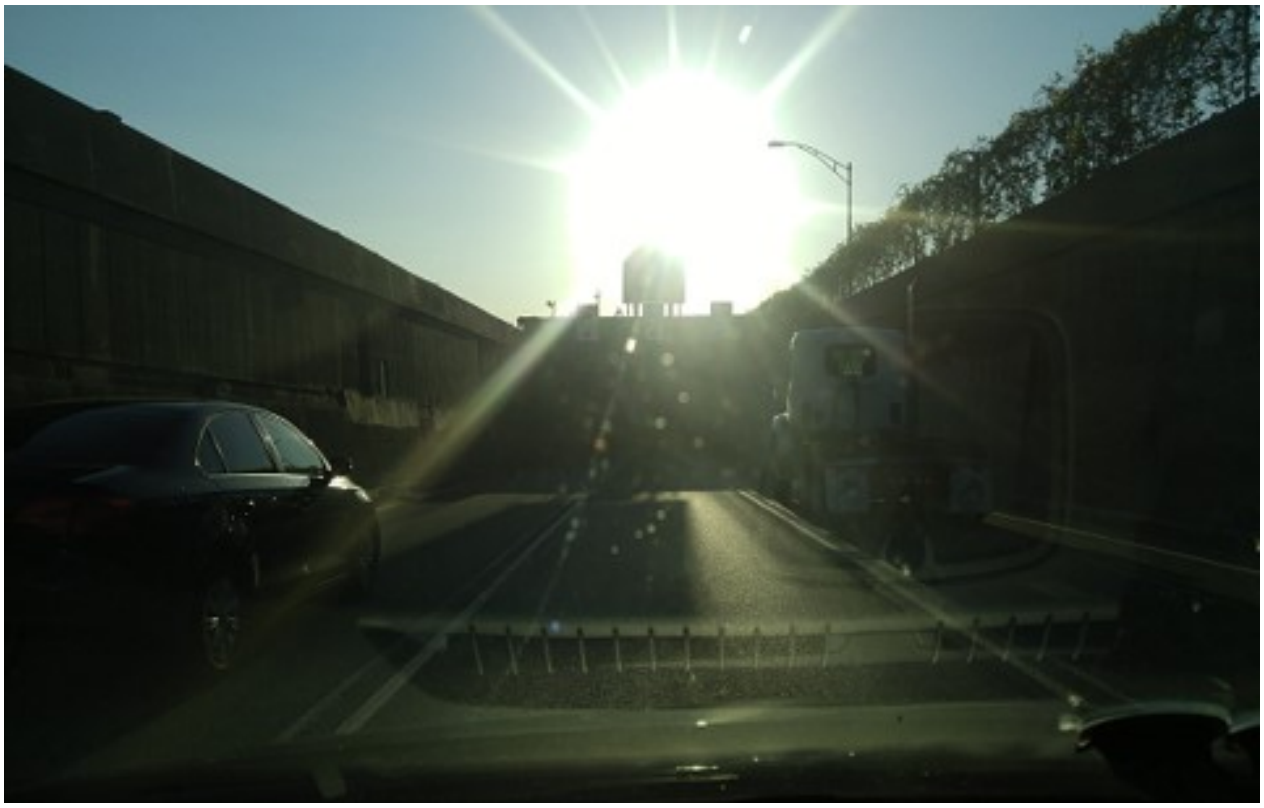

Figure 5.11: Perspective of drivers entering the tunnel Northbound circulation tube during a critical conditions. This photo was taken by D.Sun during a drive-through of the tunnel on May 24th at 7:00PM [2].

an obstruction on the road ahead. These visual impairments are even more pronounced when in a moving vehicle; considering that the posted speed limits in tunnels can range between 60 to 100 km/h, the tasks are even more difficult for motorists than illustrated in Figure 5.11.

The scenario described in Figure 5.11 occurs on a daily basis and can be easily predicted by examining the orientation of the tunnel and calculating solar angles of the sun. Moments when the sun is clearly in the viewbox of motorists as they enter the tunnel are the most dangerous and should dictate when demand for intense day-time lighting in the tunnel. These moments will be referred to as critical glare hours (CGH).

To determine when a CGH is occuring, a polar diagram was superimposed over the visualization of the motorist's perspective of the tunnel portal (see Figure 2.5). This polar diagram is used by the CIE to evaluate the contribution of each scene object on the veiling luminance subjected to motorists. CGH were defined as moments when the sun's altitude and

azimuth resulted in its placement inside the polar diagram in Figure 2.5. A sun path diagram superimposed on the 3D rhino model was used to determine when critical glare hours were most likely to occur during the year. By visualizing the perspective of a driver entering the tunnel using a camera view, it was possible to pinpoint the moments in time when the sun was directly in the field of view of drivers. For the east-bound approach, hours when the solar altitude was between 20° to 30° and the azimuth was between 0° to 30° south of east were considered critical glare hours. Similarly, critical glare hours for the west-bound approach were when the solar altitude was between 20° to 30° and the azimuth was between 0° to 30° north of west. The critical glare hours for the southbound and northbound approaches are summarized in Table 5.5.

These moments were considered to be the worst case scenarios considering that the sun is the greatest source of light in this thesis. In comparison to directly viewing the sun during CGH, reflections off the concrete walls were considered to be minor due to the poor reflectance of the surrounding materials.

Table 5.5: Critical glare hours (CGH) for the east-bound and west-bound approaches of a Louis-Hippolyte-La Fontaine Tunnel.

East-bound CGH	**West-bound CGH**
Sun-rise (Spring and Autumn)	Sun-set (Summer)
7h00 - 8h00	17h00 - 18h00
8h00 - 9h00	18h00 - 19h00
9h00 - 10h00	19h00 - 20h00
10h00 - 11h00	20h00 - 21h00

Visualizations

Having properly defined what the perspective of motorists is and when critical conditions for glare are most likely to occur, point-in-time glare simulations were used to evaluated disability glare within these parameters. Visualizations of the base and STPV scenarios were

generated and the equivalent veiling luminance was determined for every CGH and every sun-lit hour of the year using a clear-sky model. The base scenario simulations were used to demonstrate the poor visibility that motorists currently experience, and the STPV-SS scenarios were used to quantify the improvement that the structures can provide.

5.4.2 Evaluation

Illuminance uniformity

To avoid the visual flickering effect and impairment that motorists experience when travelling at high speeds in an environment with alternating bright and dark surfaces, the STPV-SS structure must transmit light uniformly on the road. Initially, matrix-based STPV technologies were the primary consideration, however results have shown that they will lead to poor illuminance uniformity on the road under the structure in all scenarios. This leads to a high probability of experiencing flicking effects. Therefore, matrix-based STPV-SS structures were not considered due to the extreme contrast illustrated in Figure 5.12. Figure 5.13 shows that using intrinsically semi-transparent PV on a sunscreen will have better uniformity. Alternatively, the integration of matrix-based STPVs with sunscreen structures can be reconsidered if they are combined with glazings with translucent finishing or directional transmission characteristics such as prismatic glazings to direct light to areas shaded by the opaque PV materials.

The recommended uniformity coefficient, U_o, is usually used to evaluate street lighting conditions at night. In these scenarios, the lighting designer usually has the ability to control uniformity by spacing and selecting appropriate luminaires [3]. When this metric is used to evaluate lighting conditions during the day when daylight and shading dictates conditions, it can be more difficult to reach the CIE recommendations. In the particular case of the LHLF tunnel, the retaining walls adjacent to the approach of the tunnel makes it inherently difficult to have uniform lighting conditions during the day, throughout the entire year. The cyclical change in solar angles is difficult to address without a structure that can dynamically adapt to current conditions.

U_o is still an applicable metric but based on the results of the base scenario (Table

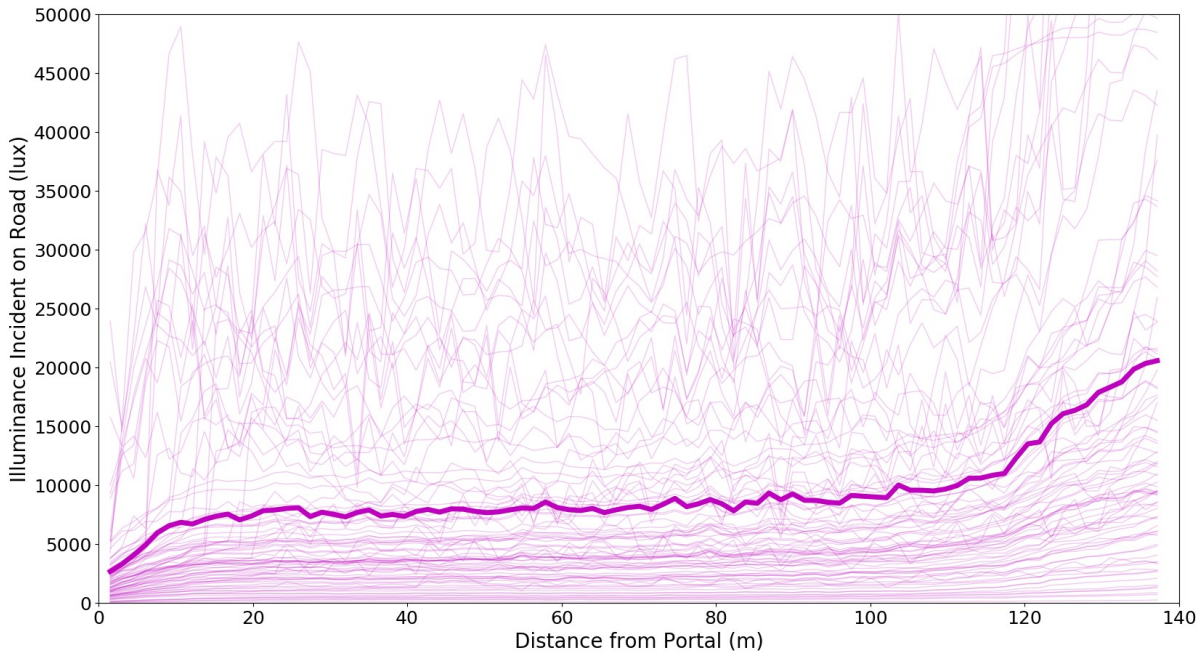

Figure 5.12: Results of annual simulations showing the luminous flux incident on the road surface at different distances - starting from the tunnel portal (left) - under the matrix-based STPV-SS structure [2].

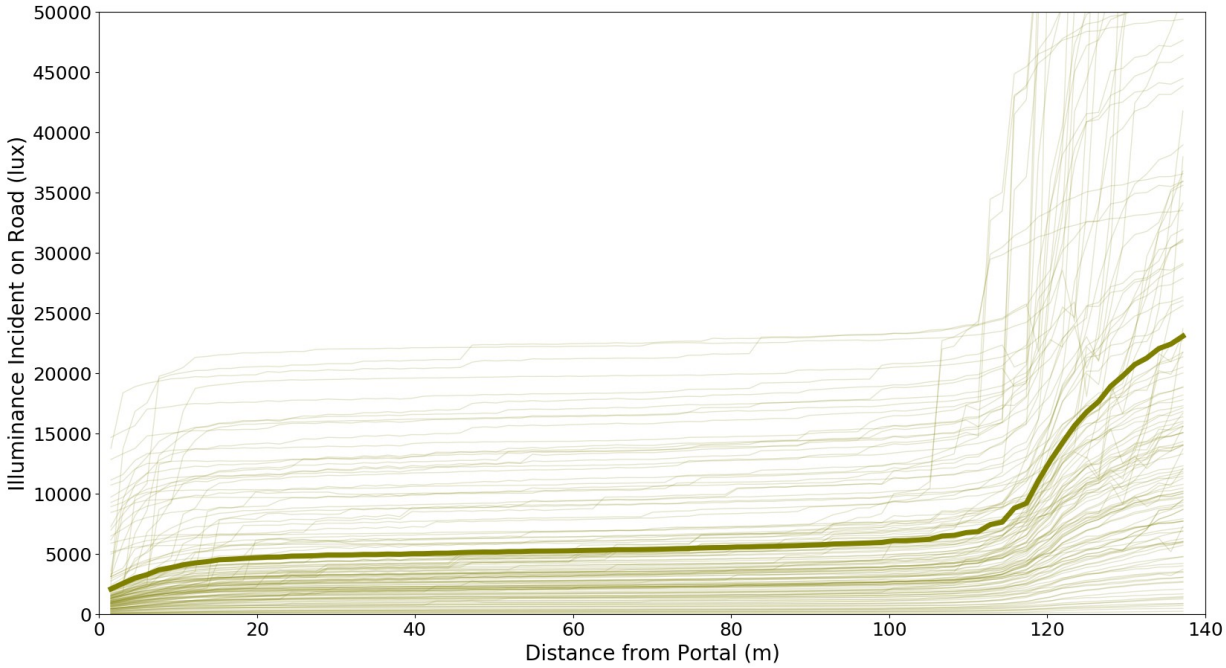

Figure 5.13: Average road surface illuminance (dark olive) under an intrinsically semi-transparent PV sunscreen with an effective transparency of 30%. The light olive lines represent hourly data [2].

5.6), the recommended minimum uniformity (0.40) may be too high of a standard given the specific conditions of underwater road tunnels entrances. The uniformity of the STPV-SS sunscreens will instead be evaluated based on their deviation from the base case simulations. Of the four transparent scenarios studied (I20, I30, I40, and I50), Table 5.6 showed that none of them resulted in any remarkable differences in uniformity coefficients. However, the IT20 scenario with translucent STPV material had uniformity coefficients that conformed to CIE recommendations and had the most consistent uniformity throughout the year. The translucent material improves the uniformity on the road because of its greater transmission of diffuse light [65]. The area of the road shaded by the retaining walls receive more light and the non-shaded surfaces are exposed to less specular direct sunlight, reducing the overall contrast under the structure.

Table 5.6: Illuminance uniformity of different STPV sunscreen structures. U_{90}, U_{75}, U_{50}, and U_{25} values are calculated for each transparency of STPV-SS. U_n is the uniformity that was exceeded 'n' percent of the time over the total number of simulations run.

Transparency (%)	$\mathbf{U_{90}}$	$\mathbf{U_{75}}$	$\mathbf{U_{50}}$	$\mathbf{U_{25}}$
Base	0.094	0.23	0.43	0.49
IT20	0.47	0.48	0.48	0.50
I20	0.11	0.26	0.43	0.48
I30	0.11	0.26	0.44	0.49
I40	0.094	0.23	0.44	0.52
I50	0.11	0.26	0.45	0.50

Veiling luminance

The veiling luminance was computed for every CGH and day-lit hour of the year to determine if the application of a STPV-SS structure could reduce visual impairment of motorists. Table 5.7 shows the veiling luminance of each STPV-SS scenario greatly reduces the occurrence of extreme CGH conditions. The most intense disability glare condition is reduced to

approximately a third.

Table 5.7: Comparison between disability glare conditions between different STPV-SS structures.

Transparency (%)	Percentiles				
	90th	**75th**	**50th**	**25th**	**Max**
	cd/m_2				
Base	6515	1748	151.4	35.8	12477
I50	2609	834.9	62.6	28.4	3710
I40	2175	590.6	57.5	24.3	3719
I30	1694	390.0	87.5	28.8	3894
I20	1132	212.4	66.9	21.6	3715

Additionally, Figure 5.14 shows the equivalent veiling luminance results of four STPV-SS structures with different VLTs (50, 40, 30, and 20%) plotted against the results of the base-case scenario. The data points are simulated CGHs and show that there are three distinct relationships that can be drawn from these results:

i) The group of data circled in Red in Figure 5.14 shows that there is roughly no change in veiling luminance. This occurs when the STPV-SS is unsuccessful in shading the sun from the perspective of motorists (Figure 5.15). During these moments, the STPV-SS has no impact, regardless of its VLT. The frequency of this type of occurrence is 608 hours out of 1395 annual CGH.

ii) The second linear relationship (center) in Figure 5.14 shows a dramatically smaller slope between STPV-SS and base case results, demonstrating that the structures are successful in reducing disability glare by an average factor of 5.66 (slope). This occurs when the STPV-SS is successful in fully shading the sun from the perspective of the driver (Figure 5.16); the transparency of the STPV-SS structures has a impact on glare conditions. The frequency of this type of occurrence is 409 hours out of 1395 annual CGH

iii) The third 2nd order polynomial relationship shows that there is still a significant decrease in veiling glare but less prominent than the 2nd relationship. The impact of the

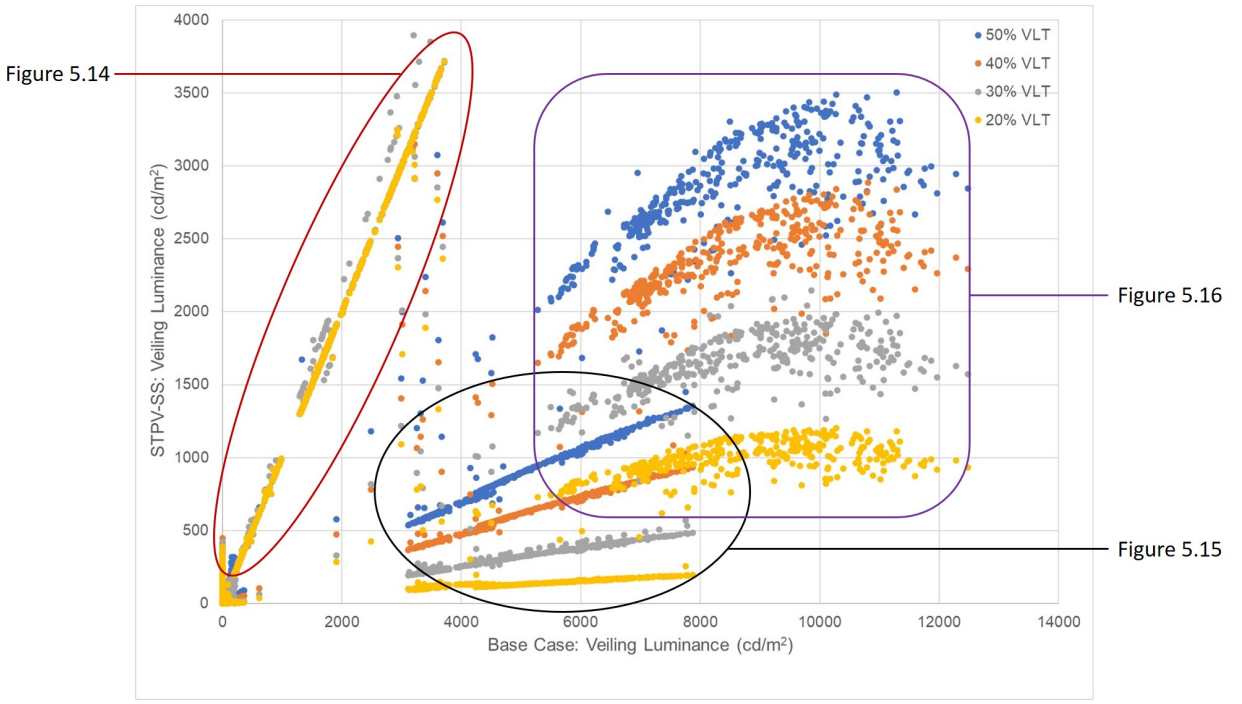

Figure 5.14: Observing the change in disability glare conditions after the application of STPV-SS structures of varying VLTs.

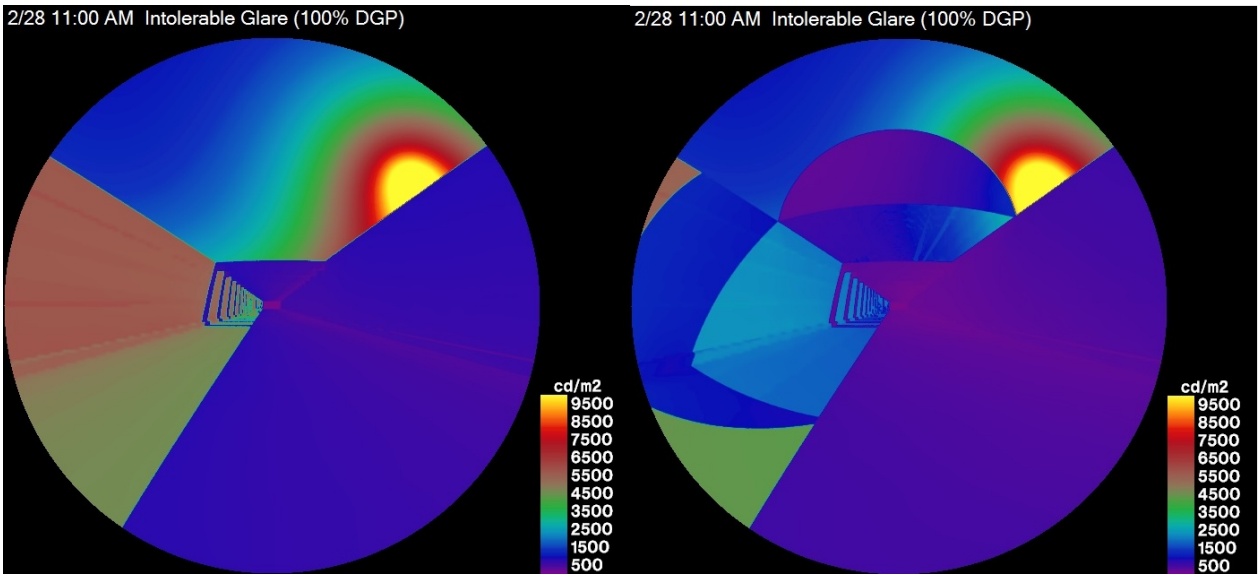

Figure 5.15: Point in time visualizations generated by the Radiance engine to illustrate the difference in disability glare (veiling luminance) between scenarios without a SS and with a STPV-SS. There was no change in veiling luminance in this scenario. VLT: 40%, Date: 02/28, Time: 11:00AM.

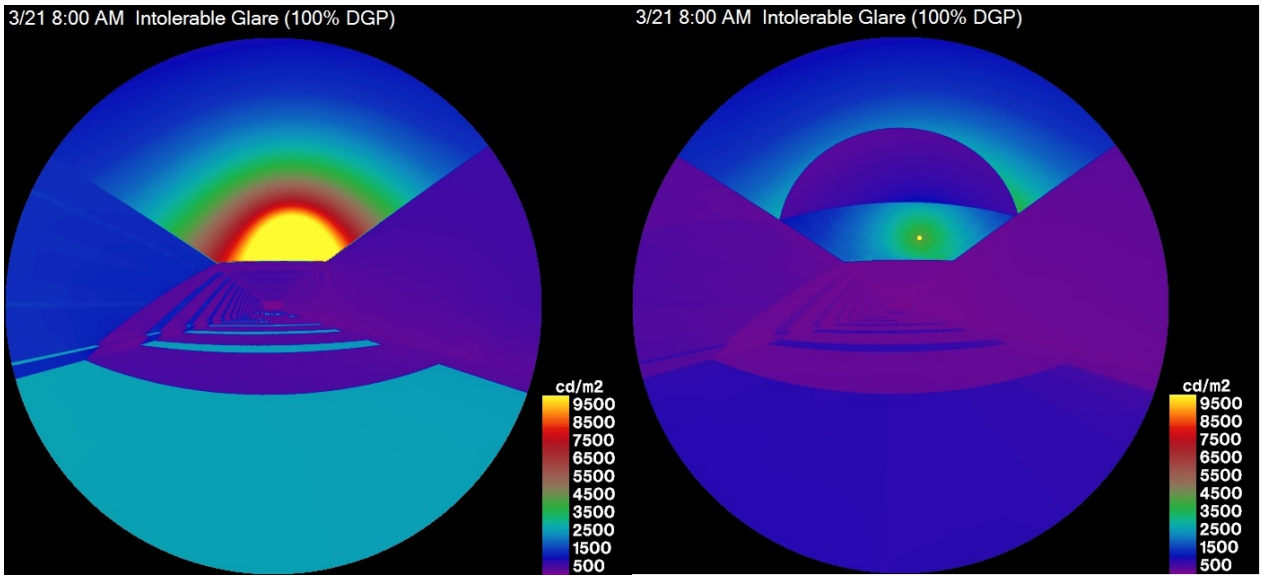

Figure 5.16: Point in time visualizations generated by the Radiance engine to illustrate the difference in disability glare (veiling luminance) between scenarios without a SS and with a STPV-SS. The shape of the STPV-SS fully shades the sun, resulting in the highest reduction in veiling luminance. VLT: 40%, Date: 03/21, Time: 8:00AM.

STPV-SS is not as prominent in these scenarios when the sun is only partially shaded by the structure and still creates significant disability glare in these conditions (Figure 5.17). The transparency of the STPV-SS structures can be increased to dramatically reduce disability glare to lower levels that can be managed by the threshold and transition zone lighting systems (see 20% VLT STPV-SS compared to 50% VLT in Figure 5.14). The frequency of this type of occurrence is 378 hours out of 1395 annual CGH

Overall, STPV-SS structures can drastically improve driver safety by reducing the veiling glare that drivers experience. Looking at the contrast between the scales of the x-axis and y-axis of Figure 5.14 shows that the worst CGH conditions in the base case were reduced by a factor of 3. Figure 5.16 illustrates the ideal function of a STPV-SS. However, due to limitations in the structures geometry, there are still many moments in the year where veiling glare is extremely high (see 'Max' column in Table 5.7). This is usually offset by the threshold and transition zone lighting systems, however, there are some cases where no lighting system can provide enough luminance to reduce veiling glare. Another option needs to be explored; for example, completely blocking critical sun positions from the field of view of motorists

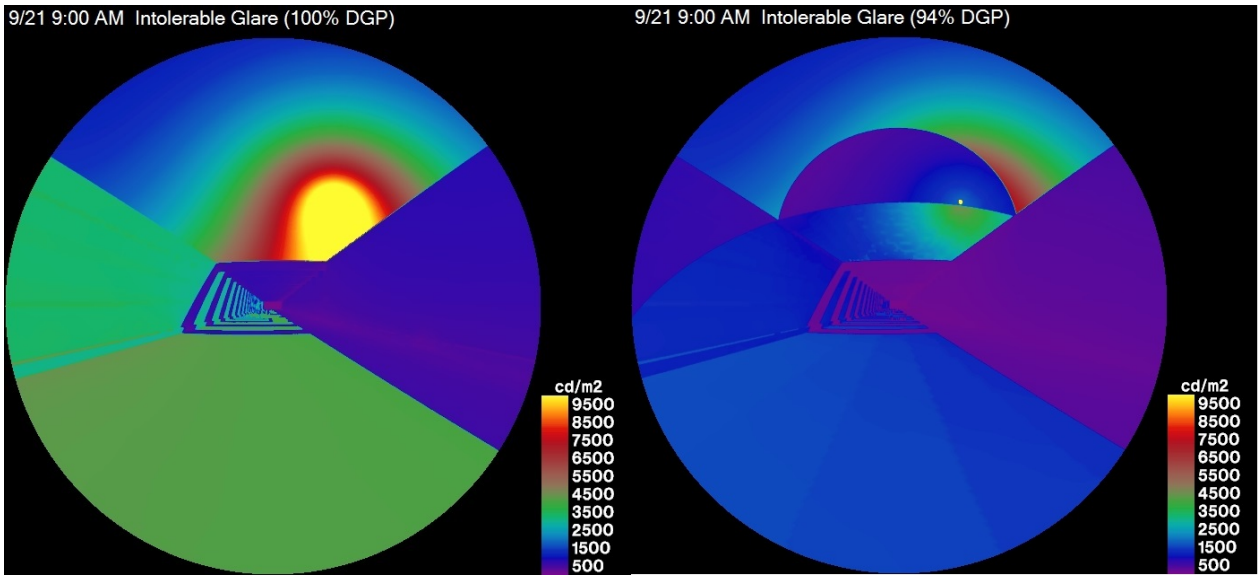

Figure 5.17: Point in time visualizations generated by the Radiance engine to illustrate the difference in disability glare (veiling luminance) between scenarios without a SS and with a STPV-SS. The shape of the STPV-SS partially shades the sun, resulting in a moderate reduction in veiling luminance. VLT: 40%, Date: 09/21, Time: 9:00AM.

with an optimized geometry for the SS would eliminate the more moments with the highest disability glare.

Recommendation

For tunnels with significant obstacles that shade the road, such as an underwater tunnel with a declination, explore a model that uses a more translucent material that has more diffuse light transmission to spread light onto the shaded parts of the road. Structures should have a higher VLT than 20% and use materials that allow for more diffuse transmission than direct transmission of light.

Limitations of Radiance

Only predefined material types include the specular indirect component of light transmitted or reflected on a surface. There exist two pre-defined translucent materials in the Radiance library that can be used to evaluate the effects of the specular indirect component of light transmitted through the STPV-SS structures. However, they do not necessarily

match the properties of the STPV materials considered in the study. A future study that calculates the diffuse light transmission using the radiosity method (RM) can be done to account for this. By considering this component of transmitted light, uniformity coefficients are expected to improve. However, the challenge in using RM is that gross simplifications of the geometry of the structure and surroundings will be made, resulting in less realistic results. Furthermore, RM cannot be used to calculate the direct component of light transmitted through the structure, and because of the differences in geometries, the calculated specular indirect component cannot be logically added the simulation results to create a complete overview of illuminance conditions.

5.5 Conclusion

This chapter has demonstrated that the LHLF tunnel has financial and safety incentives to install STPV-SS structures its approaches.

The combined net-energy savings from generating PV energy and reducing day-time lighting system demands increases the viability of PV technology in this application. While intrinsically transparent PVs have much lower annual energy generation yields than matrix-based crystalline sicilicon STPVs, they are ultimately a better selection because of the superior uniformity of light that they can provide on the road. The ability to reduce lighting system energy demands is the greatest impact that STPV-SS structures have on annual net-energy use. In some cases, the energy saved from reducing the activation of day-time lighting stages is more than 5 times greater than the energy produced from the STPVs.

Alternatively, matrix-based STPV-SS can be used to greatly reduce the net energy use of tunnels because of their superior PV efficiencies (Figure 5.2), however this will come at the cost of reducing illuminance uniformity on the road. Certain measures can be taken to improve uniformity of these structures such as using glazings that have translucent finishes or directional light transmission characteristics to reduce the effect of shadows on the road.

STPV-SS structures are most valuable when it come to improvements to motorist safety through reducing disability glare during critical glare hours. By reducing extreme glare conditions by a factor of 3, and reducing worst case disability glare conditions from over

12,000 cd/m_2 to 3900 cd/m_2, the structures can reduce the risk of incidents due to the black hole effect. These effects can be even greater with an improved structure with an shape optimal for shading the sun during CGH.

CHAPTER 6

Conclusion

6.0.1 Conclusion

This thesis has presented a study of the major electrical service systems of underground road tunnels. Literature and a survey of tunnels around the world have indicated that lighting, ventilation, and, when present, heating systems are the greatest consumers of energy. The typical functions of these systems were studied and an overview of renovation projects specific to these systems was presented. Semi-transparent photovoltaic sunscreen structures (STPV-SS) were identified as a renovation that can provide improvements to all major systems (specifically lighting) and improve the safety of motorists.

To identify which system had the highest financial potential for an energy retrofit, the utility bill of the Louis-Hippolyte-La Fontaine tunnel was studied in depth by developing numerical models of the major service systems. The monthly energy consumption and 15-minute power demand of its three most energy intensive systems were estimated; these major systems were confirmed to be (in order of decreasing magnitude: the lighting, heating, and ventilation systems. The lighting system was the largest consumer of annual energy, while heating was responsible for the annual peak load of the tunnel. After applying the rate structure of the local utility to these major system loads, lighting was estimated to have the

highest financial cost over the course of a year.

The residuals that were not modeled were studied analytically using the difference between the total power demand of the tunnel and the power demand of the three modeled systems. Through analysing these Residuals, a continuous base load and variable loads were observed in the data and it was concluded that they could reasonably be attributed to basic building system services and plug loads that were described in Chapter 4. Temperature dependent loads were also observed in the data that were due to cooling and heating in occupied spaces and un-modeled elements from the heating subsystem.

Having determined lighting as the system with the highest potential for energy retrofitting, a STPV-SS was presented as a solution. An estimate of the potential financial savings that would result from the installation of STPV-SS was calculated. The savings were a result of net-energy use from a reduction in lighting demand and energy production from the integrated STPV system. This dual function of STPV integrated sunscreen structures resulted in annual savings ranging between 14,000 to 37,000$. Energy generation and lighting energy savings increased when structures with lower a transparency was used. These annual savings can be used as a foundation to calculate the payback period of investing in STPV-SS for the LHLF tunnel.

Using STPV-SS structures lead to major improvements in the visual performance of motorists entering the tunnel by reducing disability glare by shading the sun during critical glare hours (CGH). During CGHs, the veiling luminance is so great that it results in threshold lighting requirements so large that they are unrealistic to implement. As an alternative, STPV-SS structures as shading devices that reduce the direct transmission of light from the sun can reduce glare conditions to levels that are more manageable by lighting systems. It has been demonstrated that when these structures are shading the sun, veiling luminance values can be reduced to threshold lighting requirements that are outlined in international guidelines for tunnel lighting [3], [4]. Resulting glare conditions were reduced when structures with lower effective visible light transmissions were analyzed.

Additionally, conventional sunscreen structures, such as paralumes and pergola structures [18], [17] can result in poor illuminance uniformity ratios and flickering effects that impair the vision of motorists. Daylighting simulation results showed that matrix-based

STPV-SS structures can cause the same uniformity and flickering effect problems as conventional sunscreens. These issues can be potentially be resolved by combining the structures with glazings that have translucent finishing or directional light transmission properties. Alternatively, intrinsically STPV technologies with translucent exterior finishes are better suited for integration with sunscreen structures because they are better at maintaining illuminance uniformity ratios on road surfaces and avoiding issues with flickering by evenly distributing transmitted light in all directions.

The approaches of underground tunnels are the areas with the highest risk for vehicular conditions due to their declination, the tendency for vehicles to abruptly reduce their speeds, and the most potential for large contrast in illumination. Using STPV-SS structures to create a solar powered threshold lighting zone, designers will be better equipped to improve the safety and visual performance of motorists in this area with adequate illuminance uniformity ratios and lower magnitudes of disability glare.

Bibliography

[1] I. Mocanu, J. Peeling, J. Potter, J. Rands, and M. Wayman, "REETS : Assessment of technologies with potential for energy reduction," tech. rep., CEDR Transnational Road Research Programme, 2015.

[2] D. Y.-J. Sun, A. K. Athienitis, and K. D. Avignon, "Application of Semi-Transparent Photovoltaics in Transportation Infrastructure for Energy Savings and Solar Electricity Production: Towards Novel Net-Zero Energy Tunnel Design," (Montreal, Canada), pp. 1496–1503, EU PVSEC, 2018.

[3] CIE 2004, "CIE 88:2004. Guide for the lighting of road tunnels and underpasses," 2004.

[4] I. E. Society, "Tunnel Lighting," tech. rep., 2011.

[5] K. Kapsis, *Modelling, Design and Experimental Study of Semi-Transparent Photovoltaic Windows for Commercial Building Applications*. PhD thesis, Concordia University, apr 2016.

[6] C. Kapsis, "Lecture 4: Advanced Lighting Calculations in BLDG6731 Building Illumination and Daylighting," 2016.

[7] G. Antonutto and A. Mcneil, "Radiance Primer," tech. rep.

[8] Ministère des Transports Québec, *Manuel d'exploitation: Tunnel Louis-Hippolyte-La Fontaine*. 2011.

[9] Hydro-Québec, "Electricity Rates Effective April 1, 2016.," tech. rep., Hydro-Québec, 2016.

[10] I. Mocanu, P. Nitsche, J. Peeling, J. Rands, and M. Wayman, "REETS : Realistic Energy Efficient Tunnel Solutions Initial review of technologies," tech. rep., CEDR Transnational Road Research Programme, 2015.

[11] R. Dzhusupova, J. F. G. Cobben, and W. Kling, "Zero energy tunnel: Renewable energy generation and reduction of energy consumption," in *Universities Power Engineering Conference (UPEC), 2012 47th International*, (London, UK), pp. 1–6, 2012.

[12] U. department of energy, "Photovoltaic Cell Basics," 2013.

[13] A. O. Abdul Salam and K. A. Mezher, "Energy saving in tunnels lighting using shading structures," *Proceedings of 2014 International Renewable and Sustainable Energy Conference, IRSEC 2014*, no. October 2014, pp. 519–524, 2014.

[14] D. Drakou, C. Burattini, F. Bisegna, and F. Gugliermetti, "Study of a daylight 'filter' zone in tunnels," *2015 IEEE 15th International Conference on Environment and Electrical Engineering, EEEIC 2015 - Conference Proceedings*, no. June, pp. 649–652, 2015.

[15] A. Peña García, L. Gil-Martín, A. Espín Estrella, and F. Aznar Dols, "Energy saving in road tunnels by means of transparent tension structures," in *International Conference on Renewable Energies and Power Quality*, 2010.

[16] A. Peña-Garćia, L. M. Gil-Martin, R. Escribano, and A. Espín-Estrella, "A scalemodel of tension structures in road tunnels to optimize the use of solar light for energy saving," *International Journal of Photoenergy*, vol. 2011, no. September, 2011.

[17] A. Peña-garcía and L. M. Gil-martín, "Study of pergolas for energy savings in road tunnels. Comparison with tension structures," *Tunnelling and Underground Space Technology*, vol. 35, pp. 172–177, apr 2013.

[18] L. M. Gil-Martín, A. Gómez-Guzmán, and A. Peña-García, "Use of diffusers materials to improve the homogeneity of sunlight under pergolas installed in road tunnels portals for energy savings," *Tunnelling and Underground Space Technology*, vol. 48, pp. 123–128, 2015.

[19] Z. Zhang, Y. Zou, and Z. Gou, "Lighting Analysis at Access Zone of Tunnel Entrance of IJEScA," vol. 3, no. May, pp. 97–110, 2016.

[20] A. S. Derakhtenjani, A. K. Athienitis, and K. D'Avignon, "Analysis of thermal dynamics of hydronic de-icing system designs by means of control-oriented thermal models," no. October, pp. 21–25, 2019.

[21] S. Lykke, E. Skotting, J. Ebben, and M. Braestrup, "Fire hazard mitigation for the Øresund link immersed tunnel," *Proceedings of the IABSE Colloquium*, pp. 251–262, 1998.

[22] PIARC Committee on Road Tunnels. Working Group 1. and Permanent International Association of Road Congresses., "Réduction du cout dexploitation des tunnels routiers : rapport et recommandations = Reduction of operational cost of road tunnels : report and recommendations," tech. rep., 1999.

[23] F. Salata, I. Golasi, S. Bovenzi, E. Vollaro, F. Pagliaro, L. Cellucci, M. Coppi, F. Gugliermetti, A. Vollaro, F. Salata, I. Golasi, S. Bovenzi, E. D. L. Vollaro, F. Pagliaro, L. Cellucci, M. Coppi, F. Gugliermetti, and A. D. L. Vollaro, "Energy Optimization of Road Tunnel Lighting Systems," *Sustainability*, vol. 7, pp. 9664–9680, jul 2015.

[24] A. Peña-García and T. P. L. Nguyen, "A global perspective for sustainable highway tunnel lighting regulations: Greater road safety with a lower environmental impact," *International Journal of Environmental Research and Public Health*, vol. 15, no. 12, 2018.

[25] Government of Canada, "Tecnological Readiness Levels," 2018.

[26] A. Peña-García, J. López, and A. Grindlay, "Decrease of energy demands of lighting installations in road tunnels based in the forestation of portal surroundings with climbing plants," *Tunnelling and Underground Space Technology*, vol. 46, pp. 111–115, 2015.

[27] G. Kavlak, J. McNerney, and J. E. Trancik, "Evaluating the causes of cost reduction in photovoltaic modules," *Energy Policy*, vol. 123, no. October, pp. 700–710, 2018.

[28] F. québécoise des coopératives forestières, "Commission sur les enjeux énergétiques du Québec," tech. rep., 2013.

[29] Y. Poissant, L. Dignard-bailey, and P. Bateman, "Photovoltaic Technology Status and Prospects Canadian Annual Report 2015," tech. rep., Natural Resources Canada, 2015.

[30] L. M. Fraas, *Low-Cost Solar Electric Power*. 2014.

[31] A. Athienitis and W. O'Brien, *Modeling, Design, and Optimization of Net-Zero Energy Buildings*. Montreal: Ernst & Sohn, 2015.

[32] S. A. Kalogirou, "Building integration of solar renewable energy systems towards zero or nearly zero energy buildings," *International Journal of Low-Carbon Technologies*, vol. 10, pp. 379–385, dec 2015.

[33] Z. Ioannidis, *Double Skin Facades Integrating Photovoltaic Panels, Motorized Shades and Controlled Air Flow*. PhD thesis, Concordia University, 2016.

[34] L. Aresti, R. Agathokleous, P. Christodoulides, and S. A. Kalogirou, "Air flow effect on the temperature of a building integrated PV-panel," p. 6, 2013.

[35] G. Bizzarri, M. Gillott, and V. Belpoliti, "The potential of semitransparent photovoltaic devices for architectural integration: The development of device performance and improvement of the indoor environmental quality and comfort through case-study application," *Sustainable Cities and Society*, vol. 1, pp. 178–185, oct 2011.

[36] M. Makha, P. Testa, S. B. Anantharaman, J. Heier, S. Jenatsch, N. Leclaire, J.-N. Tisserant, A. C. Véron, L. Wang, F. Nüesch, and R. Hany, "Ternary semitransparent

organic solar cells with a laminated top electrode.," *Science and technology of advanced materials*, vol. 18, no. 1, pp. 68–75, 2017.

[37] Federal Highway Administration (FHWA), "Alternative Uses of Highway Right-of-Way - Accomodating Renewable Energy Technologies and Alternative Fuel Facilities," 2012.

[38] P. M. Jochems, *The potential of PV panels near road infrastructure in the Netherlands*. PhD thesis, Eindhoven, 2012.

[39] D. Ponder, J. Proudfoot, and S. Luftig, "Solar Highway Program: From Concept to Reality: A Guidebbook for Departments of Transportation to Develop Solar Photovoltaic Systems in the Highway Right-of-Way," tech. rep., 2011.

[40] C. Kapsis, "Lecture 2: Fundamentals: Basic Concepts and Lighting Metrics," 2017.

[41] J. B. Murdoch, *Illuminating Engineering: From Edison's Lamp to the LED*. New York: Vision Communications (2003), 2nd editio ed., 2003.

[42] C. Reinhart, *Daylighting Handbook 1: Fundamentals Designing with the Sun*. Cambridge: Christoph Reinhart, 2013.

[43] E. J. Patterson, G. Bargary, and J. L. Barbur, "Understanding disability glare: light scatter and retinal illuminance as predictors of sensitivity to contrast," *Journal of the Optical Society of America A*, vol. 32, no. 4, p. 576, 2015.

[44] T. Kruisselbrink, R. Dangol, and A. Rosemann, "Photometric measurements of lighting quality: An overview," *Building and Environment*, vol. 138, no. February, pp. 42–52, 2018.

[45] T. M. Aslam, D. Haider, and I. J. Murray, "Principles of disability glare measurement: An ophthalmological perspective," *Acta Ophthalmologica Scandinavica*, vol. 85, no. 4, pp. 354–360, 2007.

[46] W. K. Osterhaus, "Discomfort glare assessment and prevention for daylight applications in office environments," *Solar Energy*, vol. 79, no. 2, pp. 140–158, 2005.

[47] J. Vos, B. Cole, H. Bodmann, C. Elisa, T. Takeuchi, and T. Van Den Berg, "Cie equations for disability glare," *CIE Collection*, vol. 135, pp. 1–9, 01 2002.

[48] J. J. Vos, "OPTOMETRY On the cause of disability glare and its dependence on glare angle , age and ocular pigmentation," *Clinical and Experimental Optometry*, pp. 363–370, 2003.

[49] J. Vos, "Disability glare - a state of the art report," *Computers in Entertainment - CIE*, vol. 3, 12 1984.

[50] L. Holladay, "Action of a Light-Source in the Field of View in Lowering Visibility," *Journal of the Optical Society of America*, vol. 14, no. 1, 1926.

[51] L. A. Issolio, P. A. Barrionuevo, S. A. Comastri, and E. M. Colombo, "Veiling luminance as a descriptor of brightness reduction caused by transient glare," *Journal of the Optical Society of America A*, vol. 29, no. 10, p. 2230, 2012.

[52] G. A. Fry and M. Alpern, "The effect of a peripheral glare source upon the apparent brightness of an object," *J. Opt. Soc. Am.*, vol. 43, pp. 189–195, Mar 1953.

[53] J. Wienold and J. Christoffersen, "Evaluation methods and development of a new glare prediction model for daylight environments with the use of CCD cameras," *Energy and Buildings*, vol. 38, no. 7, pp. 743–757, 2006.

[54] J. A. Jakubiec and C. F. Reinhart, "The 'adaptive zone'-A concept for assessing discomfort glare throughout daylit spaces," *Lighting Research and Technology*, vol. 44, no. 2, pp. 149–170, 2012.

[55] G. Antonutto and A. Mcneil, "Radiance Online," 2017.

[56] R. Mcneel, "Rhinoceros 5 User's Guide Table of Contents Section I: Introduction," 2014.

[57] S. Davidson, "Grasshopper Algorithmic Modeling for Rhino," 2019.

[58] J. Niemasz, "Diva For Rhino," 2019.

[59] Environment Canada, "Canadian Climate Normals 1981-2010 Station Data - Climate - Environment and Climate Change Canada," tech. rep., 2017.

[60] Hydro-Québec, "Hydro-Québec."

[61] Statistics Canada, "Survey of Commercial and Institutional Energy Use (SCIEU)," tech. rep., 2016.

[62] ANSI/ASHRAE, "ASHRAE Guideline 14-2002 Measurement of Energy and Demand Savings," *Ashrae*, vol. 8400, p. 170, 2002.

[63] K. Janssen, J. Lantinga, and J. Naber, "Working Towards a Zero-Energy Tunnel." 2017.

[64] M. I. H. Omer, *Peak Load Shaving and Power Quality Improvement for the Louis-Hippolyte-La Fontaine Tunnel in Montréal*. PhD thesis, Concordia University, 2018.

[65] A. Jacobs, *Cookbook*. No. October, 2014.

APPENDIX A

Radiance Parameters

The Radiance engine has a series of parameters (shown in table A.1 that are used to determine the quality of simulations and results. These parameters can be manually adjusted to the user's preference, however there are also pre-determined settings that can be used. A description of each parameter's effect on the execution time of the simulations is given in table A.2.

Table A.1: Description of the pre-determined radiance parameters settings for different quality of simulations, adapted from [7].

Parameter	Description	Simulation Quality				Notes
		Min	Fast	Accu	Max	
ps	pixel sampling rate	16	8	4	1	
pt	sampling threshold	1	.15	.05	0	
pj	anti-aliasing jitter	0	.6	.9	1	A
dj	source jitter	0	0	.7	1	B
ds	source substructuring	0	.5	.15	.02	
dt	direct thresholding	1	.5	.05	0	C
dc	direct certainty	0	.25	.5	1	
dr	direct relays	0	1	3	6	
dp	direct pretest density	32	64	512	0	C
sj	specular jitter	0	.3	.7	1	A
st	specular threshold	1	.85	.15	0	C
ab	ambient bounces	0	0	2	8	
aa	ambient accuracy	.5	.2	.15	0	C
ar	ambient resolution	8	32	128	0	C
ad	ambient divisions	0	32	512	4096	
as	ambient super-samples	0	32	256	1024	
lr	limit reflection	0	4	8	16	
lw	limit weight	.05	.01	.002	0	C

Note: (A) Does not affect rendering time, (B) Adversely affects image smapling,
(C) Maximum value disables optimization and can be very computationally expensive.

Table A.2: A summary of how sensitive simulation execution time is to adjustments of each radiance parameter, adapted from [7].

Paramter	**Effect on Execution Time**
ps	inverse, halving value increases rendering time up to four times
pt	minor, decreasing value causes modest increase in rendering time
pj	no effect
dj	indirect, increasing value requires ps parameter to be reduced
ds	inverse, halving value causes rendering time to approximately double
dt	inverse, halving value causes rendering time to increase about 50%
dc	direct, affects rendering time up to 50% over its 0 to 1 range
dr	direct, depending on the scene each new reflection can double time
dp	minor, affects start-up time only, higher values take longer
sj	no effect
st	minor, a value of zero may increase rendering by 50% over maximum of 1
ab	direct, doubling this value can double rendering time
aa	direct, doubling this value approximately quadruples rendering time
ar	direct, effect depends on scene, can quadruple time for double value
ad	direct, doubling value may double rendering time
as	direct, effectively adds to ad parameter and its cost
lr	minor, increase causes very slightly longer rendering time
lw	minor, decrease causes very slightly longer rendering time

APPENDIX B

Heating subsystems

Results of the heating model show that the heating system is only active during the winter and that most heating subsystems are linearly correlated with temperature B.1, aside from a few that are activated by temperature set points B.2.

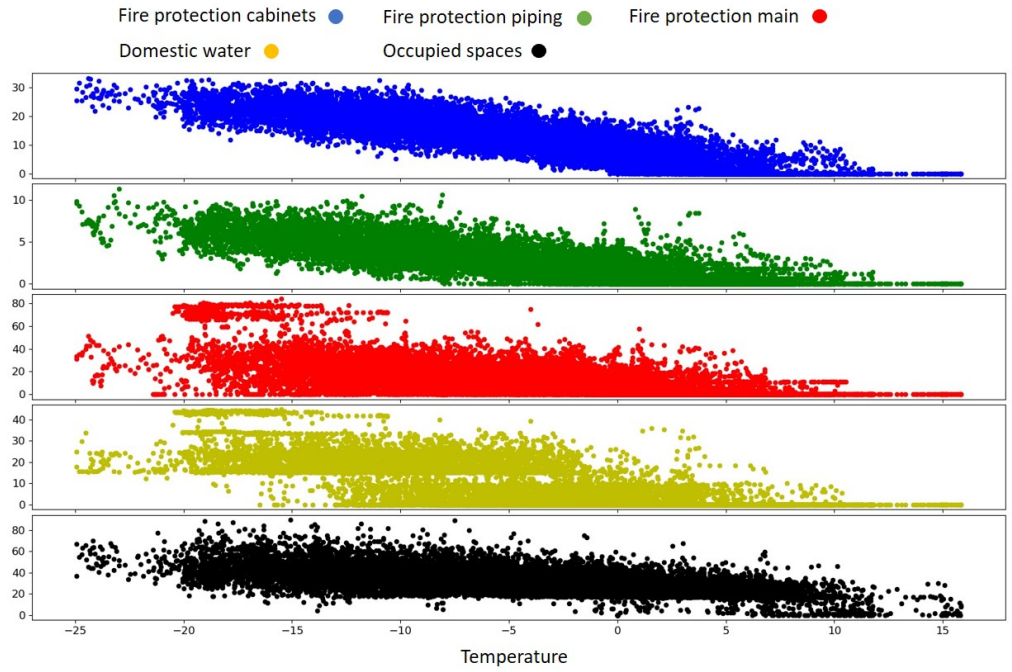

Figure B.1: Heating subsystems with controls that are linearly correlated with outdoor temperature.

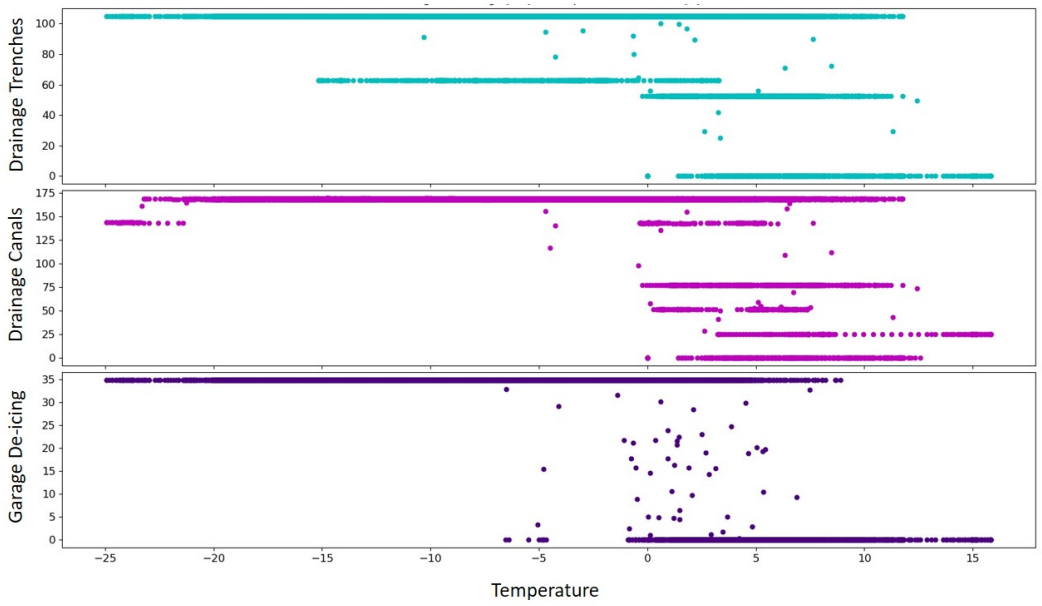

Figure B.2: Heating subsystems that are controlled/activated by temperature setpoints.

APPENDIX C

Predicted Temperature Coefficients

Table C.1: Goodness of fit of data measured at main electricity meter

R^2	Parameter	Value	Interval for 95%
0.77	α	13.2	$\pm$ 0.0931
	β	19.4	$\pm$ 0.141

Table C.2: Goodness of fit of Residuals

R^2	Parameter	Value	Interval for 95%
0.66	α	14.6	$\pm$ 0.117